DECHEMA
FORSCHUNGSINSTITUT
Stiftung bürgerlichen Rechts

Materials
Chemical Engineering
Biotechnology

Forschungsberichte Nr. 14

Markus Stöckl

2018

Attachment under current – biofilm formation by electroactive bacteria

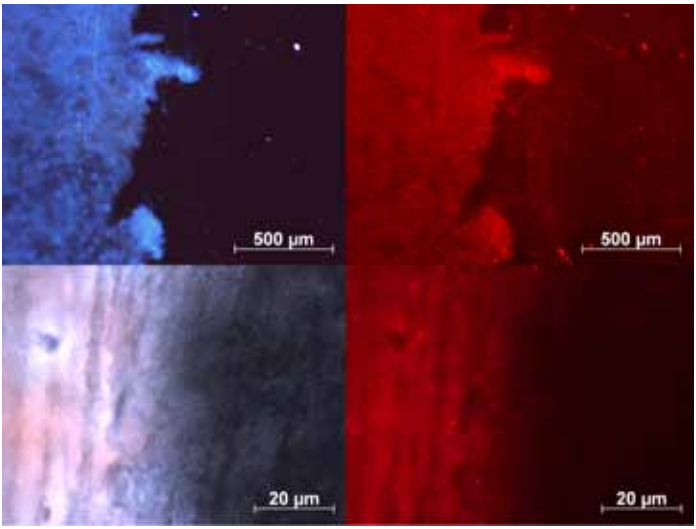

Herausgeber: DECHEMA-Forschungsinstitut • Stiftung bürgerlichen Rechts
Vorstand: Prof. Dr. Jens Schrader
Sitz der Stiftung: Frankfurt am Main
www.dechema-dfi.de

University of Duisburg – Essen

Aquatic Biotechnology in the Biofilm Centre of the Faculty of Chemistry

Attachment under current – biofilm formation by electroactive bacteria

Dissertation

for attainment of the academic degree of

Doktor der Naturwissenschaften

- Dr. rer. nat -

presented by

Markus Stöckl

(Neuss)

2017

1. Gutachter der Arbeit:	Prof. Dr. Wolfgang Sand
2. Gutachter der Arbeit:	Dr. Klaus-Michael Mangold
3. Gutachterin der Arbeit:	Prof. Dr. Anna Gorbushina

Tag der mündlichen Prüfung: 15.01.2018

Schriftenreihe des DECHEMA-Forschungsinstituts

Band 14

Markus Stöckl

Attachment under current – biofilm formation by electroactive bacteria

Shaker Verlag
Aachen 2018

Bibliographic information published by the Deutsche Nationalbibliothek
The Deutsche Nationalbibliothek lists this publication in the Deutsche Nationalbibliografie; detailed bibliographic data are available in the Internet at http://dnb.d-nb.de.

Zugl.: Duisburg-Essen, Univ., Diss., 2017

Printed in Germany.

ISBN 978-3-8440-5799-7
ISSN 2197-6155

Shaker Verlag GmbH • P.O. BOX 101818 • D-52018 Aachen
Phone: 0049/2407/9596-0 • Telefax: 0049/2407/9596-9
Internet: www.shaker.de • e-mail: info@shaker.de

Abstract

Bioelectrochemical systems (BES) are hybrid systems using electroactive bacteria and electrochemical techniques. Solid electrodes serve as electron donor for or acceptor from microorganisms for the production of current and/or the generation of valuable substances. Research conducted on BES in this thesis ranged from fundamental investigations on microbial attachment to electrodes to the development of electrode materials for advanced reactor concepts.

The first part of this theses was the biochemical analysis of the extracellular polymeric substances (EPS) secreted by *G. sulfurreducens* under electroactive conditions. *G. sulfurreducens* was cultivated in MFC-mode on graphite based electrodes polarized to +400 mV vs. Ag/AgCl for 8 d. A maximum current density of 172 ± 29 µA cm^{-2} was reached after 7 d. Routine methods for the biofilm harvest and the EPS processing were established. Electroactive cultures secreted significantly more EPS compared to cells grown under standard heterotrophic conditions (fumarate respiration). With 116 pg $cell^{-1}$, the highest amount of EPS was measured for the soluble EPS fraction of *G. sulfurreducens* using anode respiration, followed by the tightly bound (18 pg $cell^{-1}$) and loosely bound (11 pg $cell^{-1}$) fractions of the EPS. Proteins were found to dominate all EPS fractions of the biofilms grown under electrochemical conditions.

The second part was the development of a membrane separated flow cell for the simultaneous electrochemical impedance spectroscopy (EIS) and confocal laser scanning microscopy (CLSM) [Stöckl et al. 2016]. A flow cell made from PEEK was constructed, using a transparent indium tin oxide electrode as working electrode. A fluorescent *S. oneidensis* was cultivated under MFC conditions. A decrease of the charge transfer (R_{CT}) from 292 kΩ to 120 kΩ was observed with an increased current of 0.52 µA cm^{-2} after 17 h of operation. The CLSM images revealed an increasing cell number of *S. oneidensis* on the WE electrode to a monolayer with 26 cells 100 μm^{-2} after 17 h under MFC conditions.

As final part a straight forward approach to synthesize magnetic electrode particles allowing the artificial fixation of electroactive bacteria was developed [Stöckl, et al. 2016, DE102014112685A, Frankfurt, Germany]. The microwave assisted synthesis of magnetite was applied for the production of the magnetic electrode particles with activated carbon ($P_{MAG/AC}$). The surface area is around 300 m^2 g^{-1} and the particle size ranges between 20 and 200 µm. Resting cells of *S. oneidensis* attached to a maximum concentration of $8 \cdot 10^{10}$

± 3 · 10^9 resting cells g^{-1} $P_{MAG/AC}$. Electrochemical examination revealed that magnetically immobilized $P_{MAG/AC}$ showed a capacitive current response during cyclic voltammetry. Linear sweep voltammetry indicated that particles were stable down to a potential of –680 mV vs. Ag/AgCl.

Key words: bioelectrochemical systems, anode respiration, extracellular polymeric substances, impedance spectroscopy, confocal laser scanning microscopy, magnetic electrode particles

Zusammenfassung

Bioelektrochemische System (BES) sind Hybridsysteme, in denen elektroaktive Bakterien und Methoden aus der Elektrochemie kombiniert werden. Elektroden dienen dabei als Elektronendonor oder Akzeptor für Mikroorganismen bei der Stromproduktion und/oder der Herstellung von Biokraft-stoffen oder Prozesschemikalien. Der Fokus dieser Arbeit erstreckt sich von den Grundlagen des mikrobiellen Anheftens bis zur Entwicklung von Elektrodenmaterialien für komplexe Reaktorkonzepte.

Im ersten Teil wurde eine biochemische Analyse der extrazellulären polymeren Substanzen (EPS) von *G. sulfurreducens* Biofilmen unter elektroaktiven Bedingungen durchgeführt. *G. sulfurreducens* wurde in mikrobiellen Brennstoffzellen bei +400 mV vs. Ag/AgCl für 8 d kultiviert. Maximale Stromdichten von 172 ± 29 µA cm^{-2} wurden nach 7 d erreicht. Die elektroaktiven Zellkulturen produzierten deutlich mehr EPS als Zellen, die bei heterotrophen Standardbedingungen (Fumarat-Atmung) wachsen. Die höchste Konzentration an EPS wurde mit 116 pg $Zelle^{-1}$ in der löslichen Fraktion der EPS der elektroaktiven Kultur (Anoden-Atmung) gefunden, gefolgt von den kapsulären (18 pg $Zelle^{-1}$) und den kolloidalen (11 pg $Zelle^{-1}$) EPS Fraktionen. Proteine stellten dabei in allen EPS Fraktionen die größte Hauptgruppe der EPS Komponenten dar.

Die Entwicklung einer durch eine Membran geteilte Durchflusszelle zur Erfassung des mikrobiellen Wachstums mittels simultaner elektrochemischer Impedanzspektroskopie (EIS) und konfokalen Laser Scanning Mikroskopie (CLSM) bildet den zweiten Teil der Arbeit [Stöckl et al. 2016]. Die Durchflusszelle wurde mit einer transparenten Indium Zinnoxid Elektrode aus PEEK hergestellt. Ein selbstfluoreszierender *S. oneidensis* Stamm wurde unter MFC Bedingungen in der Durchflusszelle kultiviert. Der Ladungsdurchtrittswiderstand (R_{CT}) verringerte sich im Laufe der Messung von 292 kΩ auf 120 kΩ und eine maximale Stromdichte von 0,52 µA cm^{-2} wurde nach 17 h gemessen. Mittels CLSM wurde eine einschichtige Zelllage mit einer Dichte von 26 Zellen 100 μm^{-2} detektiert.

Letzter Teil dieser Arbeit war die Entwicklung von magnetischen Elektrodenpartikeln zur Fixierung von elektroaktiven Bakterien [Stöckl, et al. 2016, DE102014112685A, Frankfurt, Germany]. Diese magnetischen Partikel ($P_{MAG/AC}$) wurden mittels Mikrowellen-assistierter Magnetisierung von Aktivkohle hergestellt. $P_{MAG/AC}$ Partikel haben eine Oberfläche von 300 m^2 g^{-1}, die Größenverteilung liegt zwischen 20 und 200 µm. Ruhende *S. oneidensis* Zellen haften mit einer maximalen Zelldichte von $8 \cdot 10^{10} \pm 3 \cdot 10^9$ ruhenden Zellen g^{-1} an den

Partikeln an. Elektrochemische Messungen mit zyklischer Voltammetrie zeigten hauptsächlich kapazitives Verhalten der magnetisch immobilisierten $P_{MAG/AC}$. Linear sweep Voltammetrie konnte darüber hinaus zeigen, dass die Partikel bis zu einem Potential von –680 mV vs. Ag/AgCl stabil sind.

Schlüsselwörter: Bioelektrochemische Systeme, Anodenatmung, extrazelluläre polymere Substan-zen, Impedanzspektroskopie, Konfokale Laser Scanning Mikroskopie, magnetische Elektrodenpartikel

Preface

The mayor part of this study was accomplished at the

DECHEMA-Forschungsinstitut

Electrochemistry

Theodor-Heuss-Allee 25

60486 Frankfurt am Main, Germany

Under the supervision of

Dr. Klaus-Michael Mangold

Head of the working group electrochemistry

The flow cell construction and CLSM imaging was conducted at the

Technical University of Kaiserslautern

Institute of Bioprocess Engineering

Gottlieb-Daimler-Straße 44

67663 Kaiserslautern, Germany

Under the supervision of

Prof. Dr. Roland Ulber

Head of the Institute of Bioprocess Engineering

The biochemical EPS analysis was conducted at the

University of Duisburg Essen

Aquatic Biotechnology in the Biofilm Centre of the Faculty of Chemistry

Universitätsstr. 5

45141 Essen

Under the supervision of

Prof. Dr. Wolfgang Sand (former head of the Aquatic Biotechnology, Biofilm Centre)

With the permission of

Prof. Dr. Rainer Meckenstock

Head of the Aquatic Microbiology, Biofilm Centre

1. Gutachter der Arbeit: Prof. Dr. Wolfgang Sand

2. Gutachter der Arbeit: Dr. Klaus-Michael Mangold

3. Gutachterin der Arbeit: Prof. Dr. Anna Gorbushina

Acknowledgements

I would like to sincerely thank Dr. Klaus-Michael Mangold for being an outstanding supervisor of this work. He has always discussed my questions warmly independent on how long it took to find an answer. These discussions resulted in fruitful outcomes and new ideas. These thanks also belong to the whole working group Electrochemistry of the DECHEMA Forschungsinstitut for being the most helpful and familiar colleagues one could ask for. Additionally I would like to thank Anne Christin Wenck for her contribution as Bachelor student.

I would like to express my gratitude to Prof. Dr. Wolfgang Sand for his excellent guidance of the thesis and supervision of EPS analysis experiments of *G. sulfurreducens*. His constant supply with interdisciplinary literature, his critical questions and the availability, spanning even distances of more than 10000 km, marked a significant contribution to the success of this dissertation.

Furthermore, my great thanks belong to Dr. Dirk Holtmann. His continuous providing with new ideas and encouragement as well the arrangement of collaborations had a tremendous positive impact on this work. My thanks also go the whole working group Industrial Biotechnology of the DECHEMA Forschungsinstitut for including me as one of their group members and their unlimited support.

I also would like to thank Prof. Dr. Roland Ulber and Dr. Christin Schlegel for an excellent cooperation in designing a flow cell and the possibility to use the CLSM for the biofilm monitoring of *S. oneidensis*.

Many thanks also belong to Prof. Dr. Rainer Meckenstock and Natascha Caroline Teubner for the possibility of analyzing the EPS of *G. sulfurreducens*. Thank you also for the professional and enduring help.

I also gratefully acknowledge the financial support from the German Federal Ministry of Education and Reseach (No. 031A226).

Finally, I want to thank my family, friends and my partner Valeska for encouraging me to follow my plans not only during this thesis, and creating an environment of thought freedom.

Table of Contents

List of Abbreviations

AC	activated carbon
BCA	bicinchoninic acid
BES	Bioelectrochemical system
BET	Brunauer Emmett Teller
BSA	bovine serum albinum
C	control
CE	counter electrode
CLSM	confocal laser scanning microscopy
CM	cellular membrane
ConA	Concanavalin A
CP	cytoplasm
CPE	constant phase element
CV	cyclic voltammetry
CW	18-crown-6-ether
DAPI	4',6-diamidino-2-phenylindole
DET	direct electron transfer
DIR	dissimilatory iron-reducing
DOW	DOWEX®
eDNA	extracellular DNA
EDTA	ethylen diamin tetra acetic acid
EET	extracellular electron transfer
EFM	epifluorescence microscopy
eGFP	enhanced green fluorescent protein
EIS	electrochemical impedance spectroscopy
EPS	extracellular polymeric substances
ER	extraction reagent
EXP	exponential
FL	flavin
G. sulfurreducens	*Geobacter sulfurreducens*
GC	Glassy carbon
IET	indirect electron transfer

ITO	indium tin oxide
LB	loosely bound
LM	lactate medium
LSV	linear sweep voltammetry
MEC	microbial electrolysis cell
MEM	membrane
MET	mediated electron transfer
MES	microbial electrosynthesis
MIC	microbiologically influenced corrosion
MFC	microbial fuel cell
Mtr	metal reducing
OCP	open circuit potential [V]
OD_{600}	optical density at λ = 600 nm
OM	outer membrane
Omc	outer membrane cytochrome
ORR	oxygen reduction reaction
PBS	phosphate buffered saline
PEEK	poly ether ether ketone
P_{MAG}	magnetic particles without activated carbon
$P_{MAG/AC}$	magnetic particles with incorporated activated carbon
PP	periplasm
R_{CT}	charge transfer resistance [Ω]
RE	reference electrode
R_U	solution resistance [Ω]
S. oneidensis	*Shewanella oneidensis*
SCB	sodium chloride buffer
SEM	scanning electron microscopy
SHE	standard hydrogen electrode
SOL	soluble
STAT	stationary
TCA	tricarboxylic acid
TB	tightly bound

US	ultra sound
WE	working electrode
W_D	Warburg diffusion
Z_{IMAG}	imaginary part of the impedance [Ω]
Z_{REAL}	real part of the impedance [Ω]
Z_{TOT}	total impedance [Ω]

1 General introduction

Climate change and increasing environmental pollution are two of the main challenges of humanity in the twenty first century. With a prospected world population of around 10 billion humans in the year 2050 [United Nations 2015b] and the limited capacities our planet, poverty is one of the main problems related to global warming and pollution. Therefore, limiting global warming to a maximum of 2 °C compared to pre-industrial values was set as one of the key countermeasures [United Nations 2015a].
Based on the Kyoto protocol from 1997 [United Nations 1998] 195 member states of the United Nations Framework Convention on Climate Change signed in 2016 the Paris Agreement and acknowledged, inter alia, the following phrases [United Nations 2015a]:

- *"Recognizing the need for an effective and progressive response to the urgent threat of climate change on the basis of the best available scientific knowledge,"*

- *"Emphasizing the intrinsic relationship that climate change actions, responses and impacts have with equitable access to sustainable development and eradication of poverty,"*

- *"Recognizing the fundamental priority of safeguarding food security and ending hunger, and the particular vulnerabilities of food production systems to the adverse impacts of climate change."*

It is scientifically well accepted that the emission of greenhouse gases is the main contribution to the climate change and global warming. Amongst these, emissions related to the energy consumption sector are by far the highest category [Bundesumweltamt 2016b]. As can be seen in Figure 1 for the year 2014, more than 80 % of the emitted CO_2-equivalents in Germany originated from energy consumption. In order to decrease the emission of greenhouse gases, modernization and innovations in the energy sector are needed. Consequently, a future energy management including sustainable energy generation as well as efficient storage systems is a key parameter towards fulfilling global political agreements and a minimization of global warming.

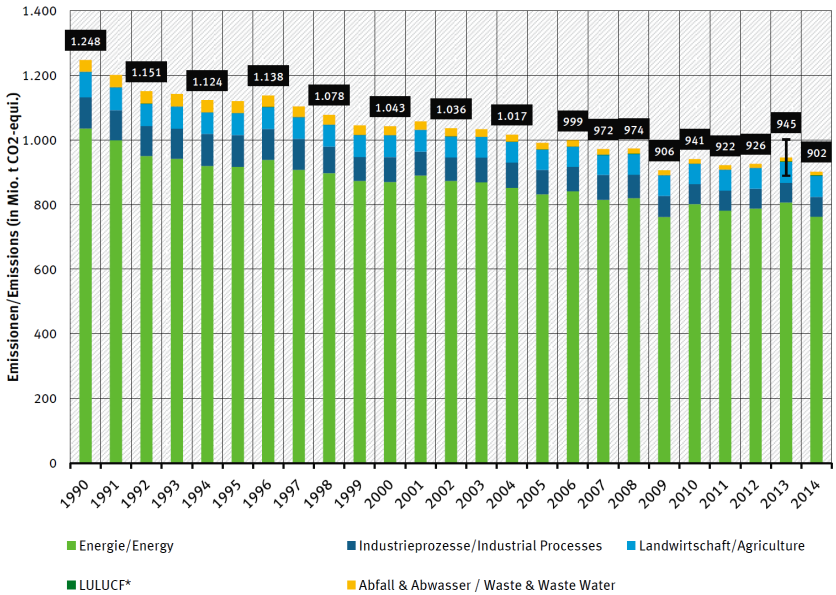

Figure 1: Emission trends in Germany since 1990 divided into the following categories: Energy, industrial processes, agriculture, LULUCF (Land Use, Land Use Change and Forestry), waste and waste water. Adapted from [Bundesumweltamt 2016b].

1.1 Future energy management

Since the highest reduction potential lies in the emission of greenhouse gases, a variety of measures were taken into account for future energy management. In the past decades research focused on the development of alternative and renewable energy sources including solar, wind, water and biomass. Common for the majority of renewable energy sources is, that energy is derived in the form of electricity [Ausfelder et al. 2015].

Renewable ways of energy generation are strongly characterized by both temporal (seasonal and daily) and spatial fluctuations. Prediction of available sunlight or wind for example is limited, as well as their availability. In the context of sustainable energy management, the residual load has to be taken into account. It is defined as the difference between the required (demand) and the generated energy (supply) [Ausfelder et al. 2015].

In the case of a positive residual load, more energy is generated than consumed, leading to the possibility or the need to store energy. Available technologies range from mechanical (mainly pumped hydro storage) and thermal storage (e.g. ad- and desorption processes) to

chemical (e.g. hydrogen production) and electrochemical techniques (batteries) [Ausfelder et al. 2015].

In the case of a negative residual load, the demand on energy is higher than the available energy, leading to the short or near term onset of additional energy production. So far, this buffering is mainly achieved by the combustion of fossil fuels.

Independent from the need to store or generate energy, the development of sustainable technologies is an ongoing process. One main parameter indicating this development might be the funding with 3.5 billion euros in the years from 2013 to 2016 by the Federal Republic of Germany for this purpose [Bundesministerium für Wirtschaft und Energie 2017].

Research is thereby not only focused on one discipline but pluralistic, since a variety of solutions for sustainable energy generation and storage are required when facing the complex future energy demand [Bundesumweltamt 2016a].

Bioelectrochemical systems might be one part in a sustainable energy management, since they are characterized by a high flexibility [Rabaey et al. 2008]. They can provide the possibility to buffer fluctuations in the residual load by either the production of current from waste streams or the generation of storage chemicals by a consumption of available current (positive residual load).

1.2 Bioelectrochemical systems

Bioelectrochemical systems (BES) are hybrid systems using electroactive bacteria and electrochemical techniques. Solid electrodes serve as electron donor or acceptor for microorganisms (or enzymes) for the production of current and/or the generation of valuable substances.

By the combination of microbiology with electrochemistry it is possible to merge the advantages of both disciplines. Characteristics of microbiological catalysts such as a high reaction specificity and self-replication fuse with a high reaction control through applied current or potential and high coulombic efficiencies typical for electrochemical systems. This combination in BES offers the opportunity for the development of innovative, sustainable and efficient processes for current generation as well as energy storage via a number of valuable products [Krieg et al. 2014].

In environmental habitats with only minor amounts of oxygen or without, some bacteria have the ability to transport electrons originating from their metabolisms to or from extracellular electron acceptors. Consequently these bacteria offer the opportunity to serve as microbial electrocatalysts in BES. In general, BES are at least comprised of two electrodes, an anode and a cathode, which are often separated by a membrane (Figure 2). Electrical contact between the two electrodes can thereby be realized via a resistor, a potentiostat, or another power supply. A schematic of a BES generated by the combination of the bioelectrochemical half-cell systems of a microbial fuel cell (MFC) at the anodic side and a microbial electrosynthesis (MES) at the cathodic side is presented in Figure 2.

As all electrochemical systems, BES can be divided into current consuming (electrolysis, e.g. MES, MEC) or current generating systems (galvanic element, e.g. MFC). The first developed BES were MFCs, harvesting current by the microbial oxidation of organic matter in combination with an anode as sole/main electron acceptor [Potter 1912; Stirling et al. 1983; Reguera et al. 2006; Logan and Regan 2006]. The anode respiration is thereby mostly coupled with an abiotic reduction at the cathode, such as oxygen reduction or other terminal electron acceptors [Manohar and Mansfeld 2009; Mohan et al. 2009; Q. Deng et al. 2010].

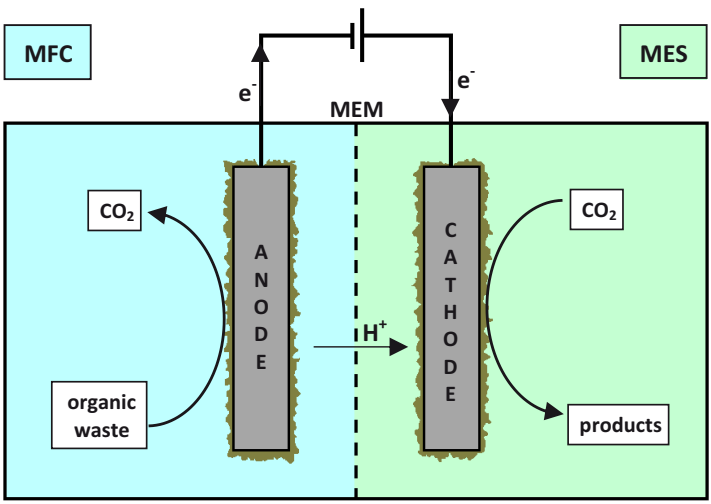

Figure 2: Schematic of a bioelectrochemical system (BES) composed of microbial fuel cell (MFC) and microbial electrosynthesis (MES) half cells. Sessile electroactive bacteria are schematically displayed in brown on the electrodes surfaces. Abbreviations: e^-: electron, H^+: proton, MEM: membrane (dashed line).

A second type of BES are microbial electrolysis cells (MEC). Thereby, a MFC process is used at the anodic side of the system to minimize the energy demand for cathodic electrosynthesis such as the production of hydrogen [Call and Logan 2008; Tartakovsky et al. 2009; Kuntke et al. 2014]. This process was also described as microbially assisted electrosynthesis [Rabaey and Rozendal 2010]. Most recently the ability to feed bacteria with electrons to produce valuable products was discovered, leading to the term microbial electrosynthesis (MES) [Nevin et al. 2010; Rabaey and Rozendal 2010]. Since MFC and MES represent the two most important applications in BES focusing on either the anode or the cathode these two will be explained in more detail in the following.

1.2.1 Microbial fuel cells

Microbial fuel cells (MFC) are type of BES employing electroactive microorganisms at the anode to catalyze the oxidation of organic substances under the generation of electrical current. They work on the principle of biological catalyzed conversion of chemical energy into electrical energy. Reduced organic molecules of high chemical energy (fuel/waste) are oxidized to molecules of low energy (waste/CO_2) by electroactive microorganisms. Thereby, the electroactive microorganisms transfer (respire) the electrons in the absence of alternative electron acceptors to the anode (more detailed information on the extracellular electron transfer is given in section 1.3). The electrons are then further transferred to the cathode of the MFC and the terminal electron acceptor gets reduced. The theoretical redox potential of a MFC is thereby defined by the difference in the standard redox potentials (ΔE^0) between the oxidized compound (anode) and the reduced compound (cathode). As example, the theoretical maximum potential of a MFC oxidizing acetate ($\Delta E^0 = -0.28\ V$) coupled with the oxygen reduction reaction (ORR) ($\Delta E^0 = 0.82\ V$) is 1.1 V.

The first MFC was reported in 1912 by Potter, employing yeast for the oxidation of glucose in a "not ordinary galvanic cell" [Potter 1912] generating a potential difference of 0.32 V. In 1931 Barnett constructed a stack of bacterial batteries with synthetic mediators involved in the biological redox reactions to reach a stack potential of 35 V [Barnett 1931]. 35 years later, Allen described the metabolic behaviour of *Escherichia coli* with mixed substrates employing an electrochemical cell [Allen 1966], and in 1983 Stirling introduced the name

microbial fuel cell [Stirling et al. 1983]. Since then, a plethora of MFC´s has been developed, focusing on the respective components of an MFC and the fields of operation.

MFC´s have successfully harvested current from a variety of different fuels like alcohols [Kim et al. 2007; Luo et al. 2009], carbohydrates [Pant et al. 2010], or even insects [Ieropoulos et al. 2005]. More important, the main energy sources for MFC´s are waste water streams of different origin containing high organic loads. Examples are urban waste water [Rodrigo et al. 2007; Mohan et al. 2009], beer brewery waste water [Wang et al. 2008], paper recycling waste water [Huang and Logan 2008] or food processing waste water [Oh and Logan 2005].

Concerning the electroactive microbial catalysts used in a MFC, a high variety can be found as well. By far the most prominent model organisms belong to the *Geobacter* and *Shewanella* families and have been used in a plethora of studies [Bond et al. 2002; Reguera et al. 2006; Nevin et al. 2008; Marsili et al. 2008; Rosenbaum et al. 2010; Brutinel and Gralnick 2012; Sun et al. 2016]. However, in the majority of MFC´s applied for current production from waste water streams, mixed cultures dominate the anodic space of the fuel cells [Du et al. 2007; Rodrigo et al. 2007; Mohan et al. 2008; Daniel et al. 2009]. Besides that, the dissimilatory iron-reducing (DIR) bacterium *Klebsiella pneumoniae* has been successfully grown in a MFC [Yuvraj and Aranganathan 2016].

Different electrode materials have been tested for their application as anode. Key factors for the material selection are conductivity, bio-compatibility, accessible surface area and cost. Besides stainless steel mainly carbon based materials were applied as terminal electron acceptor for the electroactive bacteria [Krieg et al. 2014]. A comprehensive study on different electrode materials for *Shewanella oneidensis* was published [Kipf et al. 2013].

Since the reduction reaction at the cathode is supposed to be one of the main limiting factors in MFC´s, different studies focused on the optimization and cost effectiveness of this reaction. Activated carbon [He et al. 2006; L. Deng et al. 2010] has been used as well as platinum [He et al. 2006; Roy et al. 2014] or gas diffusion electrodes open to air [You et al. 2011; Pasupuleti et al. 2015]. Furthermore, algae have been used to enhance the ORR by in situ production of oxygen directly in front of the cathode surface [Rosenbaum et al. 2005]. Additionally, a very interesting approach applied current for the electrochemical reduction of metal ions such as copper to recover it from copper-containing waste water streams such as acid mine drainage [Heijne et al. 2010; Nancharaiah et al. 2015].

In conclusion, it can be stated that MFC´s are an economical technology to combine waste water treatment with current generation. A company claimed that MFC systems are already commercially available (emefcy, Caesarea, Israel). Implemented in the purification process of a waste water treatment (WWTP) plant, a full-scale MFC would notable reduce overall energy demand of the WWTP [Hiegemann et al. 2016]. To the author´s opinion, implementation of a MFC into the waste water treatment system is mostly hindered by political and municipal issues than by scientific problems.

1.2.2 Microbial electrosynthesis

The most recent technology emering from the field of BES is microbial electrosynthesis (MES). It represents the possibility to convert electrical energy into chemicals and biofuels. Electrical current is provided at the cathode of a bioelectrochemical cell and converted under the reduction of carbon based molecules (substrate/CO_2) to substances of high energy (product) and value. Comparable to the theoretical cell potential of a MFC, standard redox potentials of the desired products determine the theoretically applied cathode potential.

So far, the spectrum of products generated with MES is rather in its infancy but is quickly emerging. Already in 1988 Kim found that butanol fermentation with *Clostridium acetobutylicum* was enhanced under current supply via a mediator [Kim and Kim 1988]. The first MES starting from CO_2 as substrate was reported by Nevin in 2010 [Nevin et al. 2010]. The organism *Sporomusa ovata* produced acetate from CO_2 and the current was derived from a solar cell. Further studies demonstrated mainly the conversion of CO_2 to acetate [Marshall et al. 2013; Patil et al. 2015; Mohanakrishna et al. 2015]. More complex and recent MES products are mainly organic acids or alcohols consisting of up to four carbon atoms. Nevin showed the generation of acetate, 2-oxobutyrate and formate with *Clostridium ljungdahlii* and *Clostridium aceticum* in the µ-molar range [Nevin et al. 2011]. Additionally, Ganigue produced acetate, ethanol, butyrate and buthanol in a MES with an inoculum dominated by species of the genus *Clostridium* [Ganigué et al. 2015].

A different approach of MES is the generation of methane catalyzed by methanogenic bacteria, representing the "power to gas" approach. Cheng reported the generation of methane from CO_2 at a cathode polarized to –700 mV vs. SHE or even more negative values with a mixed culture biofilm dominated by *Methanobacterium palustre* [Cheng et al. 2009]. Comparable to these findings, Villano presented autotrophic methane production by

hydrogenophilic methanogenic bacteria at a potential more negative than –650 mV vs. SHE [Villano et al. 2010]. However, due to the relatively high negative potentials applied in these studies, hydrogen production is assumed to serve as precursor for microbial methanogenesis. In contrast to this, Beese-Vasbender presented in their publication that already at a cathode potential of –160 mV vs. SHE methane production with the *Methanobacterium*-like archaeon strain IM1 was observed. Since hydrogen production appears only at potentials below –400 mV vs. SHE, the organism was shown to utilize electrons directly from the cathode without hydrogen as electron carrier [Beese-Vasbender et al. 2015].

In the field of future energy management MES might present a promising technology to produce biochemicals and biofuels to store excessive energy (positive residual loads) provided from renewable energy. However, MES still needs to overcome a variety of biological, electrochemical, logistical and economic challenges [Rabaey et al. 2011].

1.3 Extracellular electron transfer mechanisms

The key function behind the working principle of BES is the ability of a group of bacteria, frequently named electroactive bacteria [Rabaey et al. 2008], electrogenic bacteria [Borole et al. 2011] or electrogens [Cheng et al. 2009], to exchange electrons with an electrode. In the last decade, different mechanisms for the interaction of bacteria with solid electrodes have been discovered, allowing a new insight look into microbial activity.

The ability to exchange electrons with extracellular compounds is thereby one of the key principles of microbial life, with a variety of mechanisms discovered for bacteria under aerobic and anaerobic conditions. Well known mechanisms under anaerobic conditions are denitrification, sulfate and sulfur respiration, acetogenesis or methanogenesis [Madigan and Martinko 2006]. Moreover, the bacterial interactions with metal ions have an important ecological role. The dissimilatory reduction of metal ions such as manganese and iron [Lovley and Phillips 1988], uranium [Lovley et al. 1993] or cobalt [Hau et al. 2008] for example were found to appear in aquatic sediments. Bacteria such as *Geobacter metallireducens* [Lovley and Phillips 1988] or *Shewanella oneidensis* [Hau et al. 2008] release electrons to metal ions in the absence of oxygen to close their respiratory chain. Besides reduction, microbial oxidation of metals is another ecological niche occupied by bacteria. Leaching bacteria use

the autotrophic oxidation of metal ions for energy generation by the uptake of electrons. Prominent examples for the electron uptake are *Acidithiobacillus ferrooxidans* or *Leptospirillum ferrooxidans* [Sand et al. 1992; Schippers et al. 1996]. When employing the thiosulfate or polysulfide mechanism, these organisms take up electrons from the oxidation of ferrous to ferric iron [Rohwerder et al. 2003]. Based on this observation, *Acidithiobacillus ferrooxidans* for example has been applied in a BES by drawing current from a graphite cathode [Carbajosa et al. 2010] and was identified as a promising organism towards the electrification of microorganisms for the production of chemicals [Tremblay and Zhang 2015].

However, in BES so far leaching bacteria play only a minor role. More prominent and frequently applied bacteria in BES are *Shewanella oneidensis* [Logan et al. 2005; Marsili et al. 2008], *Geobacter sulfurreducens* [Bond et al. 2002; Lovley et al. 2011] or *Sporomusa ovata* [Nevin et al. 2010] for example. Their ability to exchange electrons with an electrode has been studied extensively [Yang et al. 2012]. Thereby, the mechanism of extracellular electron transfer (EET) varies depending on the type of organism and can be generally differentiated into the direct electron transfer (DET) and the mediated (MET) or indirect electron transfer (IET). The types of EET are schematically displayed in Figure 3. Depending on the definition MET and IET are mainly differentiated by the type electron shuttle In the MET shuttling molecules are mainly recycled, whereas in the IET electron shuttles are consumed (e.g.Hydrogen). Two exemplary bacteria possessing the most important mechanisms, DET and MET, are *Geobacter sulfurreducens* and *Shewanella oneidensis*, respectively, which were also employed in this study.

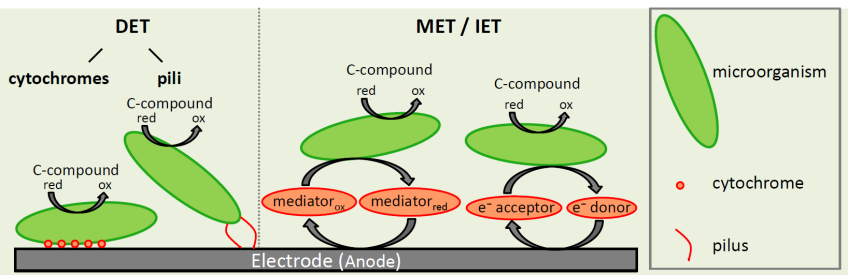

Figure 3: Different mechanisms of extracellular electron transfer (EET), exemplary for the anode respiration: direct electron transfer (DET), mediated electron transfer (MET) and indirect electron transfer (IET), modified from [Sydow et al. 2014].

1.3.1 Mediated electron transfer

For the mediated electron transfer (MET), a physical contact between microorganisms and the electrode is not required. In MET electroactive cells are mainly present in the planktonic phase and electrons are exchanged via redox-active mediators that shuttle electrons between the cells and the electrode. Mediators can be naturally excreted by microorganisms such as flavins by *S. oneidensis* or phenazines by *Pseudomonas aeruginosa* [Dietrich et al. 2006; Marsili et al. 2008; Sydow et al. 2014]. A second option are chemically synthesized and added substances such as safranin-T or methyl viologen [Fultz and Durst 1982]. When serving as electron shuttle in MES mode for example, the soluble substances get oxidized by the organism, diffuse to an electrode and are subsequently reduced, comparable to the recycling of Fe(II) and Fe(III) in the contact mechanism at the leaching of pyrite [Rohwerder et al. 2003].

For process engineering of BES employing microorganisms capable of MET is advantageous in terms of high space and time yield. The electroactive cells live in the planktonic phase and have access to medium components without diffusion limitation and, consequently, do not limit the process. Furthermore, a porous electrode can be accessed down to the nanometer scale, since mediators are magnitudes smaller than living cells. However, when employing BES with MET in continuous reactor operation, both cells and mediators have to be replaced due to constant wash out [Krieg et al. 2014]. *S. oneidensis* is the most prominent electroactive model organism using the mediated electron transfer, since it was shown to secrete flavins such as riboflavin [Marsili et al. 2008]. Analog to its ability to respire on metal ions under anaerobic conditions, the assumed pathway for the anode respiration is named Mtr (metal reducing) pathway [Ross et al. 2011]. Electrons originating from the oxidation of lactate are thereby directed from the menaquinone pool of the cell to the quinol oxidase CymA (cytoplasmic membrane) located in the cellular membrane (Figure 4). Further electron transfer takes place via the multiheme c-type cytochrome MtrA in the periplasm and further to the outer membrane bound MtrA-

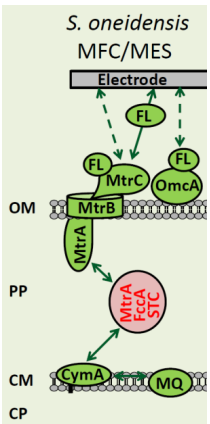

Figure 4: Schematic of the proteins involved in the mediated EET of *S. oneidensis* under MFC and MES conditions. Cellular appendages are not shown. OM: outer membrane. PP: periplasm. CM: cellular membrane. CP: cytoplasm. FL: Flavin. Modified from [Sydow et al. 2014].

MtrC-complex connected over the β-barrel protein MtrB. Via the MtrC located on the outer side of the outer membrane electrons are transferred to the shuttling mediator. Furthermore, *S. oneidensis* is assumed to be able to release electrons directly to an anode via the membrane bound MtrC and OmcA (outer membrane) cytochromes. The reverse electron trans-portation in MES mode from a cathode inside the cell is supposed to use the same protein cascade employed for the respiration [Ross et al. 2011].

1.3.2 Direct electron transfer mechanism

For the direct electron transfer mechanism (DET) from the electroactive organisms to the electrode or vice versa physical contact between cells and electrode is required. Consequently, the majority of bacteria employing the DET forms biofilms to adhere to the electrode and thereby is in contact with the surface. The thickness of these biofilms was thereby found to influence the current production for example under MFC conditions [Sydow et al. 2014]. Electrical contact to the electrode surface is realized by either the formation of conductive pili or nanowires [Reguera et al. 2006; Malvankar et al. 2011] (see also section 3.1.2) or via cytochromes located in the outer membrane of the cells [Ross et al. 2011] and is schematically displayed in Figure 3. Comparable observations have been made for cable-bacteria in marine sediments, shuttling electrons in the centimeter scale to couple spatially separated redox half reactions [Müller et al. 2016]

For process engineering by BES using microorganisms capable of DET, the retention of the cells on the electrode is thereby a great advantage. The biocatalyst remains in the system, independent from the type of reactor (batch or continuous cultivation) and is furthermore regenerated during processing due to the reproduction of the dynamic biofilm construct. Possible diffusion limitations such as the accumulation of protons resulting from thick or dense biofilms can consequently be a drawback of the surface dependent BES [Clauwaert et al. 2009].

Comparable to *S.oneidensis* and MET, by far the most applied microorganism amongst electroactive bacteria using the DET to respire on electrodes or to draw electrodes from an electrode is *Geobacter sulfurreducens*. It was found to produce biofilms with a thickness of up to 45 to 50 µm and to produce high currents under MFC conditions [Reguera et al. 2006; Nevin et al. 2008; Sun et al. 2016]. Figure 5 illustrates schematically the assumed electron pathway from the cytoplasm of the cell to an anode or vice versa from a cathode into the

cell for *G. sulfurreducens* [Sydow et al. 2014]. Initially, electrons are transferred from the menaquinone pool of the cell to a cytochrome bc-complex. Further electron shuttling takes place via the multiheme proteins MacA located in the cellular membrane and the periplasmic PpcA. From the PpcA cytochrome electrons can be transferred to a variety of outer membrane bound proteins. The cytochrome OmcZ in the outer membrane is assumed to be in direct contact with the electrode, whereas OmcS is associated to conductive pili (PilA) redirecting the electrons over a larger distance to the electrode [Lovley 2011].

In contrast to the relatively detailed model for the anode respiration, electron transport from a cathode inside the cell is characterized by a some uncertainty. Electrons are assumed to pass the outer membrane barrier through an outer membrane cytochrome (OMC) towards a GSU3274 protein and enter the cytoplasm through an inner membrane cytochrome (IMC), which is currently under debate [Sydow et al. 2014].

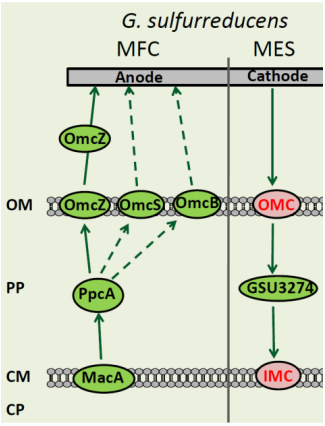

Figure 5: Schematic of the proteins involved in the direct EET of *G. sulfurreducens* under MFC and MES conditions. Cellular appendages are not shown. OM: outer membrane. PP: periplasm. CM: cellular membrane. CP: cytoplasm. Modified from [Sydow et al. 2014].

1.4 Biofilm formation

To release electrons via DET on an anode in a MFC, electroactive bacteria have to be in physical contact with the electrode surface (section 1.3.2). Consequently, the majority of microorganisms using DET forms biofilms on electrode surfaces.

Similar to the biofilm formation process of microorganisms adhering to surfaces other than electrodes, the development of an electroactive biofilm can be described by 5 phases (Figure 6) [Monroe 2007]. Initially (**I**), microorganisms bind reversibly to an (electrode) surface. This stage has also been described as conditioning phase, when initially substances such as free DNA, proteins, lipids, polysaccharides and others bind to the surface on the basis of electrostatic and van der Waals interactions [Flemming and Wingender 2010]. Cells that bind in this phase to the surface bind reversibly. The second stage (**II**) describes the irreversible

attachment. Surface related cells secrete extracellular polymeric substances (EPS) and bind thereby to the surface. EPS are self-produced hydrated biopolymers such as polysaccharides, proteins, nucleic acids and lipids. Some functions of EPS are to immobilize cells on the surface, form stable aggregates, prevent biofilms from desiccation or nutrient accumulation [Wingender et al. 1999]. In electroactive biofilms the EPS are further related to contribute to the EET [Borole et al. 2011]. More detailed information on EPS can be found in chapter 2 (3.1.3).

The third stage of biofilm formation (**III**) is defined by maturation, namely the formation of micro colonies. Cells immobilized on the substrate multiply and continue to excrete EPS. Growth of the biofilm in this phase is mainly two-dimensional. In contrast, further maturation of the biofilm in the second maturation phase (**IV**) is rather three-dimensional. Depending on a variety of factors such as the diversity and species of the sessile culture, rheological conditions or the availability of nutrients biofilm structures of mature biofilms differ. Biofilms can reach thicknesses up to several hundreds of microns, including tunnel-like systems inside the film or a mushroom like-structure after maturation [Boles et al. 2004]. Different gradients such as nutrient, oxygen or pH have been reported for biofilms resulting from the metabolic behavior of the bacterial consortium and biofilm thickness. Proton accumulation in electroactive biofilms has been assumed to lower the performance of a MFC for example [Clauwaert et al. 2009].

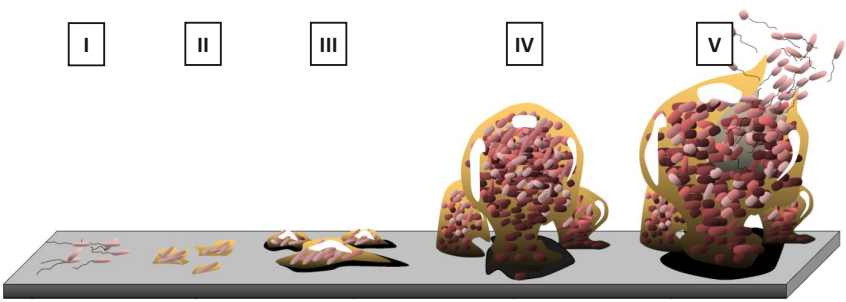

Figure 6: Schematic of the 5 phases of biofilm development adapted from [Monroe 2007]. Phases: I: reversible attachment. II: irreversible attachment. III: maturation. IV: maturation II. V: dispersion.

Since for electroactive microorganisms employing DET the physical contact to the electrode surface is essential to perform anode respiration, electroactive biofilms are rather unstructured. Electrodes are generally covered and structures are dense. Mushroom like structures, as it was observed for *Pseudomonas aeruginosa*, have not been reported for electroactive biofilms so far [Boles et al. 2004].

The final phase of the biofilm development (**V**) is characterized by the dispersion. Initialized by cell lysis of shear forces for example, sessile cells or parts of the biofilm separate from the biofilm and might form new colonies on fresh surfaces.

2 Motivation and Aims

The field of bioelectrochemistry is characterized by a broad range of applications and scientific problems. Research in the field of BES is focused on a plethora of single aspects. Examples are mechanisms behind the EET, identification of electroactive bacteria, expanding the product spectrum or optimization of reactor designs.

Based on these broad opportunities to contribute to BES, research a multidisciplinary research approach was chosen for this thesis. Several aspects of microbial electrochemistry were investigated in order to achieve a deeper understanding of the whole field of BES. Research conducted in this thesis ranged from fundamentals of microbial attachment to electrodes to the development of electrode material for advanced reactor concepts. The focus was set on three different aspects. Namely, the aims of this thesis were:

- The analysis of the EPS excreted by an electroactive organism under electroactive conditions (chapter 3).

- The development of a platform for the simultaneous electrochemical and optical monitoring of electroactive microbial attachment to electrodes (chapter 4).

- The development of a three-dimensional electrode material providing the artificial fixation of electroactive bacteria for an advanced reactor system (chapter 5).

Fulfilling these aims was supposed to significantly contribute to the progress of BES towards their application and establishment for future energy management in both sustainable energy generation and the storage of excessive energy.

3 EPS analysis of *Geobacter sulfurreducens* biofilms

3.1 Introduction

3.1.1 *Geobacter sulfurreducens*

G. sulfurreducens was reported to be capable of releasing electrons to a solid electrode as terminal electron acceptor in 2002 [Bond et al. 2002]. Since, this organism became one of the most applied bacteria in bioelectrical systems (BES). As being one of the most common electroactive microorganisms, the biofilm formation on electrodes and the extracellular electron transfer from the cells to the electrode have already been examined excessively. In contrast to this, the EPS of *G. sulfurreducens* biofilms has been studied rarely so far.

Geobacter sulfurreducens is a dissimilatory metal- and sulfur-reducing microorganism isolated from the surface sediment of a ditch [Caccavo et al. 1994]. It is an obligately anaerobic Gram-negative, chemoorganotrophic proteobacterium of the *Geobacter* family. *G. sulfurreducens* is rod-shaped, 2 to 3 by 0.5 µm in size, non-motile and does not form spores. It is able to oxidize acetate with Fe(III), S^0, Co(III), fumarate or malate as electron acceptors for growth, but can also use hydrogen as sole electron donor with Fe(III) as electron acceptor [Caccavo et al. 1994]. Optimal growth is observed between 30 and 35 °C.

Energy harvesting and carbon fixation in *G. sulfurreducens* takes place via the citric-acid-cycle and is displayed in Figure 7 for the cultivation with fumarate as electron acceptor [Galushko and Schink 2000]. Initially, acetyl-CoA is formed from acetate either over acetyl phosphate under the consumption of ATP by an acetyl-CoA synthase or coupled to the succinyl-CoA to succinate reaction (1). Fumarate is transferred to malate by a fumarate hydratase, which is then transferred to oxaloacetate by a malate dehydrogenase under the generation of one NADH (2).

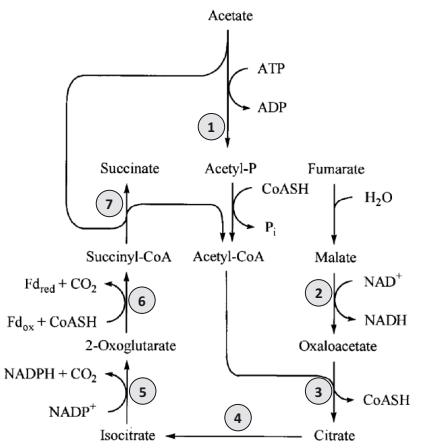

Figure 7: Pathway of acetate oxidation of *G. sulfurreducens* with fumarate as electron acceptor. Modified from [Galushko and Schink 2000].

Subsequently, a citrate synthase forms citrate from acetyl-CoA and oxaloacetate (3), which is further transferred to isocitrate by an aconitate hydratase. One NADPH is subsequently generated by the isocitrate dehydrogenase catalyzed CO_2 separation resulting in oxoglutarate (5). Under a second CO_2 separation an oxoglutarate dehydrogenase forms succinyl-CoA by the reduction of ferredoxin (6). Finally, succinyl-CoA is transferred to succinate by a succinyl-CoA synthetase with the generation of one ATP (7). In addition, minor amounts of acetyl-CoA can be formed from malate via pyruvate [Galushko and Schink 2000]. In the net reaction, two NADPH and one NADH are gained by acetate oxidation.

3.1.2 *G. sulfurreducens* and its biofilms in bioelectrochemical systems

Besides the ability to respire anaerobically using metal, sulfur, fumarate or malate reduction, *G. sulfurreducens* was also found to employ solid electrodes as terminal electron acceptors [Bond et al. 2002]. It is the most prominent organism employing the direct electron transport (DET) pathway [Lovley et al. 2011], already described in section 1.3.2. However, electrons can also be transferred to redox shuttles as electron acceptors for mediated electron transfer (MET), even though *G. sulfurreducens* was not found to secrete any mediators [Bond and Lovley 2003]. Due to this, the main EET pathway is DET. *G. sulfurreducens* has to be in direct contact with the electrode surface in order to release electrons and was consequently found to form biofilms on anode surfaces in MFCs. As one of the best biofilm formers of electroactive bacteria in pure culture, dense biofilms were observed to reach a thickness up to 45 or 50 µm [Reguera et al. 2006; Nevin et al. 2008; Sun et al. 2016]. Electrical contact of the cells with the electrode is achieved by outer membrane proteins, when cells are directly attached to the electrode. Cells, which are not directly attached to the electrode surface but located inside the biofilm are connected to the electrode by a net of conductive pili, self-produced nanowires in the extracellular space, which were found to conduct electrons on distances in the centimeter scale [Malvankar et al. 2011]. In this way anode respiration and a direct electron shuttling through the biofilm is achieved [Reguera et al. 2006].

As it was generally described for the biofilm formation processes in aquatic systems [Flemming and Wingender 2010], morphology, density and thickness of the biofilm result from a variety of internal and external factors, e.g. the bacterial consortium, external shear forces, surface morphology and nutrient availability. Furthermore, in electroactive biofilms

the surface accessibility enabling the electron release is a factor limiting the thickness of the biofilm. On one hand, thick biofilms in BES are desired since a high density of cells leads to a high current output or consumption. On the other hand, electrical conductivity or insulation inside the biofilm are determining limiting factors for spatial spacing since the respiration on the solid electrode is a surface associated and metabolism limiting step. Additionally, proton accumulation and consequent lowering of the pH value at the electrode surface also affects the biofilm formation in BES [Clauwaert et al. 2009].

3.1.3 EPS composition and analysis

In the field of EPS composition analysis, the determination of group parameters is a common way, which often can be found in literature, especially in the field of biocorrosion. Castro analyzed *Aeromonas hydrophila* biofilms for their contents of polysaccharides, proteins and uronic acids [Castro et al. 2014] and Vardanyan did protein and polysaccharide determination for biofilms of isolates of *Leptospirillum, Acidithiobacillus* and *Sulfobacillus* [Vardanyan et al. 2015]. Yang compared proteins, polysaccharides and DNA of different corrosion strains [Yang et al. 2016] and Wikiel did a comprehensive investigation on the EPS of *Desulfovibrio alaskensis* focusing on proteins, DNA, uronic acids, polysaccharides, lipids and humic acids [Wikiel 2013]. Contrary to these findings, electroactive biofilms are rarely investigated concerning their EPS composition so far, even though the composition is assumed to impact the electron transfer inside the biofilm [Yang et al. 2012]. Li showed in a series of experiments on the general redox properties of the EPS from *Shewanella oneidensis* and *Pseudomonas putida* a heme-mediated behavior of the EPS indicated by iron oxidation with CV [Li et al. 2016]. Rollefson studied the polysaccharide network in an electroactive biofilm of *Geobacter sulfurreducens* and identified OMC as essential for anchoring and arranging of electrode shuttling proteins [Rollefson et al. 2011]. Kouzuma et al. also focused on the polysaccharides in the EPS of *S. oneidensis* MR-1

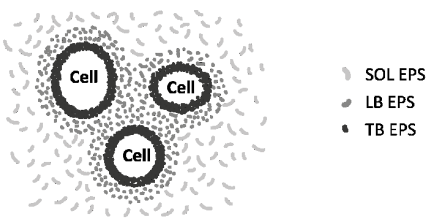

Figure 8: Schematic spatial organization of the different EPS fractions modified from Nielsen et Jahn 1999, in [Wingender et al. 1999].

biofilms [Kouzuma et al. 2010].

When analyzing the EPS a spatial organization on the cell scale and consequent harvesting of the EPS have to be taken into consideration. A scheme of the spatial organization of the EPS can be seen in Figure 8. EPS molecules that are strongly associated to the outer membrane, mainly polysaccharide and protein layers, are classified as capsular or tightly bound EPS (TB EPS) and are isolated by chemical extraction. Substances classified as colloidal or loosely bound EPS (LB EPS) are less compact and less associated to the cell membrane and can be harvested mechanically. As last fraction, the soluble EPS (SOL EPS), is secreted by the cells and accumulated in the outer sphere of the biofilm.

ince the biofilm and its EPS are very complex in both function and composition, the respective groups of the EPS (proteins, DNA, uronic acids, polysaccharides, lipds and humic acids) are supposed to play different roles in the interaction between microorganisms and the surface.

Proteins have a variety of functions in the EPS ranging from the spatial structuring to enzymatic activity such as preliminary digestion. Additionally, in electroactive biofilms proteins are also involved in the extracellular electron transfer. Nanowires, pili-like structures mainly composed of cytochromes, are synthesized by electroactive bacteria such as *Geobacter* and *Shewanella* and are capable to transport electrons even over distances on the centimeter scale to an electrode [Reguera et al. 2006; Malvankar et al. 2011; Lovley 2011]. Furthermore, Deutzman proposed that cell derived free enzymes by *Methanococcus maripaludis* bind to electrodes and take up electrons directly to catalyze hydrogen or formate formation. The subsequent consumption of those, consequently enables *Methanococcus maripaludis* to consume electrons from an electrode [Deutzmann et al. 2015].

Besides proteins carbohydrates are the second main group component of the EPS. Hydration of the biofilm is one of their functions, as well as the formation of supermolecular networks to stabilize the biofilm architecture [Wloka et al. 2004]. Rollefson showed that under electroactive conditions polysaccharides are responsible for extracellular anchoring of *Geobacter* biofilms to graphite electrodes [Rollefson et al. 2011]. Furthermore, Kouzuma indicated that extracellular polysaccharides influence both attachment to an electrode surface and current generation of *S. oneidensis* biofilms [Kouzuma et al. 2010].

Extracellular DNA (eDNA) in the EPS can originate either from the lysis of sessile cells or the excretion of the biofilm consortium. eDNA also has a stabilizing effect on the EPS structure and can play an important role in aggregation and microcolony formation [Flemming and Wingender 2010]. Furthermore, it can promote horizontal gene transfer within the biofilm. In electroactive biofilms eDNA is assumed to increase conductivity of the biofilm and is eventually involved in electron shuttling [Borole et al. 2011].

In naturally occurring biofilms humic substances mainly originate from the incomplete degradation of organic matter and are also incorporated in the EPS. In electroactive biofilms, humic acids are supposed to be employed as natural extracellular electron shuttle compounds, bridging the space between the microorganism and the electrode surface [Du et al. 2007; Torres et al. 2010]. Uronic acids were also identified as part of the EPS excreted by bacteria. Sand and Gehrke for example showed that iron(III) ions are complexed by uronic acids and accumulated in the EPS of an *Aciditiobacillus ferrooxidans* biofilm and thereby enhance leaching of iron [Sand and Gehrke 2006]. Furthermore, uronic acids were shown to serve as substrate for current production in microbial fuel cells [Catal et al. 2008].

Lipids are the last main group of substances found in the EPS. They are important in the surface conditioning and the initial biofilm formation on hydrophobic surfaces. Additionally, lipids are supposed to act as bio-surfactants in the biofilm [Davey et al. 2003]. More recent studies revealed that besides proteins *Shewanella oneidensis* nanowires are also composed of lipids, making them an important element for the EET in electroactive biofilms [Pirbadian et al. 2014]. However, lipids remain probably the least studied group of extracellular polymeric substances [Wikiel 2013].

Based on the different approaches of EPS investigation described, analysis of five main EPS group components (proteins, carbohydrates, lipids, uronic acids and eDNA) of anode respiring *G. sulfurreducens* was the main goal of this experimental series. To achieve this aim, a harvesting protocol was developed as well as a TB EPS extraction routine. Subsequently, *G. sulfurreducens* was cultivated under electroactive conditions in MFCs and the EPS was compared to cells grown heterotrophically without an electrode as terminal electron acceptor.

Cells grown under electrochemical conditions were compared with cells from a standard heterotrophic cultivation. Some EPS compounds responsible for both, the attachment to the electrode surface as well as those possibly involved in the electron transfer, are identified.

3.2 Materials and Methods

3.2.1 Microorganism

Geobacter sulfurreducens was ordered from the DSMZ (DSM-12127, Leibniz Institute DSMZ – German Collection of Microorganisms and Cell Cultures, Braunschweig, Germany) and cultivated under heterotrophic and anaerobic conditions.

3.2.1.1 Growth media

For growth curves and maintenance cultures *G. sulfurreducens* was grown on acetate as sole carbon and energy source according to the recommendation of the DSMZ. The acetate medium 826 by the DSMZ was prepared with the following contents: 10 mM sodium acetate; 28.04 mM NH_4Cl; 4.23 mM Na_2HPO_4; 1.34 mM KCl; 50 mM disodium fumarate; 29.76 mM $NaHCO_3$; 10 mL of trace element solution (with: 7.85 mM nitrilotriacetic acid; 12.17 mM $MgSO_4 \cdot 7\ H_2O$; 2.96 mM $MnSO_4 \cdot\cdot\ H_2O$; 17.11 mM NaCl; 359.70 µM $FeSO_4 \cdot 7\ H_2O$; 640.34 µM $CoSO_4 \cdot 7\ H_2O$; 421.92 µM $CaCl_2 \cdot 7\ H_2O$; 625.98 µM $ZnSO_4 \cdot 7\ H_2O$; 40.05 µM $CuSO_4 \cdot 5\ H_2O$; 42.16 µM $KAl(SO_4)_2 \cdot 12\ H_2O$; 161.73 µM H_3BO_3; 41.33 µM $NaMoO_4 \cdot 2\ H_2O$; 126.21 µM $NiCl_2 \cdot 6\ H_2O$; 1.14 µM $Na_2SeO_3 \cdot 5\ H_2O$; 1.21 µM $Na_2WO_4 \cdot 2\ H_2O$), 10 mL vitamin solution (with: 8.19 µM biotin; 4.53 µM folic acid; 59.11 µM pyridoxine-HCl; 14.82 µM thiamie-HCl $\cdot$ 2 H_2O; 13.28 µM riboflavin; 40.61 µM nicotinic acid; 20.98 µM D-Ca-pamtothenate; 0.06 µM vitamin B12; 36.46 µM p-aminobenzoic acid and 24.23 µM lipoic acid) and 1 mL selen-tungsten solution (12.5 mM NaOH; 11.41 µM $Na_2SeO_3 \cdot 5\ H_2O$ and 12.13 µM $Na_2WO_4 \cdot 2\ H_2O$). The medium was heated to 100 °C and constantly degassed with N_2/CO_2 gas mixture (80/20; v/v) with 20 mL min^{-1} during cooling to room temperature. $NaHCO_3$ was added when temperature was below 45 °C. 47.5 mL medium were filled in 250 mL septum flasks (Glasgerätebau Ochs, Bovenden, Germany) and sealed with a butyl septum and an aluminum cap. Gas atmosphere was adjusted by five consecutive steps of vacuum and refilling with N_2/CO_2 to a pressure of 1 bar. Oxygen free disodium fumarate was added as electron acceptor after autoclaving from a 1 M stock solution by sterile filtration through the butyl septum.

3.2.1.2 Heterotrophic cultivation of *G. sulfurreducens*

To prepare a fresh culture, 1 mL *G. sulfurreducens* was added with a sterile syringe and cannula from a maintenance culture, stored at 4 °C in the dark, to 49 mL medium in a septum flask to a final concentration of $5.2 \cdot 10^6$ cells mL^{-1}. Cells were incubated at 30 °C without shaking. For the production of growth curves, samples were taken periodically until stationary phase was reached. Cell growth was monitored via OD_{600} measurement. The development of both substrate and metabolite concentrations were measured with HPLC (Shimadzu, Kyōto, Japan; **Column**: Rezex-ROA, Phenomenex, California, USA; **Method**: 5 mM H_2SO_4, 0.6 mL min^{-1}, 30 °C, 25 min, wave length detector (λ = 190–210 nm)). As standards for HPLC calibration the following componenets were applied with the resulting calibration curves: sodium lactate in the range from 0–200 mM ($y = 1.643 * 10^{-5}x; R^2 = 0.999$), sodium actetate in the range from 0–200 mM ($y = 3.069 * 10^{-5}x; R^2 = 0.997$), sodium pyruvate in the range from 0–20 mM ($y = 8.699 * 10^{-7}x; R^2 = 0.999$), disodium fumarate in the range from 0–2 mM ($y = 3.446 * 10^{-8}x; R^2 = 0.999$) and disodium succinate in the range from 0–200 mM ($y = 1.357 * 10^{-5}x; R^2 = 0.995$). Finally, a correlation between OD_{600} and cell concentration was realized by cell countig with a Neubauer chamber.

To further employ *G. sulfurreducens* in electrochemical experiments, precultures were made in 1 L septum flasks containing 350 mL growth medium, prepared under the same conditions mentioned before. Cells were grown for 48 h to early stationary phase and harvested under anaerobic conditions by centrifugation at 4000 rmp and 30 °C for 15 min (Sigma 3K30, Sigma Aldrich, St. Louis, USA). Cells were then resuspended in anaerobic medium lacking disodium fumarate, since the electrode was used as an electron acceptor in this experiments.

3.2.2 Laboratory electrochemical H-cell

For the bioelectrochemical cultivation of *G. sulfurreducens*, a modified H-cell set up was developed. As described before [Reguera et al. 2006; Nevin et al. 2009; Krieg et al. 2014; Blanchet et al. 2015], two 100 mL glass bottles were connected via two flanges and separated by a circular proton exchange membrane (Nafion 117, Sigma Aldrich, St. Louis, USA) with an inner diameter of 2.6 cm to form an H-shaped reactor with a separated working electrode (WE) and counter electrode (CE) chamber. The CE chamber had three GL14 glass joints angled upright perpendicular to each other; the WE chamber had two

upright angled GL14 glass joints for the insertion of degassing cannula and sampling. Furthermore, the WE chamber was modified by the addition of a second flange with an inner diameter of 2.5 cm for the working electrode. The WE was pressed on the second flange from the outer side with a self-designed clamp system constructed by the DECHEMA work shop and sealed with a 1 mm thick circular silicon mat as can be seen in Figure 9 B.

Figure 9: Photographs of the bipolar plate counter electrode (A) and the dismounted working electrode chamber of a H-cell (B).

With an inner diameter of 2.5 cm of the flange, the resulting geometrical WE surface was 4.9 cm^2. Electrical contact to the WE was achieved by a spring wire from the outer side of the reactor. As material for the working electrode a bipolar plate (Eisenhuth GmbH & Co. KG, Osterode am Harz, Germany) was chosen. The graphite based electrode material was delivered in 200 · 300 · 5 mm (width · length · thickness) and cut to pieces of 30 · 30 mm. Prior to each experiment the electrode surface was rubbed down with SiC-paper (FEPA grain size 500, Stuers GmbH, Kernen im Remstal, Germany) to maintain a fresh electrode surface and same conditions for all experiments. As counter electrode also a bipolar plate was taken. The geometry can be seen in Figure 9 A, with a geometrical surface of 13.2 cm^2 of the electrode immersed in the electrolyte. The CE surface was roughened with SiC-paper (FEPA grain size 120). The CE was implemented with the upper rod-like part of the electrode in the silicon mat of the CE chamber lid. A magnetic stirring bar was placed into both electrode chambers. An image of a completely mounted H-cell can be seen in Figure 10.

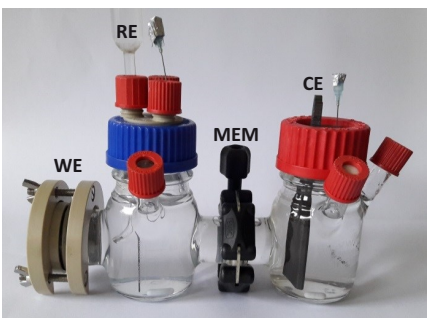

Figure 10: Photograph of a mounted glass H-cell with the clamped working electrode (WE, bipolar plate), Haber-Luggin capillary for reference electrode insertion (RE; Ag/AgCl), separation of the WE and CE chamber by a Nafion membrane (MEM) and the counter electrode (CE, bipolar plate).

Prior to each experiment the assembled H-cells were filled with water to avoid desiccation of the membrane and sterilized by autoclaving. To start an experiment the water was replaced by growth media, 110 mL in the CE and 120 mL in the WE chamber. Finally, for constant potential control a reference electrode was added to the system. Therefore a Haber-Luggin capillary filled with KCl_{sat} was sterilized with 70 % ethanol (v/v) and inserted through one of the ports in the lid of the WE chamber under a clean bench. The Ag/AgCl reference electrode was placed in the Haber-Luggin capillary after connecting the reactor system to a potentiostat.

3.2.3 Electrochemical cultivation of *G. sulfurreducens*

Electrochemical cultivation of *G. sulfurreducens* was done in MFC mode, polarizing the WE as anode.

H-cells were assembled as described in the previous chapter and filled with medium 826 without disodium fumarate, since in the set-up as MFC the WE served as terminal electron acceptor. The whole set-up was put under an incubation hood (TH 30, Edmund Bühler GmbH, Hechingen, Germany) set to 30 °C. H-cells were placed on two magnetic stirrers, one for the WE and one for the CE chamber, respectively. The electrochemical cells were connected to a multi potentiostat (IPS Elektronik GmbH & Co KG, Münster, Germany) in the following way: the bipolar plate pressed from the outer side of the WE chamber was connected as working electrode. The second bipolar plate implemented in the lid of the CE chamber was set as counter electrode and the Ag/AgCl RE placed in the Haber-Luggin capillary in the WE chamber was set as reference electrode.

Prior to anodic polarization, the open circuit potential (OCP) of the WE was monitored for 3 h. OCP indicated equilibration of the carbonate buffer of the medium depending on the CO_2 partial pressure and anaerobic conditions. After starting the OCP monitoring, gas tubings were connected to the degassing cannula of the WE over a 0.22 µm pore size PVDF syringe filter to maintain sterile conditions. N_2/CO_2 (80/20 v/v) gas flow was set 30 mL min^{-1} with a rotameter and kept constant throughout the whole experiment. The three GL14 lids of the CE chamber were opened but not completely removed to allow oxygen diffusion into the headspace of the CE chamber for the oxygen reduction at the cathode without increased contamination risk by airborne germs.

When the OCP was constant at a value of around +400 mV vs. Ag/AgCl, the WE was polarized anodically to +400 mV vs. Ag/AgCl. *G. sulfurreducens* cells were harvested in stationary phase, washed as described before and added 30 min after starting the polarization to reach an OD_{600} of 0.1 corresponding to $5 \cdot 10^7$ cells mL^{-1}. MFC mode was run for 8 d before EPS harvesting and extraction was continued. H-cells were always run in triplicates, current density was referred to the geometrical WE surface (4.9 cm^2).

3.2.4 Evaluation of the extraction reagent for EPS

Several methods for the extraction of the tightly bound EPS of microorganisms have been described in literature [Wingender et al. 1999]. Depending on the type of extraction and the corresponding extraction reagents (ER), the amounts of extracted EPS as well as the concentrations of different groups of EPS compounds might vary [Liu and Fang 2002; Takahashi et al. 2009]. However, despite the highest extraction, the lysis of cells during the extraction procedure is a crucial factor for the selection of the ER [Wikiel 2013], since a high lysis of cells would lead to a false positive concentration of eDNA in the TB EPS fraction. Due to this, cell lysis was chosen as selection parameter for the evaluation of the TB EPS extraction reagents.

Percentages of lysed cells caused by the respective extraction reagents were determined via the total protein content in the extraction supernatant. Therefore, different amounts of cells were lysed and the total protein concentration in the supernatant was measured via colorimetry, resulting in a correlation between total protein concentration and cells. From this assumption, the calculated total protein content of the cells employed for the ER evaluation was then representing 100 % cell lysis. The relation between this value and the measured protein concentration in the supernatant after the TB EPS extraction procedure is consequently the percentage of lysed cells caused by the respective extraction method. Extraction of proteins from the EPS by during reagent evaluation was neglected.

3.2.4.1 Total protein concentration – bicinchoninic acid assay

Cell lysis was evaluated via total protein concentration in the supernatant with a BCA protein assay (Pierce BCA Assay Kit 23225/23227, Thermo Fisher Scientific, Waltham, USA). Based on the reduction of Cu^{2+} ions in alkaline solution by the presence of proteins to Cu^{+} and their

subsequent complexation by bicinchoninic acid (BCA), the adsorption of this complex was measured at a wave length of 562 nm. Bovine serum albinum (BSA) served as standard for the total protein concentration in a range from 0–250 mg L^{-1} ($y = 0.0017x + 0.1628$; $R^2 = 0.999$). Briefly, reagent A (alkaline buffered solution) and reagent B (cupric sulfate solution) of the BCA assay kit were externally combined in a ratio of 50:1, added to 25 µL BSA standard or sample in a 96 well microtiter plate to reach 225 µL and mixed with a pipette. The reaction mixture was then incubated for 30 min at 37 °C in the dark before the adsorption at 562 nm was measured with a Tecan infinite M200 microtiter plate reader (Tecan, Männedorf, Switzerland).

3.2.4.2 Correlation of total protein concentration and OD_{600}

To correlate the total protein concentration to the concentration of cells, a range of cell concentrations was lysed and the total protein concentration in the supernatant was measured. Pulsed cell disruption with ultra sound (US) was chosen as method for mechanical cell lysis. In a first step, the duration of US pulsation for maximal cell lysis was examined. *G. sulfurreducens* was grown to stationary phase and washed with sterile PBS. Aliquots of 2 mL with an OD_{600} of 0.5 ($3 \cdot 10^8$ cells mL^{-1}) were filled in Falcon tubes (15 mL) and stored on ice. Each Falcon tube containing cells was placed under the US finger (Sonifier W-250 D, Heinemann Ultraschall und Labotechnik, Schwäbisch Gmünd, Germany) and the finger was immersed 1.5 cm into the cell suspension without touching the wall of the Falcon tube. An ice bath was installed around the set-up to avoid protein degradation due to temperature increase during US treatment. Pulsed US disruption was applied in time intervals of 1 s followed by 2 s relaxation according to a personally communicated protocol. Total US-time was accumulated from the time intervals of US application. As time intervals 0, 5, 30, 60, 90 and 120 s were tested and 120 s US-time were selected for further experiments based on these results. The disrupted cell fragments were separated by centrifugation at 4000 g and 4 °C for 10 min and the total protein concentration in the supernatant was quantified in triplicates with the BCA assay described before. Total protein concentration in dependence on the employed biomass was subsequently determined by 120 s of the described US disruption process of 2 mL cell suspension in PBS with OD_{600} of 0, 0.06, 0.12, 0.19, 0.26, 0.51, corresponding to cell concentrations of 0, $3 \cdot 10^7$, $6 \cdot 10^7$, $9 \cdot 10^7$, $1 \cdot 10^8$, $3 \cdot 10^8$ cells mL^{-1},

respectively. Again, total protein concentration was measured from the supernatant and correlated to the previously measured BSA standards.

3.2.4.3 Extraction reagent evaluation

As possible extraction reagents ethylene diamine tetra acetic acid (EDTA) [Liu and Fang 2002], 18-crown-6 ether (CW) [Wikiel 2013] and DOWEX® (DOW) [Takahashi et al. 2009] were examined with the focus on cell lysis during extraction procedure. The extraction routine was modified from [Wikiel 2013] and is also graphically displayed in Figure 11. As described before, *G. sulfurreducens* was grown to stationary phase with an OD_{600} of 0.52 ($3 \cdot 10^7$ cells mL^{-1}) and three aliquots of 30 mL per extraction reagent plus three aliquots of the negative control were washed and resuspended in PBS (5 mL). Subsequently, the ER were added: EDTA: 5 mL of 40 mM EDTA in PBS were added resulting in 20 mM EDTA for the extraction. CW: 5 mL of 60 mM CW in PBS resulted in 30 mM extraction concentration. DOW: 2.5 g DOW (DOWEX® Marathon™ C Na^+-form, 20 – 30 mesh, Sigma Aldrich, St. Louis, USA) and further 5 mL PBS were filled in. As negative control only PBS as ER was employed. As positive controls BSA was added to a final concentration of 125 µg mL^{-1} to the respective ERs and PBS as negative control.

Extractions were run for 6 h under gentle shaking at 80 rpm on a rotating shaker (IKA KS 130 Basic, 4 mm rotation deviation, IKA Werke Staufen, Germany) at 4 °C. After centrifugation, total protein concentration in the supernatant was measured and related to the calculated protein concentration as 100 % cell lysis.

3.2.5 EPS harvest and extraction

Due to the relatively small electrode surface and the consequently small mass of biofilm on the electrode surface, three electrochemical cultivations were run in parallel. Both, biofilms and supernatant of the WE-chamber of the three parallel cultivations, were then combined to one sample each at the end of experiments. This was done to gain EPS concentrations higher than the low detection limits of the biochemical analysis. The harvesting and EPS extraction routine followed the following procedure and can also be seen in the graphical

abstract (Figure 11). The EPS extraction routine was modified from Wikiel [Wikiel 2013] leading to a nine step process:

1: After electrochemical cultivation,

2: the graphite based working electrode was disassembled from the H-cell and remaining liquid on the electrode surface was removed with a pipette. Physical contact between the biofilm and the pipette was avoided.

3: Initially, the soluble EPS was processed. The remaining medium in the WE chamber was separated from planktonic cells by filtration through a 0.22 µm pore size PVDF syringe filter. To reduce the total volume of 350 mL of the soluble EPS sample, aliquots of 50 mL were placed in a drying oven at 50 °C for 40 h until the total volume was reduced to 50 mL.

4: The biofilm was then scratched off the electrode with a cell scraper (TPP, Trasadingen, Switzerland), transferred to a 50 mL Falcon tube and gently resuspended in 20 mL sterile PBS (136.89 mM NaCl; 2.68 mM KCl; 10 mM $Na_2HPO_4 \cdot 2\ H_2O$; 1.98 mM KH_2PO_4). Scratching off with the cell scraper and subsequent taking up in PBS was repeated several times on the electrode surface.

5: The next step was the extraction of the loosely bound EPS from the resolved biofilm. LB EPS extraction was done by centrifugation of the resuspended biofilm with 9400 g at 4 °C for 15 min. The Supernatant was separated from the cells and stored as LB EPS for further processing.

6: The TB EPS were extracted from the remaining cell pellet. Therefore, the cell pellet was gently resuspended in 20 mL PBS with a pipette and 2.5 g DOW were added. The extraction was executed for 6 h at 4 °C under constant shaking at 80 rpm on a rotating shaker. The supernatant was then separated and the remaining DOW beads were washed trice with 5 mL PBS. Remaining cells were finally separated from the TB EPS by centrifugation at 9400 g at 4 °C for 15 min. The supernatant was stored as TB EPS.

7: To remove residual media components and metabolites of cultivation from the respective EPS fractions a dialysis step was performed. Extracted EPS fractions were filled in Spectra/Por® dialysis tubing (Spectrum laboratories, Los Angeles, USA) with a 3.5 kDa cut off. Dialysis was run for 72 h against 5 L deionized water at 4 °C and the water was changed at least two times per day.

8: Subsequently, samples were dried at 55 °C in a drying cabinet and stored at -20 °C until biochemical analysis was conducted (**9**).

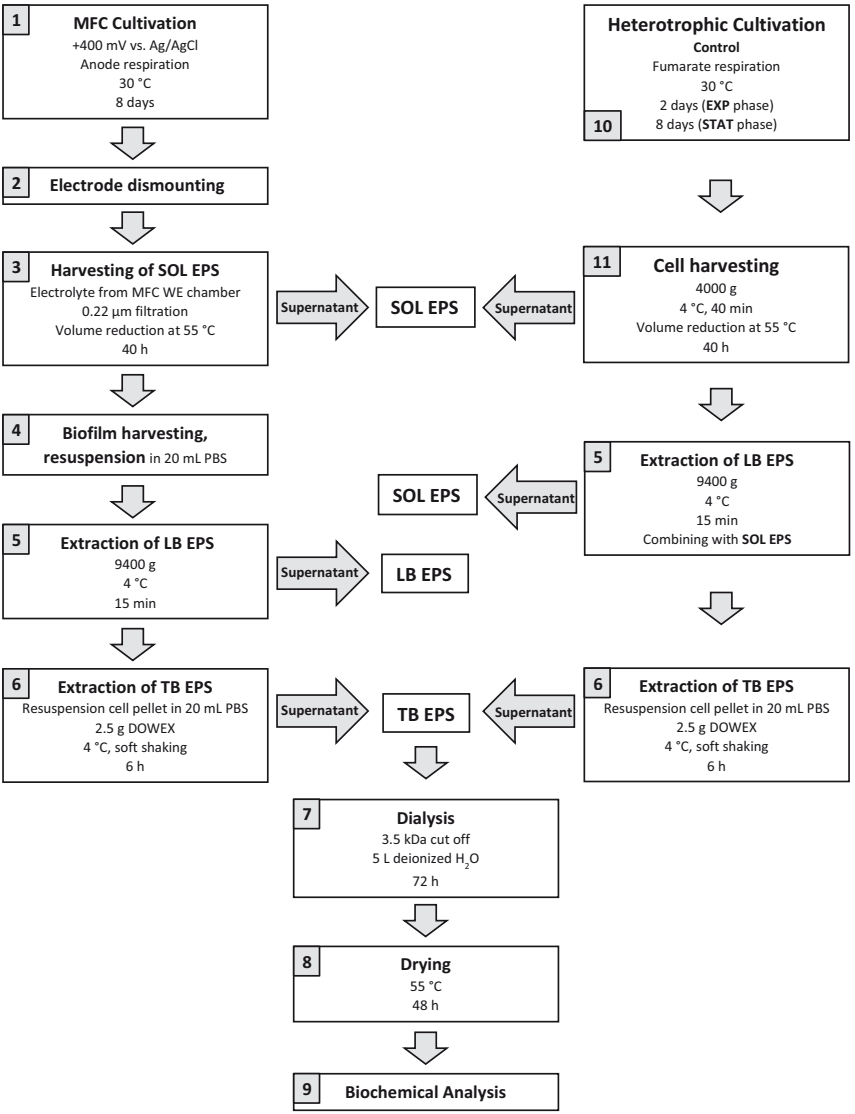

Figure 11: Schematic route of the biofilm harvest and EPS fractionation of *G. sulfurreducens* for MFC grown anode respiring cells (left) and heterotrophically grown fumarate respiring cells. Fractionation in soluble (SOL EPS), loosely bound (LB EPS) and tightly bound EPS (TB EPS).

3.2.6 EPS harvest of heterotrophically cultivated *G. sulfurreducens* (controls)

Besides the EPS of anode-respiring cells cultivated in a MFC, as control heterotrophically-grown *G. sulfurreducens* cells respiring on fumarate were analyzed for their EPS composition. Therefore, cells grown to exponential phase (EXP) for 2 d as well as grown to stationary (STAT) phase for 8 d were harvested. Cultivation conditions were the same as already described (section 3.2.1.2). Schematically, the EPS harvesting can be seen in Figure 11, which was the same as for the MFC-grown cells, if not stated otherwise. Initially, heterotrophically grown cells (**10**) were separated from the culture broth containing the SOL EPS via centrifugation at 4000 g for 40 min at 4 °C (**11**). LB EPS was then harvested from the remaining cell pellet as described for the MFC grown cells. It was assumed that by harvesting *G. sulfurreducens* from liquid culture via centrifugation at 4000 g for 40 min the LB EPS was already partly detached from the cells and combined with the SOL EPS. Consequently, LB EPS harvested at 9400 g (**5**) was merged with the SOL EPS, resulting in the analysis of TB and SOL EPS fractions only for the contdrols. TB EPS was finally extracted from the remaining cell pellets similar to the MFC grown cells (**6**), as well as further dialysis (**7**) and drying (**8**). Both controls, exponential and stationary phase were grown in duplicate.

3.2.7 Biofilm staining and electrode imaging after harvesting

To qualitatively evaluate biofilm harvesting from the electrode surface with a cell scraper, both Epifluorescence Microscopy (EFM) and Scanning Electron Microscopy (SEM) images were made from a biofilm attached to a WE. Therefore, *G. sulfurreducens* was grown on a bipolar plate WE as described in section 3.2.3. After dismounting the WE half of the biofilm was scratched off the electrode whereas the other half remained on the surface. After three washing steps with PBS samples were dried in a desiccator and either used for SEM or stained for EFM imaging.

3.2.7.1 Fluorescence staining and epifluorescence microscopy imaging

Epifluorescence microscopy was performed to differentiate between cells and EPS in the biofilm. Biofilms were stained with a mixture of 4'.6-Diamidino-2-phenylindole dihydrochloride (DAPI) for the sessile cells and a TRITC labelled Concanavalin A (ConA) for

the EPS. Working concentrations were 1 µg mL^{-1} and 100 µg mL^{-1} in PBS respectively. Half of the biofilm was scratched off before samples were incubated for 20 min at room temperature in the dark. Subsequently, excessive staining solution was removed by three gentle washing steps with PBS with a pipette.

Imaging was done with an upright EFM (Axio imager Z1m, Carl Zeiss, Oberkochen, Germany) equipped with a camera (AxioCam MRc5), mercury vapor lamp (HBO 100), DAPI, FITC and TRITC filters and air (50, 200 and 400-fold) or oil immersion (100-fold) objectives. Images were processed with Axiovison Rel. 4.6 software.

3.2.7.2 Scanning electron microscopy imaging

The scanning electron microscope was employed to image the graphite based roughened electrode surface of a fresh WE and of an intact biofilm as well as the edge of a partially harvested biofilm. The microscope was a Philips XL 40 with a Tungsten cathode (Philips, Amsterdam, Netherlands). Spot size, applied voltage, type of detector, and magnification can be found in the corresponding SEM images. For sample preparation, the electrode was dismounted from the H-cell reactor, half of the biofilm was scratched off and the surface was gently rinsed with deionized water with a pipette to remove salts and media components interfering with SEM imaging.

3.2.8 Biochemical EPS analysis

For biochemical EPS analysis, samples were dissolved in 2 mL nuclease free and sterile H_2O. Determinations were conducted in 96 well microtiter plates and a Tecan microtiter plate reader. Methods were partially adapted from Wikiel [Wikiel 2013] and modified according to personal communication (Biofilm centre, University Duisburg-Essen, Germany). Concentrations of the EPS compounds were referred to single cells. Therefore, *G. sulfurreducens* was cultivated electro-chemically in a H-cell in duplicate. Biofilms were harvested as described before (section 3.2.5) and resuspended in 30 mL PBS with a vortexer. Total amount of cells was determined by cell counting with a Neubauer chamber. For the controls, OD_{600} of the heterotrophically grown cultures in EXP and STAT phase was used to determine the total amount of cells. Standard deviations of the respective EPS components were calculated from the three biologically independent replicates.

3.2.8.1 Protein determination

Protein concentration was determined with a BCA assay as already described in section 3.2.4.1.

3.2.8.2 Carbohydrate determination

Concentration of carbohydrates was measured according to Dubois [Dubois et al. 1956]. Briefly, carbohydrates get oxidized initially by sulfuric acid under the separation of water and subsequently react with phenol characterized by a color change. Therefore, 20 µL sample or standard were mixed with 220 µL concentrated H_2SO_4 and 40 µL of 5 % (v/v) phenol and incubated at 30 °C for 10 min in an electric heating block (ThermoMixer, Eppendorf, Hamburg, Germany) under a fume hood. Light absorption was then measured at wavelengths of 485 and 570 nm. Glucose was used as standard with concentrations from 0–100 mg L^{-1} ($y = 0.0022x + 0.0113$; $R^2 = 0.999$).

3.2.8.3 Uronic acid determination

According to Blumenkrantz and Asboe-Hansen uronic acids were determined using $Na_2B_4O_7$ and ß-hydroxydiphenyl [Blumenkrantz and Asboe-Hansen 1973]. Briefly, uronic acids get oxidized by heating to 100 °C in a sulfuric acid/tetraborate mixture and subsequently react with ß-hydroxydiphenyl to form a chromogen. The method is based on the appearance of a chromogen, if a Glucuronic acid was used as standard ranging from 0–100 mg L^{-1} ($y = 0.0013x + 0.0003$; $R^2 = 0.99$). 35 µL sample or standard were mixed with 315 µL of 0.0125 M $Na_2B_4O_7$ in concentrated H_2SO_4 on ice. After heating to 100 °C (electric heating block) for 5 min and quickly cooling down on ice again, background absorbance of 200 µL was measured at 520 nm in a microtiter plate. Subsequently, 4.5 µL of 0.15 % (w/v) ß-hydroxydiphenyl in 0.5 % (v/v) NaOH were added and incubated for 5 min at room temperature. Again, absorbance at 520 nm was measured and the background was subtracted.

3.2.8.4 Lipid determination

Lipids were initially extracted with a chloroform/methanol mixture from the water phase of the dissolved EPS and then analyzed by colorimetry with vanillin according to van Handel [Van Handel 1985]. Briefly, lipids get oxidized by sulfuric acid and a color change can be observed after the reaction with vanillin. To 175 µL sample or standard, 300 µL chloroform-methanol solution (2:1 v/v) were added and mixed well. After 5 min of incubation, phase separation of the lipid containing chloroform phase (lower phase) from the methanol - water phase (upper phase) was accelerated by centrifugation (3 min at 12000 rpm). 70 µL of the lower phase were carefully transferred to a 2 mL reaction tube with a pipette and the chloroform was evaporated at 95 °C in an electric heating block under a fume hood. Then, 100 µL concentrated H_2SO_4 were added and the background absorbance was measured at 525 nm in a microtiter plate. Finally, 900 µL vanillin phosphoric acid mixture (1.5 mg mL^{-1} vanillin in 17 % (w/v) H_3PO_4) were added to 100 µL sample or standard and again absorbance was measured at 525 nm in microtiter plates and the background values were subtracted. Olive oil was used as standard in a range from 0–50 mg mL^{-1} ($y = 0.0012x + 0.078$; $R^2 = 0.994$).

3.2.8.5 eDNA determination

As last parameter, eDNA was determined according to the PICOGREEN® dsDNA assay (Invitrogen, California, USA). Working principle of the assay is based on the quantitative binding of a fluorescence labelled probe to the DNA structure. Initially, an aqueous working solution of PicoGreen Reagent (1:200 v/v) was prepared from 10 mM Tris-HCl and 1 mM EDTA (TE) with a pH value of 7.5. Due to the possibility of photodegradation the working solution was protected from light. 100 µL sample or standard were combined with 100 µL working solution and incubated for 2–5 min at room temperature in the dark. Sample fluorescence was measured at excitation and emission wavelengths of 480 and 520 nm, respectively. DsDNA in TE buffer was applied as standard in a range from 0–2 mg L^{-1} ($y = 22544x + 653$; $R^2 = 0.999$).

3.3 Results

3.3.1 Growth curves for heterotrophic *G. sulfurreducens* cultivation

To initially characterize the growth of *G. sulfurreducens* under standard heterotrophic cultivation conditions, cultures were observed over approximately 55 h until stationary phase was reached. The optical density at 600 nm, pH and substrate consumption is displayed over time in Figure 12. Furthermore, concentrations of fumarate, succinate and pyruvate were monitored as indicators for microbial growth (Figure 13). Correlation between the cell concentration via total cell count and the optical density ($y = 4.962 * 10^8 x$; $R^2 = 0.999$) can be found in Figure 14.

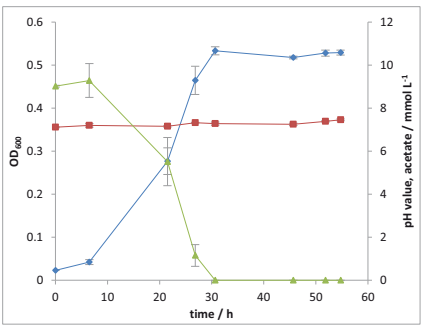

Figure 12: Growth curve for *G. sulfurreducens* under standard heterotrophic cultivation (minimal medium + acetate; electron acceptor: fumarate; 30 °C, anaerob). Left y-axis: OD_{600} (—◆—); right y-axis pH (—■—) and acetate (—▲—, in mmol L^{-1}). Mean values of three biologically independent cultures are given with standard deviations presented in grey error bars.

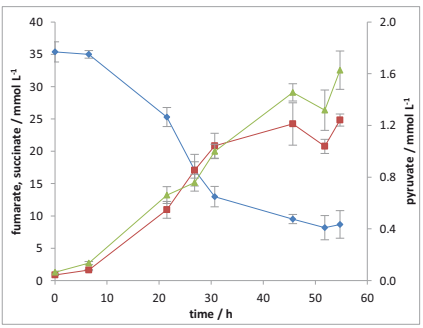

Figure 13: Metabolite concentrations by *G. sulfurreducens* under standard heterotrophic cultivation (minimal medium + acetate; electron acceptor: fumarate; 30 °C, anaerob). Left y-axis: fumarate (—◆—) and succinate (—■— in mmol L^{-1}), right y-axis: pyruvate (—▲—, in mmol L^{-1}). Mean values of three biologically independent cultures are given with standard deviations presented in grey error bars.

As can be seen in Figure 12, growth was characterized by a very short lag phase. Cell multiplication was already observed after 6.5 h with an OD_{600} of 0.05 ($2 \cdot 10^7$ cells mL^{-1}). After 21.5 h the culture was in the middle of the exponential phase at an OD_{600} of 0.32 ($1 \cdot 10^8$ cells mL^{-1}). The stationary phase was reached after 30 h and after a small decrease the cell concentration remained constant around at an OD_{600} of 0.52 ($3 \cdot 10^8$ cells mL^{-1}). The pH remained around 7.5 in the carbonate buffered system, whereas the acetate

concentration in the medium followed a course opposite to the cell concentration. A substrate depletion was reached after 30 h. Analogous to the acetate concentration the fumarate concentration (Figure 13) also decreased during the experiment (from 35.4 to 8.7 mmol L^{-1}), since it served as electron acceptor for cell respiration and gets thereby reduced to succinate. Accordingly, the succinate concentration increased during the experiment in the same molar range as fumarate decreased (from 0.8 to 24.8 mmol L^{-1}). A small increase of pyruvate as a metabolic side product to a maximum concentration of 1.2 mmol L^{-1} during cultivation was also detected.

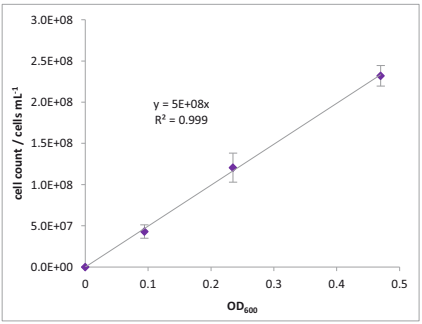

Figure 14: Correlation between the total cell count of heterotrophically cultivated *G. sulfurreducens* (minimal medium + acetate; electron acceptor: fumarate; 30 °C, anaerob) and the optical density (OD_{600}). Given are mean values of three biologically independent cultivations counted with a Neubauer-chamber. Standard deviations are presented in grey error bars.

3.3.2 Electrochemical cultivation

G. sulfurreducens was grown under electrochemical conditions in a microbial fuel cell to maintain electroactive and anode respiring biofilms. EPS fractionating in TB, LB and SOL EPS and biochemical analysis for typical sum parameters were the following steps. Therefore, always three H-cells were run in parallel and biofilms were harvested and combined after approximately 8 d.

Initial to the inoculation of *G. sulfurreducens* cells to the MFC, the medium in the WE chamber was degassed with N_2/CO_2 and the OCP was monitored, as can be seen in Figure 15. Under aerobic conditions and an unsaturated carbonate buffer system, the OCP started around 130 mV versus Ag/AgCl. Directly after starting degassing the OCP increased and reached a plateau at 400 mV after approximately 2 h, indicating a saturated carbonate buffered system and stabilization of the pH around 7.5. Thereby, reaching the plateau was depending on the N_2/CO_2 gas flow, reaching 400 mV fast with high volume flow (data not shown).

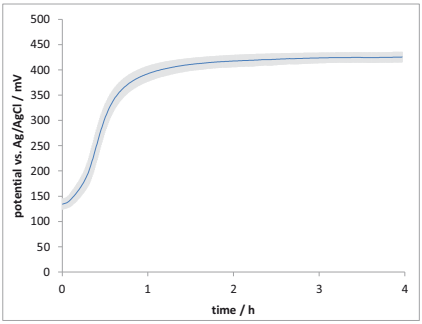

Figure 15: Open circuit potential development of the bipolar plate working electrode during N_2/CO_2 degassing (30 mL min^{-1}) prior to *G. sulfurreducens* inoculation (acetate minimal medium, no fumarate, 30 °C). Mean OCP versus a saturated Ag/AgCl reference electrode of three independent MFC is presented with standard deviations given in grey.

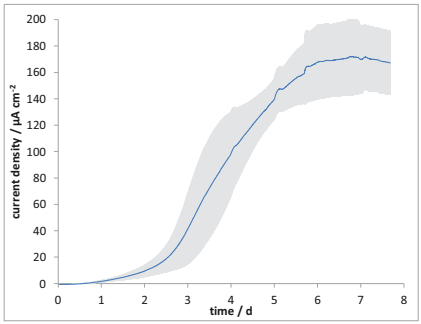

Figure 16: Mean current density curve for 9 biologically independent cultivations of *G. sulfurreducens* in H-cell microbial fuel cells (minimal medium + acetate; electron acceptor: anode; 30 °C; anaerob). Current density is referred to geometrical WE surface (4.9 cm^2). Standard deviations are given in grey.

The WE was then polarized to 400 mV vs. Ag/AgCl and *G. sulfurreducens* cells were added at $5 \cdot 10^7$ cells mL^{-1}. Directly after cell addition a current increase was observed (Figure 16). Comparable to the number of cells in the growth curves under heterotrophic conditions, development of the current can be described also by a lag phase (day 0–day 1), an exponential phase (day 1–day 6) and a stationary phase (day 6–day 8). The maximum current density was reached after approximately 7 d at a value of 172 ± 29 µA cm^{-2} (referred to geometrical WE surface of 4.9 cm^2). A small additional current decrease was observed prior to the end of the electrochemical cultivation.

3.3.3 Biofilm harvesting and EPS extraction

After electrochemical cultivation of *G. sulfurreducens*, biofilm harvest (i), EPS fractionation (ii) and biochemical EPS analysis (iii) were the subsequent steps towards the EPS characterization of *G. sulfurreducens* biofilms under electrochemical conditions.

Preliminary to the actual biofilm harvest and fractionation into the individual EPS groups (SOL, LB and TB EPS), the selection of the EPS extraction reagents and routine was conducted.

3.3.3.1 Evaluation of the EPS extraction reagent

As mentioned in section 3.1.3, a variety of (TB) EPS extraction reagents and methods can be found in literature depending on the EPS producing organism and the EPS compound of interest. Since the influence of the EPS extraction on membrane integrity was chosen as selection parameter for an EPS extraction reagent in this study, cell lysis during the extraction with EDTA, CW and DOW was tested. The protein content was therefore related to the cell count via cell lysis experiments and colorimetric protein determination. Cell lysis during EPS extraction was then evaluated by the protein concentration in the extraction supernatant and referred to the total protein concentration of the used amount of cells.

3.3.3.1.1 Total protein concentration and cell lysis

To determine the total protein content of a given cell concentration, cells were disrupted with US and the protein content in the supernatant was measured with the BCA assay. Different time intervals of US treatment were tested and the total protein concentration in the supernatant was analyzed to indicate cell lysis (Figure 17). As can be seen, without US treatment, the protein concentration was around 0. Total protein concentration in the supernatant increased with increasing US treatment up to a time of 90 s (135 ± 5.5 µg mL^{-1}) and reached a plateau at 129 ± 2.3 µg mL^{-1} after 120 s applied US. In further experiments, 120 s of US treatment were chosen to achieve maximum cell lysis.

By testing the disruption of different cell concentrations and the subsequent determination of the total protein concentration in the supernatant, the amount of proteins was correlated to the cell concentrations at 100 % cell lysis. Figure 18 illustrates protein concentration in dependence of the amount of lysed cells and gives $y = 207.18x - 0.2937$ ($R^2 = 0.999$) as correlation.

Based on the values for total cell disruption, lysis caused by the different extraction reagents was calculated in the next step and the reagent causing the lowest membrane damage was chosen for further EPS fractionation.

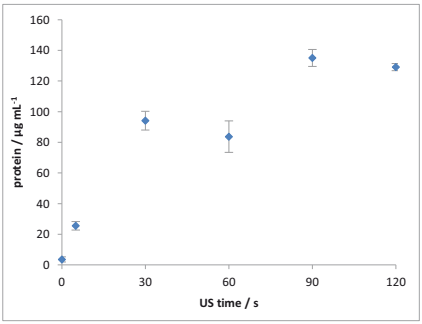

Figure 17: Protein concentrations in the supernatant indicating cell lysis caused by ultra sound (US) treatment. Mean values for three biologically independent experiments are presented over increasing ultra sound (US) treatment, applied in intervals of 1 s. Cells were heterotrophically cultivated (minimal medium + acetate; electron acceptor: fumarate; 30 °C, anaerob) Standard deviations are implemented with grey error bars.

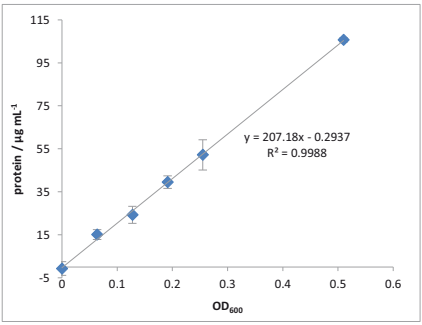

Figure 18: Protein concentrations in the supernatant for cell densities (OD_{600}) from 0 to 0.5 after disruption with ultra sound for 120 s. Presented values are mean values from three independent and heterotrophically grown *G. sulfurreducens* cells (minimal medium + acetate; electron acceptor: fumarate; 30 °C, anaerob) Standard deviations are given with grey error bars.

3.3.3.1.2 Extraction reagent evaluation

As final step of the extraction reagent evaluation *G. sulfurreducens* cells were used to test membrane damage and consequent protein release during the extraction procedure.

Therefore, *G. sulfurreducens* cells were incubated with EDTA, CW and DOW as ER and PBS as control. Additionally and as positive control for the BCA assay validation, 125 µg mL^{-1} BSA standards were run in parallel with the three ER and PBS, as well as negative controls with only PBS and the ER. Results of the positive (+) controls of extraction routine (Figure 19) indicate good BSA recovery rates for CW (117.0 ± 2.6 µg mL^{-1}), DOW (124.0 ± 9.9 µg mL^{-1}) and PBS (118.3 ± 4.5 µg mL^{-1}) of 94, 99 and 94 %, respectively. However, the positive EDTA control produced a negative BSA concentration (-2.1 ± 3.6 µg mL^{-1}) indicating that the BCA assay was affected by EDTA. Similar to this, the negative control without the BSA standard and EDTA as ER gave a negative BSA concentration (-18.4 ± 3.9 µg mL^{-1}). The negative control of CW gave a false positive result with 20.9 ± 1.7 µg mL^{-1}, whereas both DOW and PBS negative controls showed neglect able effects on the BCA assay with 3.5 ± 2.2 and -3.9 ± 4.1 µg mL^{-1}.

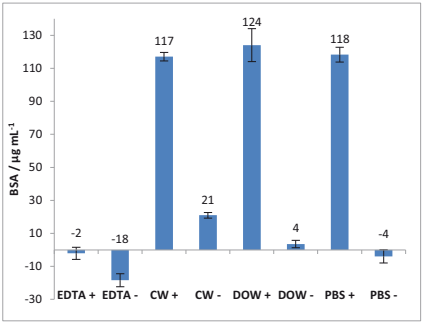

Figure 19: Positive (+) and negative (-) controls of the three different extraction reagents EDTA, CW and DOW and PBS of the BCA assay. 125 µg mL^{-1} BSA were applied as positive control. Calculated BSA values are given above the respective bars, standard deviations implemented with black error bars.

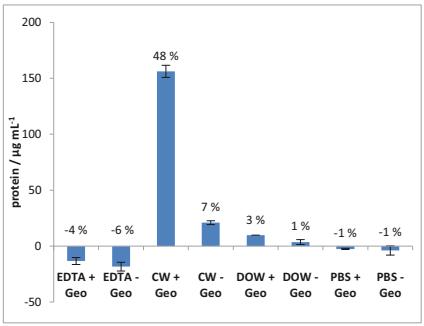

Figure 20: Total protein concentration in the supernatants after extraction of *G. sulfurreducens* cells (+ Geo) with the three different extraction reagents EDTA, CW and DOW and PBS. Extractions without *G. sulfurreducens* cells (- Geo) were run as controls. Calculated cell lysis is given as percentage values above the respective bars, standard deviations implemented with black error bars.

Analysis of the extraction supernatants (Figure 20) show that CW caused the highest cell lysis with 48 % (156 ± 5.3 µg mL^{-1}), which correlated with a light brown coloring of the supernatant after centrifugation. EDTA gave a negative cell lysis of -4 % (-13.4 ± 3.2 µg mL^{-1}) also combined with a color change of the supernatant to light brown. The lowest cell lysis was observed with DOW at 3 % (9.8 ± 0.05 µg mL^{-1}) correlating with no visible color change of the supernatant after extraction.

The control without ER and only PBS gave a slightly negative cell lysis of -0.8 ± 0.2 % (-2.6 ± 0.5 µg mL^{-1} BSA) and also no color change was observed.

In general, it has to be stated that the BCA assay was characterized by an uncertainty concerning the functionality of the assay in combination with the ER. EDTA produced false negative results, whereas CW gave false positive BSA values in the controls. However, the extraction with DOW gave the lowest cell lysis combined with a good recovery of the BSA standard, a low value for the negative control and no color change of the supernatant after extraction.

Consequently, DOW was chosen as extraction reagent for the tightly bound EPS in biofilm fractionation, taking the observed cell lysis into account for the interpretation of TB EPS values.

3.3.3.2 Biofilm harvest and subsequent imaging

The procedure of harvesting of the electrochemically cultivated biofilm from the dismounted anode is displayed by the series of images in Figure 21. As can be clearly seen, scratching off the biofilm with a cell scraper resulted in a complete removal of the visible part of the attached cells from the surface.

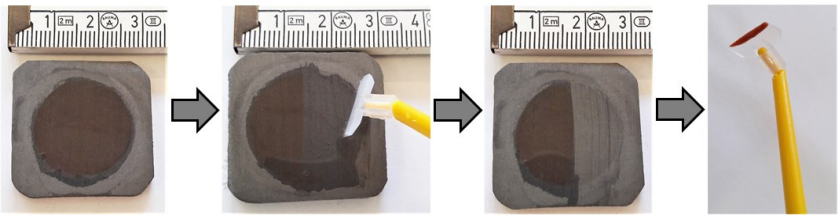

Figure 21: Series of images of the harvesting procedure of the electroactive biofilm from the bipolar plate working electrode with a cell scraper. Biofilm cultivation in a membrane separated H-cell under (minimal medium + acetate; electron acceptor: anode; 30 °C; anaerob).

Both, EFM and SEM imaging were performed to qualitatively evaluate biofilm harvest from the electrode surface by scratching of the attached biomass with a cell scraper. In this experiments, only half of the biofilm was scratched off to visualize both, intact biofilm and electrode surface after harvest. Subsequently, either a staining step for EFM imaging was performed or the electrode was dried in a desiccator for SEM imaging.

3.3.3.2.1 Fluorescence staining and EFM imaging of anode respiring biofilm

Electrode samples were stained with both DAPI and ConA (TRITC-labelled) to visualize DNA and EPS, respectively. By the simultaneous combination of the two fluorescent dyes, scratching off of *G. sulfurreducens* cells and remaining EPS on the electrode surface after biofilm harvesting could be visualized. EFM images with different magnification from both DAPI and TRITC channel can be found in Figure 22. As can be seen in all images, fluorescent staining with DAPI and TRITC-labelled ConA was successful. Pictures indicate that electrochemically cultivated *G. sulfurreducens* formed a homogenous biofilm covering the electrode surface (left half of each image), as it was also observed optically after dismounting the electrode from the H-cell set up. In general, DAPI and ConA signals are very

strong at the intact biofilm and very low or not present on the electrode after harvest. Images A and C point out, that the cells were successfully removed from the electrode with the cell scraper, since no single cells are visible on the harvested electrode area (right part of the images).

Figure 22 E shows stained single cells at the border of the multilayered biofilm. As can be seen from images B and D, the EPS were mainly removed from the surface, however in image B the TRITC signal might indicate that removing of the EPS from the electrode surface was not complete. Furthermore, EPS fragments or agglomerates can be detected on both images B and D. Based on these findings, repeated steps of scratching with a cell scraper and taking up in PBS were implemented in the harvesting routine.

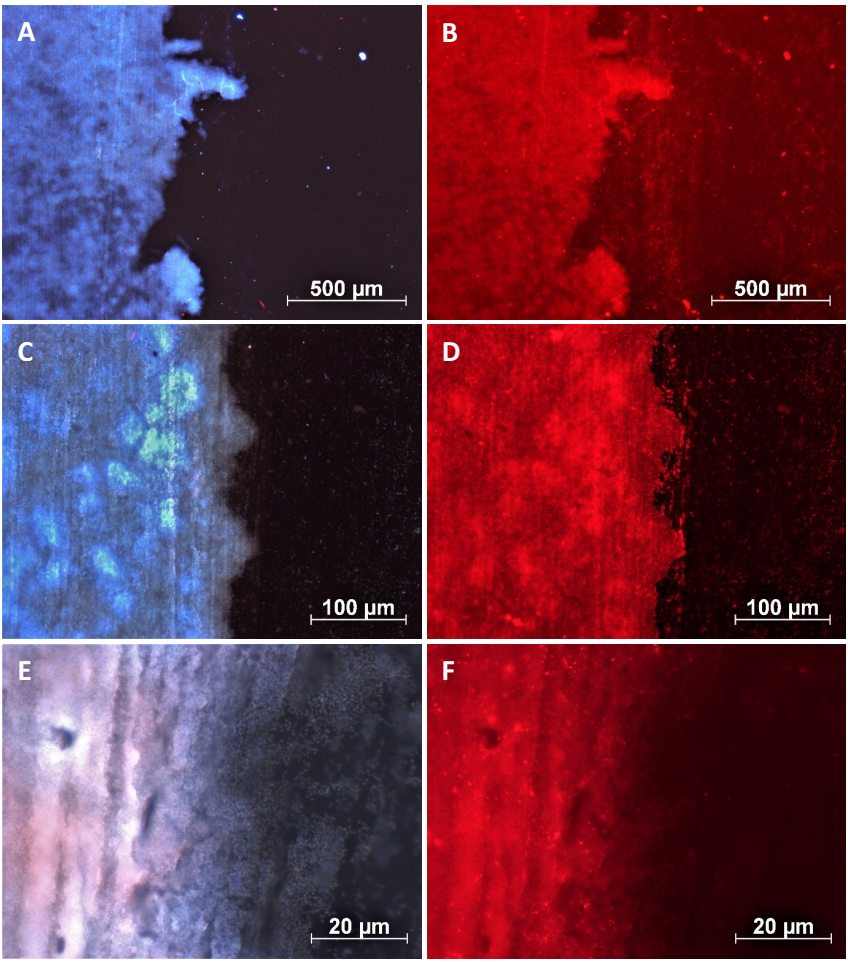

Figure 22: EFM images of *G. sulfurreducens* biofilm border after harvesting half of the biofilm from the WE dismounted from a H-cell operated as MFC (minimal medium + acetate; electron acceptor: anode (bipolar plate); 30 °C; anaerob). Images A, C and E display the DAPI signals (1 µg mL^{-1} DAPI), images B, D and F are ConA-TRITC (100 µg mL^{-1} TRITC-labelled ConA) signals. Images were taken with increasing magnification: A and B with 50-fold, C and D with 200-fold and E and F with 1000-fold magnification. Staining procedure with DAPI and TRITC-labelled ConA.

3.3.3.2.2 SEM images of anode respiring *G. sulfurreducens* biofilm

Figure 23 and Figure 24 show micro- and macro-scale SEM images of a freshly polished bipolar plate electrode (Figure 23 A) and an electrode after electrochemical cultivation of *G. sulfurreducens* and the harvest of biofilm (Figure 23 B). On the microscale, the fresh electrode surface (Figure 23 A) is amorphously and irregularly structured. Additionally, it can be characterized by a high amount of cavities. The scratching direction of SiC-paper can be seen in the vertical direction. After biofilm harvest the biofilm and further cleaning, the electrode surface remains similar. The dark shadows in Figure 23 B might indicate some residual EPS on the surface of the bipolar plate as well as the more smooth transition between the particle-like structures and cavities. However, both general pattern of the surface morphology and the initial structure originating from the SiC-paper can be clearly identified. Furthermore, no remaining single cells or biofilm fragments could be observed in the SEM images after biofilm harvesting.

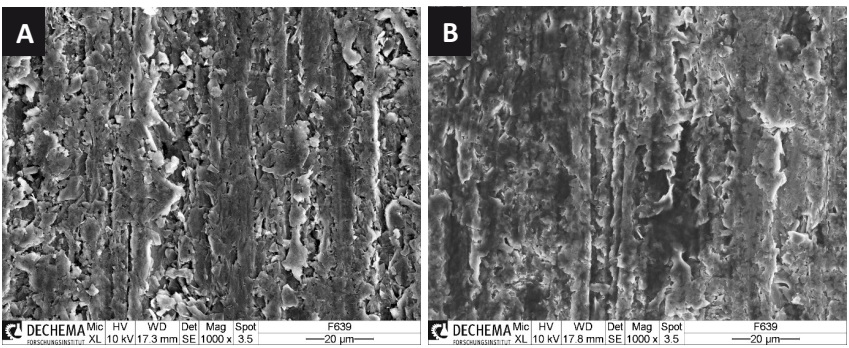

Figure 23: SEM images (SE-detector) of bipolar plate electrodes at 1000-fold magnification, surface roughened with SiC-paper (FEPA grain size 500). A: SEM image of a fresh electrode after surface conditioning with SiC-paper. B: SEM image a bipolar plate electrode after electrochemical cultivation of *G. sulfurreducens* as MFC (minimal medium + acetate; electron acceptor: anode; 30 °C; anaerob) and subsequent biofilm removal with a cell scraper.

Similar results can be observed on the macroscale in Figure 24. Comparable to the high resolution image of the fresh electrode surface (Figure 23 A), the pattern of the SiC-paper roughening process can be identified clearly (Figure 24 A). The harvesting process imaged in Figure 24 B shows that the scratching off with a cell scraper removed the biofilm and neither

EPS nor biofilm residuals were left on the surface after harvest (left corner and top of the image).

To summarize, it can be stated that the biofilm harvesting process with a cell scraper from the planar electrode sufficiently removed both EPS and cells from the surface, resulting in a nearly quantitative recovery of EPS for the subsequent biochemical analysis.

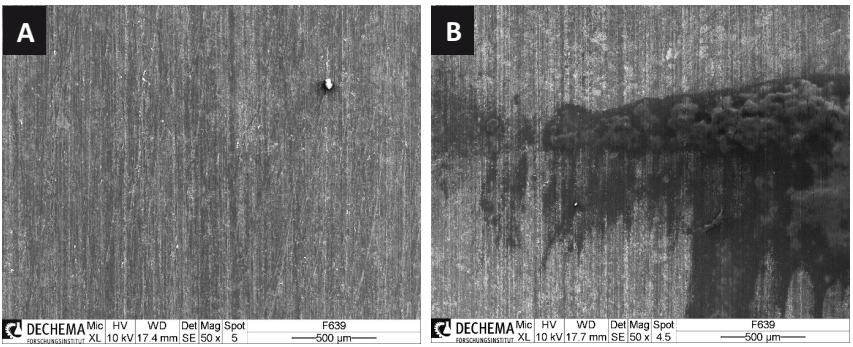

Figure 24: SEM images (SE-detector) of bipolar plate electrodes at 50-fold magnification. Surface was roughened with SiC-paper (FEPA grain size 500). A: SEM image of a fresh electrode after surface conditioning with SiC-paper. B: SEM image of a bipolar plate electrode after electrochemical cultivation of *G. sulfurreducens* as MFC (minimal medium + acetate; electron acceptor: anode; 30 °C; anaerob). The residual biofilm was left intentionally on the electrode to visualize biofilm harvest with a cell scraper.

3.3.4 Biochemical EPS analysis

The harvested and extracted EPS fractions of both anode respiring *G. sulfurreducens* in a MFC and of heterotrophically grown and fumarate respiring cells as control were analyzed for their amounts of total proteins, total carbohydrates, total uronic acids, total lipids and total eDNA. Concentrations referred to single cells and are presented individually for each compound (sections 3.3.4.1 – 3.3.4.5) and summarized for all EPS compounds (section 3.3.4.6).

3.3.4.1 Total protein concentration in EPS

Results for the total protein concentrations found in the extracted fractions of the electroactive biofilms (MFC) and the heterotrophically grown cells (C) can be found in Figure 25. By far the highest protein concentration was found in the SOL EPS of the electroactive

biofilm with 97 ± 18 pg cell^{-1} followed by the SOL EPS (12 ± 1 pg cell^{-1}) of the EXP control. TB EPS of the MFC grown cells was 10 ± 7 pg cell^{-1} and 4 ± 2 pg cell^{-1} proteins were found in the LB fraction of the electroactive biofilm. Compared to the electroactive cells, heterotrophically grown cells had a significantly reduced protein concentrations in both EPS fractions. As mentioned before, the highest protein concentration is found in the SOL EPS of cells harvested in the exponential phase (C EXP SOL). Total proteins in the TB EPS of the culture harvested in exponential phase (C EXP TB) as well as TB and SOL EPS of the culture grown to stationary phase are in the lowest range with 0.5 ± 0.03, 3 ± 0.3 and 3 ± 0.2 pg cell^{-1}, respectively. It has to be stated that total protein concentrations in the electrochemically grown cultures are characterized by a high heterogeneity indicated by the high standard deviations for TB, LB and SOL EPS of the MFCs.

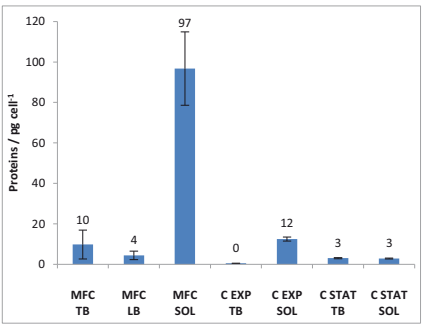

Figure 25: Total protein concentration per cell for EPS fractions (tightly bound: TB; loosely bound: LB; soluble: SOL) extracted from cells grown electrochemically (MFC) or heterotrophically (C) to exponential (EXP) and stationary phase (STAT). Bovine serum albinum served as standard. Concentrations are given as number and standard deviations presented in black error bars.

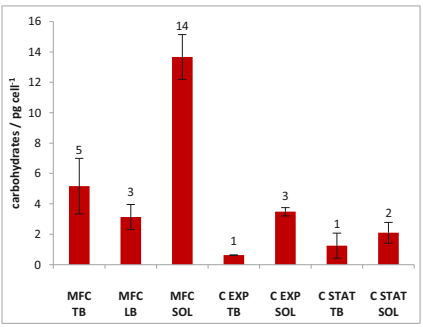

Figure 26: Total carbohydrate concentrations per cell for EPS fractions (tightly bound: TB; loosely bound: LB; soluble: SOL) extracted from cells grown electrochemically (MFC) or heterotrophically (C) to exponential (EXP) and stationary phase (STAT). Glucose served as standard. Concentrations are given as number and standard deviations presented in black error bars.

3.3.4.2 Total carbohydrate concentrations in EPS

Values for carbohydrates, the second group of compounds, are presented in Figure 26. Similar to the total protein concentrations the highest amount of carbohydrates was found in the SOL EPS fraction of the electroactive biofilm (14 ± 1 pg cell^{-1}), followed by the TB EPS

(MFC) and the SOL EPS of the fumarate respiring cells harvested in EXP phase (C EXP) with 5 ± 2 and 3 ± 0.3 pg cell^{-1}, respectively. 3 ± 1 pg carbohydrates cell^{-1} were found in the LB EPS of the MFC. Carbohydrate concentrations in both controls (C), EXP and STAT, were in the same range and in general lower compared to the anode respiring cells. For both controls more carbohydrates were found in the SOL EPS fraction than in the TB EPS fraction. With 3 ± 0.3 pg cell^{-1} the amount in the SOL EPS of the EXP harvested culture was higher than the STAT phase harvested cells (2 ± 1 pg cell^{-1}). The TB EPS concentration in the STAT control was at 1 ± 0.8 pg cell^{-1} followed by the smallest amount in the EXP control (0.6 ± 0 pg cell^{-1}). Again, standard deviations were significantly higher for the MFC grown cells in all EPS fractions than for the controls. However, values were lower compared to the standard deviations of the values for the total protein concentrations.

3.3.4.3 Total uronic acid concentration in EPS

The third parameter was uronic acids in the EPS. Total concentrations of uronic acids for the respective samples are displayed in Figure 27. Again, the highest concentration was found in the SOL EPS of the anode respiring cells with 4 ± 1 pg cell^{-1}. Contrary to proteins and carbohydrates, the second highest uronic acid concentration was found in the LB fraction (MFC) followed by the TB EPS (MFC) fraction (1 ± 0.7 and 0.7 ± 0.3 pg cell^{-1}, respectively). Compared to the electroactive cells, fumarate respiring cells showed significantly lower concentrations for uronic acids, independently from the phase of growth in which they were harvested or the EPS fraction. The highest concentration was found in the SOL EPS of the EXP phase harvested cells (0.3 ± 0.13 pg cell^{-1}) followed by the SOL EPS of the STAT control (0.3 ± 0.1 pg cell^{-1}) and the TB EPS of the EXP control (0.3 ± 0.2 pg cell^{-1}). TB EPS of the control harvested in exponential phase was the smallest value with 0.1 ± 0.04 pg cell^{-1}. For uronic acid values the standard deviations were relatively high.

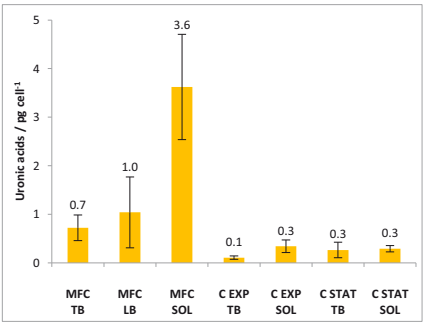

Figure 27: Total uronic acid concentrations per cell for EPS fractions (tightly bound: TB; loosely bound: LB; soluble: SOL) extracted from cells grown electrochemically (MFC) and heterotrophically (C) to exponential (EXP) and stationary phase (STAT). Glucuronic acid served as standard. Concentrations are given as number and standard deviations presented in black error bars.

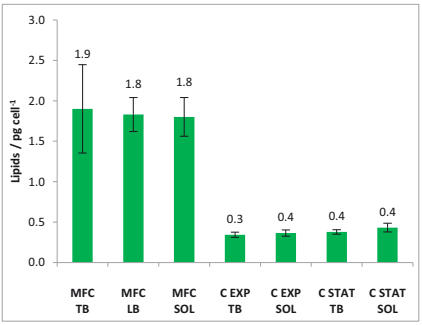

Figure 28: Total lipid concentrations per cell for EPS fractions (tightly bound: TB; loosely bound: LB; soluble: SOL) extracted from cells grown electrochemically (MFC) and heterotrophically (C) to exponential (EXP) and stationary phase (STAT). Olive oil served as standard. Concentrations are given as number and standard deviations presented in black error bars.

3.3.4.4 Total lipid concentration in EPS

The analysis of the total lipid concentrations in the harvested EPS fractions is presented in Figure 28. In general, concentrations of the lipids were significantly higher for the electrochemically cultivated cells compared to the fumarate respiring cells. In contrast to the findings for the protein, carbohydrates and the uronic acid values, lipids were equally distributed in the EPS fractions of equal cultivation conditions. MFC grown cells produced concentrations of 2 ± 0.6, 2 ± 0.2 and 2 ± 0.2 pg $cell^{-1}$ in the TB, LB and SOL EPS respectively. Lipid concentrations for the controls were smaller compared to the electroactive biofilms by approximately a factor of 10. Moreover, the values did not indicate an accumulation of lipids in any of the fractions. Concentrations were 0.3 ± 0.03, 0.4 ± 0.04, 0.4 ± 0.03 and 0.4 ± 0.05 pg $cell^{-1}$ for TB EPS (EXP), SOL EPS (EXP), TB EPS (STAT) and SOL EPS (STAT), respectively.

3.3.4.5 Total eDNA concentration in EPS

As last parameter of the biochemical EPS analysis the total eDNA concentration were determined. Again the anode respiring cells exhibited higher concentrations than the fumarate respiring controls (Figure 29). The highest concentration was found in the SOL EPS of the electroactive (MFC) biofilm (0.17 ± 0.06 pg cell^{-1}) followed by the LB and TB EPS of the MFC (0.14 ± 0.12 and 0.07 ± 0.05 pg cell^{-1}, respectively). As mentioned before, eDNA concentrations in the EPS fractions of the controls were significantly smaller and in the same range for all controls. The highest eDNA amount of the control samples was found in the SOL EPS of the STAT control (0.03 ± 0.005 pg cell^{-1}), followed by the TB EPS of the EXP control (0.03 ± 0.006 pg cell^{-1}), the SOL EPS of the EXP control (0.02 ± 0.001 pg cell^{-1}) and finally the TB EPS of cells harvested in the stationary growth phase (0.01 ± 0.002 pg cell^{-1}). Furthermore, it has to be stated, that samples harvested from the electrode surface showed a high heterogeneity in eDNA concentrations, indicated by high standard deviations.

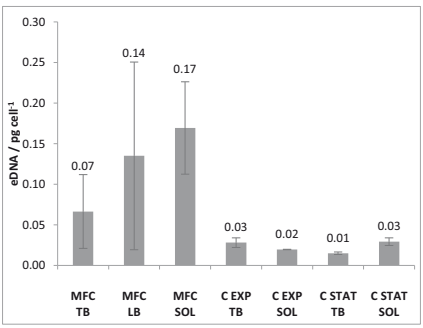

Figure 29: Total eDNA concentrations per cell for EPS fractions (tightly bound: TB; loosely bound: LB; soluble: SOL) extracted from cells grown electrochemically (MFC) and heterotrophically (C) to exponential (EXP) and stationary phase (STAT). dsDNA served as standard. Concentrations are given as number and standard deviations presented in black error bars.

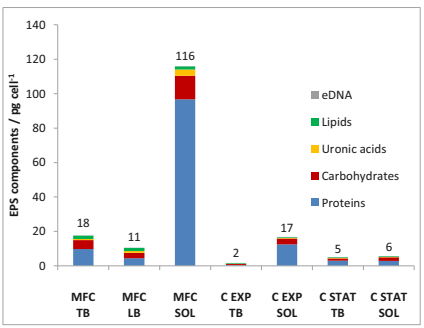

Figure 30: Summarized concentrations for EPS compounds per cell of EPS fractions (tightly bound: TB; loosely bound: LB; soluble: SOL) extracted from cells grown electrochemically (MFC) and heterotrophically (C) to exponential (EXP) and stationary phase (STAT). Summarized concentrations are given as number.

3.3.4.6 Summary for analysis on EPS composition of *G. sulfurreducens*

Figure 30 summarizes the concentrations of the five parameters for the EPS fractions and cultivation conditions. It can be clearly seen that the fraction of SOL EPS of the MFC-grown *G. sulfurreducens* cells contains the highest amount of EPS with a value of 116 ± 21 pg cell^{-1}. The second highest EPS concentration is measured for the TB EPS of the electroactive biofilms with 18 ± 10 pg EPS cell^{-1}. The lowest values are detected for the anode respiring cells with LB EPS at 11 ± 4 pg cell^{-1}. All controls cultivated under non-electroactive conditions showed smaller EPS concentrations compared to the electroactive fractions. The highest EPS concentration was measured in the SOL fraction of the controls harvested in EXP phase with 17 ± 1 pg cell^{-1}. The SOL fraction of cells harvested in the STAT phase were found to have the second highest EPS concentration (6 ± 1 pg cell^{-1}) followed by the TB fraction of the same cultures (STAT, 5 ± 1 pg cell^{-1}) and the TB fraction of cells harvested in the EXP phase (2 ± 0 pg cell^{-1}). As mentioned before, standard deviations for the electroactive biofilms are high. Besides the EPS concentration, Figure 30 also illustrates the composition of the respective fractions and cultures. Under electrochemical conditions *G. sulfurreducens* mainly secrets proteins into the electrolyte, followed by carbohydrates and residual compounds. The same pattern can be observed for the TB fraction of the MFC cells, however, proteins are not as dominant as in the SOL EPS. In the LB EPS, again proteins represent the biggest group followed by carbohydrates. In all samples eDNA is the smallest fraction of the EPS.

3.4 Discussion and Conclusions

The aim of the experiments presented in this chapter was the biochemical EPS analysis of anode respiring *G. sulfurreducens*. In order to fulfil this aim the following steps were conducted:

- electrochemical cultivation of *G. sulfurreducens* biofilms
- evaluation of a tightly bound EPS extraction reagent
- establishment of an EPS extraction routine for electroactive biofilm samples
- biochemical analysis of electrochemically cultivated *G. sulfurreducens* biofilms.

3.4.1 Electrochemical cultivation in H-cells

As already described by a plethora of studies, *G. sulfurreducens* is one of the most applied model organisms in the field of microbial current production. Results presented in section 3.3.2 show a typical current density curve for a strain initially grown on fumarate as electron donor and then added to a polarized electrode [Nevin et al. 2009]. Analog with the heterotrophic growth curves, presented in section 3.3.1, current production in the MFC was also characterized initially by a lag phase, followed by an exponential phase and a stationary phase, indicating the maturation of the anode respiring biofilm. The small current decrease at the end of the experiment is typical for a MFC and is often related to an acidification of the biofilm resulting from proton accumulation, since 8 protons are released during the conversion of one acetate to CO_2 using the anode as electron acceptor [Franks et al. 2009].
Final current densities of around 172 µA cm^{-2} are comparable to values reported by Nevin et al. (215 µA cm^{-2}) for *G. sulfurreducens* biofilms fed with acetate in a H-cell set-up [Nevin et al. 2009]. However, current densities up to 1000 µA cm^{-2} and higher have also been published for *G. sulfurreducens* biofilms growing in a flow through cell [Malvankar et al. 2012]. The values indicate that our MFC set-up was not designed to realize maximum current densities. The internal resistance resulting from the high distance between the WE and CE and the low electrode surface to electrolyte volume were assumed to be the main limiting factors. Additionally, electrochemical reactors providing an increased WE surface

might be used in future studies in order to harvest an increased amount of biofilm. Nonetheless, the modified H-cell reactor provided an established electrochemical system and allowed precise electrochemical cultivation conditions. Furthermore, the main advantage of the used system was the possibility to quickly dismount the WE by the designed clamp system in order to harvest the biofilms without loss because of mechanical disruption during dismounting. Finally, operation of the MFC in batch mode allowed the accumulation of the SOL EPS fraction during cultivation.

3.4.2 Extraction reagent evaluation

The extraction reagent evaluation was conducted in order to obtain a reagent promoting the extraction of the tightly bound EPS combined with a low amount of cell lysis. Cell lysis was chosen as main parameter since false positive concentrations in the TB EPS fraction would be a consequence of high lysis of cells during the extraction routine. It was rather accepted to extract a reduced amount of TB EPS from the bacteria than eventually extracting more TB EPS, but taking an increased cell lysis into account.

Results revealed that from the three tested extraction reactions DOW caused the lowest cell lysis under the given conditions and CW the highest amount of cells. Lysis caused by EDTA was not quantifiable with the BCA assay, but it was assumed that EDTA might also cause a high amount of cell lysis, because both EDTA and CW function as chelating agents complexing cations, when extracting the TB EPS. Consequently, effects of both ER on the membrane integrity might be comparable. Compared to other studies such as Wikiel, the observed cell lysis of 3 % with DOWEX as ER appears relatively high [Wikiel 2013]. However, taking into consideration that *G. sulfurreducens* was described as very sensitive towards a damaging of the membrane [Coppi et al. 2001], the observed cell lysis for DOW seems to be acceptable. Furthermore, comparing the results of the biochemical analysis of the TB EPS fractions of MFC grown cells and both fumarate respiring controls, the influence of the cultivation conditions on the EPS composition strongly overlaid possible effects from cell lysis during the extraction procedure. Concentrations of all major EPS compounds differ between the controls and the anode-respiring cells. The total amount of TB EPS of the control, harvested in EXP phase for example, was more than tenfold lower than the amount of TB EPS of the MFC cells (Figure 29). This resulted in the conclusion that the effect of cell lysis was of minor importance since all cell were treated equally.

However, besides cell lysis as evaluation parameter, other parameters such as the maximum extraction capacity for the respective EPS compounds (proteins, carbohydrates etc.) should be tested in future studies to achieve a maximum EPS recovery as it was described before [Liu and Fang 2002; Takahashi et al. 2009; Wikiel 2013].

3.4.3 Biofilm harvest

Evaluation of the biofilm harvest with a cell scraper was performed optically and monitored via fluorescence staining combined with epifluorescence microscopy and scanning electrode microscopy. Therefore, biofilms were cultivated electrochemically, harvested partially and examined optically. All imaging techniques proved that the vast majority of the biofilms were harvested by the scratching process, especially when this process was repeated. Nevertheless, it has to be taken into account that cells or at least parts of the EPS may remain on the electrode surface, so that the biofilm could not be harvested completely in this way. To ensure a maximum EPS recovery from the WE surface a chemical extraction procedure from the electrode should be established in future studies.

In general, all three ways to monitor biofilm formation on an electrode surface (optical, via EFM or SEM) illustrate a homogenously covered electrode surface. The complete electrode coverage is typical for electroactive *Geobacter* biofilms [Nevin et al. 2009; Sun et al. 2016], but different from the colonization of sulfur for example as it observed by Zhang [Zhang et al. 2015].

3.4.4 Biochemical EPS analysis

As final step of this series of experiments the EPS fractions were analyzed biochemically to compare the major compounds of the EPS of anode respiring *G. sulfurreducens* cells with fumarate respiring cells.

The results clearly indicate that anode respiration of *G. sulfurreducens* strongly promotes the production of EPS. Proteins were secreted to the electrolyte (SOL EPS) almost tenfold more under electrochemical conditions as compared to the controls harvested in exponential phase and more than 30 times more as compared to the cells harvested in stationary phase. A similar pattern but with smaller differences was observed for the soluble fraction of the carbohydrates. They were secreted around 3.5 times more under MFC conditions as

compared to EXP phase culture and almost 7 times more as compared to the STAT phase culture. Uronic acids and eDNA complete these findings also following the same pattern. Again the concentrations in the SOL EPS were around ten times higher in the anode respiring culture as compared to the controls. It might be assumed that the electrochemical cultivation leads on the one hand to an upregulation of genes responsible for the expression of the respective EPS compounds as already has been reported for cells of *G. sulfurreducens* on graphite electrodes. Nevin found that e.g. genes responsible for expression of transport and binding proteins were overexpressed, whereas other genes were down regulated [Nevin et al. 2009]. On the other hand, transport of the substances from cytoplasm or periplasm beyond the outer membrane might be enhanced in the course of anode respiration leading to an accumulation of EPS in the electrolyte (SOL EPS). The observation, that proteins dominate the composition of the SOL EPS fraction (Figure 30) might be a result of the extracellular electron transfer mechanisms of *G. sulfurreducens.* This is involving mainly proteins such as cytochromes to transfer electrons to the electrode, e.g. via nanowires [Malvankar et al. 2011].

The general trend that more EPS were produced by electroactive cells was valid also for the tightly-bound EPS. All EPS compounds occurred in increased concentrations with the MFC harvested cells than with the control cells. Again, proteins were most abundant, indicating their importance for the EET, followed by carbohydrates, which are connected to the surface attachment [Rollefson et al. 2011].

LB EPS were analyzed only for cells harvested from the MFC, since they were combined with the SOL EPS fraction in case of the controls (section 3.2.5, Figure 11). But also under these conditions electroactive cells produce significantly more EPS compared to cells grown with fumarate respiration.

When explaining the large differences between MFC grown cells and the control cells, anode respiration is assumed to have the biggest impact on EPS secretion. However, heterotrophically grown cells were present partially as a biofilm on the glass wall of the septum flask, with the major part occurring as planktonic cells. In contrast, MFC cells were mainly sessile cells. The need to form a biofilm under heterotrophic conditions was low, since fumarate respiration is not a surface limited process. The second parameter, that was different apart from the applied potential, was the stirring of the WE chamber. Both factors

have been reported to influence biofilm formation and, consequently, also influence the EPS secretion [Wingender et al. 1999]. Influence of stirring on *G. sulfurreducens* EPS production should be tested in future studies.

The relatively high standard deviations found for all major EPS compounds independent from cultivation and fraction might be a result of the complex routine towards the biochemical analysis of EPS. The main steps were MFC cultivation (**1**), electrode dismounting (**2**), biofilm harvest (**3**), resuspension (**4**), fractionation (**5**), dialysis (**6**), drying (**7**), resolving (**8**) and biochemical analysis (**9**). This variety of steps towards the EPS analysis illustrates the high potential leading to quantitative differences between the individual samples.

Comparing the data for EPS concentrations found in this study with data from leaching bacteria for example, indicates that *G. sulfurreducens* produces high amounts of EPS e.g. values around 140 pg total EPS cell^{-1}. Wikiel for example found concentrations ranging at values lower than 1 pg EPS cell^{-1} for *Desulfovibrio alaskensis* under various corrosion conditions [Wikiel 2013]. Castro described concentrations around 50 pg EPS cell^{-1} for *Aeromonas hydrophila* under reducing conditions [Castro et al. 2014]. Hence, the electrochemical cultivation of *G. sulfurreducens* involving anode respiration strongly promotes biofilm formation and EPS production. Proteins dominate the secreted EPS, probably because they are mainly involved in the EET from and to cells of *G. sulfurreducens*.

To the best of the authors knowledge, these experiments are the first approach towards a complete analysis of *G. sulfurreducens* EPS under electroactive conditions. The data indicate a strong promoting effect of an anodically polarized electrode on EPS production. However, since microbial EPS are very complex and the results strongly depend on the type of analysis, further studies are needed. A more detailed analysis of the major EPS compounds such as proteins or carbohydrates analysis [Yang et al. 2016; Castro et al. 2014], should be performed as well as a further evaluation of TB EPS extraction reagents [Takahashi et al. 2009]. This will lead to a deepened understanding of electroactive biofilm formation and function. Furthermore, varying electrochemical parameters such as the applied anode potential might also influence the EPS composition and should therefore be tested in future studies.

4 Combination of EIS and CLSM for simultaneous biofilm monitoring

4.1 Introduction

A major part of this chapter has been published previously in Stöckl et al. 2016.

4.1.1 Monitoring of electroactive biofilms

The implementation of bioelectrochemical systems into industrial energy generation or compound synthesis is limited by a variety of parameters including appropriate reactor concepts, efficient power outputs, suitable reactions or genetically engineered organisms. Since BES requires the electron transfer from microorganisms to an electrode or vice versa, the interaction between an organism and the electrode also has to be taken into account as a limiting factor in BES. Monitoring of cell attachment to the electrode surface, subsequent biofilm formation and electrode interaction and consequently, the understanding of the fundamental mechanisms are necessary to overcome these limitations [Logan and Regan 2006]. In contrast to the majority of corrosion studies, in BES applications the formation of a biofilm is beneficial causing an efficient electron transfer between organism and electrode.

A large variety of biofilm monitoring techniques has been developed in the last decades, ranging from spectroscopic methods [Wolf et al. 2002] to gravimetry [Bressel et al. 2003], over several microscopical techniques to electrochemical detection methods. Online biofilm monitoring techniques were reviewed in detail by Janknecht [Janknecht and Melo 2003]. The incorporation of electrodes in the experimental set-up is one major advantage for the biofilm monitoring in BES, since they are essential for the operation of BES. It is obligate to investigate electrochemically the attachment of electroactive organisms at electrodes, because these methods only require a working and a counter electrode plus an optional reference electrode. Electrochemical biofilm monitoring methods can be performed continuously over the time scale of an experiment and do not determine the experiment. Commonly applied electrochemical methods to detect microbial activity on electrodes are cyclic voltammetry (CV) [Fricke et al. 2008; Richter et al. 2009], spectro-electrochemistry [Jain et al. 2011] and chronoamperometry [Rollefson et al. 2011; Estévez-Canales et al. 2017]. Furthermore, electrochemical impedance spectroscopy (EIS) becomes more and more important for a deeper understanding of biological as well as electrochemical processes in BES [He et al. 2006; He and Mansfeld 2009]. EIS is a non-invasive method, which allows a

detailed examination of electron transfer, surface capacity and morphology [Ende and Mangold 1993].

Besides the named electrochemical methods, a huge number of different types of microscopy have been established to visualize bacterial adhesion to electrodes or other surfaces. Well investigated methods are atomic force microscopy [Fang et al. 2000; Mangold et al. 2008], Raman microscopy [Virdis et al. 2012; Lebedev et al. 2014], scanning electron microscopy [Priester et al. 2007; Alhede et al. 2012], and epifluorescence (EFM) respectively confocal laser scanning microscopy (CLSM) [Surman et al. 1996; Möhle et al. 2007; Neu and Lawrence 2014].

However, due to the versatile interactions and the dynamic behavior of biofilms, the application of one single analytical method is often not sufficient to achieve a thorough understanding of the complex interactions between the electroactive bacteria and the electrode surface. Therefore, a combination of two (or more) techniques is a promising approach for biofilm monitoring. Jain reported the combination of spectroscopy with chronoamperometry for the analysis of a *Geobacter* biofilm [Jain et al. 2011]. Additionally, Ben-Yoav described a device for EIS and detection of surface coverage with optical microscopy in an undivided cell applied for non-electroactive bacteria [Ben-Yoav et al. 2011]. The simultaneous electrochemical and optical measurements can be used to characterize both, the electrochemical parameters as well as the microbial attachment behavior, morphology of a biofilm or the surface coverage on an electrode. Consequently, the aim of this project was to develop and characterize a flow cell, which enables the parallelized application of an electrochemical and an optical biofilm monitoring method, namely EIS and CLSM. The addressed flow cell was defined to fulfill the following requirements:

I. Applicability as bioelectrochemical system (e.g. microbial fuel cell)
II. Enabling continuous and non-destructive in-situ microscopy for the characterization of cell attachment or biofilm growth on the electrode surface
III. Suitable design for EIS measurements and further electrochemical measurements such as cyclic voltammetry

IV. Separated working and counter electrode (two chamber system in order to separate the electrodes and corresponding electrolytes)

Summarized, this novel flow cell should enable the electrochemical characterization of biofilm processes by the noninvasive method EIS. Furthermore, the parallelized visualization of surface related microorganisms by CLSM allows the characterization of cell attachment and biofilm formation. The application of both EIS and CLSM in parallel will allow a deepened understanding of the behavior of electroactive organisms [Stöckl et al. 2016].

4.1.2 Electrochemical impedance spectroscopy

The electrochemical impedance spectroscopy (EIS) is an electrochemical method for the characterization of surface related chemical reactions, processes or surface morphology. In general, impedance (Z) is defined as the resistance under an alternating current or potential. In the past, EIS has been mainly applied for the detection of corrosion, studying the corrosion inhibition, polymer layers, pitting corrosion or microbiologically influenced corrosion (MIC) [Marcus and Mansfeld 2005; Manohar et al. 2008]. Additionally, in the last decade, EIS turned out to be a powerful tool in BES, mainly for the characterization of the anodic electron transfer and biofilm formation [Ramasamy et al. 2008; He and Mansfeld 2009; Borole et al. 2010; Dominguez-Benetton et al. 2012].

The working principle of EIS is based on the application of small sinusoidal alternating potential (E) (or current) to a specimen (working electrode) in an electrolyte around a certain fixed potential (e.g. open circuit potential, OCP). The amplitude of the applied potential thereby strongly depends on the impedance of the system. Typically for the analysis of BES potential amplitudes around 10–15 mV are applied. During an EIS measurement, the frequency (ω) of the applied alternating voltage is varied over a wide frequency range, from usually 100 kHz down to 50 mHz or even lower. As consequence of the applied voltage (ΔE), a resulting current (ΔI) is monitored. Depending on the frequency (ω) and the characteristics of the specimen the resulting current is thereby measured in phase ($\varphi = 0$; Faraday current) or characterized by a certain phase shift ($\varphi \neq 0$; capacitive or inductive current). As can be seen below, the impedance is described as the quotient of the applied potential (ΔE) and the resulting current (ΔI), in dependence on the frequency (ω),

phase shift (φ) and time (t). By mathematical transformation, it can further be differentiated in the real (Z_{REAL}) and imaginary (Z_{IMAG}) part of the impedance (with: $i = \sqrt{(-1)}$ as imaginary number) [Ende and Mangold 1993]:

$$Z(i\omega) = \frac{|\Delta E| e^{i\omega t}}{|\Delta I| e^{i(\omega t + \varphi)}} = |\Delta Z| e^{-i\omega} = Z_{REAL} - i\, Z_{IMAG}$$

Subsequent visualization of measured impedance data is realized mainly by two different types of diagrams: the Nyquist plot enables the differentiation between the imaginary (Z_{IMAG}) and the real (Z_{REAL}) part of the total impedance (Z_{TOT}), whereas the Bode plot shows the frequency dependence of both the total impedance (Z_{TOT}) and the phase shift (φ). Interpretation of EIS measurement is finally managed by creation of an equivalent circuit based on graphical examination (pattern of the curves), and subsequent fitting with a software.

4.1.3 Confocal laser scanning microscopy

Confocal laser scanning microscopy (CLSM) visualizes and produces highly resolved 3D images of fluorescent samples. Due to the possibility to image three dimensional organic structures CLSM has been established as one of the major biofilm imaging techniques [Staudt et al. 2004; Neu and Lawrence 2014; Zhang et al. 2015].

Similar to the principle of epifluorescence microscopy, a fluorescent sample is excited by a laser at a certain wavelength and emits light with a higher wavelength. By the insertion of a pinhole in the beam path prior to the detector, signals that do not originate from the focus of the lenses are eliminated. Specimens are scanned point by point and a software subsequently merges the signals to a complete image. To produce images via CLSM, samples have either to be naturally fluorescent or to be stained with fluorescent dyes. Usual fluorescent markers are DAPI (labelling DNA) [Castro et al. 2014], lectins (e.g. ConA labelling EPS) [Zhang et al. 2015] or eGFP produced by genetically modified cells [Stöckl et al. 2016].

4.1.4 *Shewanella oneidensis*

To approve the feasibility of our developed flow cell for the monitoring of biofilm formation simultaneously with EIS and CLSM, *Shewanella oneidensis* was selected to serve as electroactive model organism. *S. oneidensis* was chosen due to its tolerance towards oxygen, the well-studied EET and the possibility to monitor bacterial attachment via fluorescence microscopy with an engineered eGFP producing strain.

4.1.4.1 Strain description

Shewanella oneidensis MR-1 was initially described in 1999 as a Gram-negative and rod shaped bacterium with 2–3 µm in length and 0.4–0.7 µm in diameter with an optimal growth temperature of 30 °C [Venkateswaran et al. 1999]. Cells are non-spore-forming and motile by a single unsheathed polar flagellum and were found mainly in aquatic sediments. *S. oneidensis* is able to harvest energy from a variety of substrates such as acetate, lactate, pyruvate, succinate, fumarate, serine and other amino acids [Tang, Adam L Meadows, et al. 2007]. As facultative anaerobic organism, *S. oneidensis* is capable to respire on oxygen as well as dissimilate by the reduction of metal ions such as manganese and iron oxides (Mn(IV) and Fe(III)), sulfur, nitrate, and fumarate.

S. oneidensis uses some metabolic pathways (serine, Entner-Doudoroff, tricarboxylic acid and pentose phosphate pathways) for energy conversion [Tang, Hwang, et al. 2007]. With lactate as primary substrate the tricarboxylic acid (TCA) pathway presented in Figure 31 is the major carbon metabolism route under both aerobic and oxygen limited conditions [Tang, Hwang, et al. 2007]. Thereby, lactate is initially oxidized to pyruvate with the formation of one NADH or one quinone, followed by an oxidation to acetyl-CoA and the formation of one formate or one NADH. Acetyl-CoA is then either oxidized to acetate or transferred to the TCA cycle.

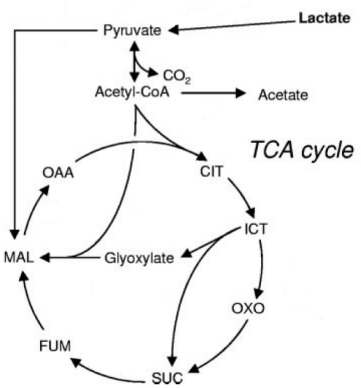

Figure 31: Scheme of the TCA cycle employed by *S. oneidensis* MR-1 for lactate metabolism. Adapted and modified from Tang [Tang, Adam L. Meadows, et al. 2007].

4.1.4.2 *S. oneidensis* in bioelectrochemical systems

Besides *G. sulfurreducens*, *S. oneidensis* is one of the most applied and best studied electroactive organisms for bioelectrical systems (BES). As mentioned before, it was initially described to respire dissimilatorily on metal oxides under anaerobic conditions, until it was also found to release electrons to solid electrodes as terminal electron acceptor [Logan et al. 2005; Marsili et al. 2008]. Due to its tolerance towards oxygen, its molecular accessibility and the ability to transfer electrons either directly (DET) or via mediators (MET) to the electrode surface, it became a model organism in many studies [Rosenbaum et al. 2010; Sydow et al. 2014]. Mediated electron transfer is mainly realized by the excretion of riboflavin. However, flavin mononucleotide (FMN) and flavin adenine dinucleotide (FAD) were assumed also to be possible compounds produced by *S. oneidensis* for electron shuttling [Marsili et al. 2008; Brutinel and Gralnick 2012]. In contrast to *G. sulfurreducens*, cultivation under anaerobic conditions leads to the formation of very thin biofilms, since mediated electron transfer is the main EET applied under these conditions and the majority of cells is present in the planktonic phase. However, the presence of oxygen leads to an increased biofilm formation on electrodes [Rosenbaum et al. 2010].

The majority of the results presented in this chapter were already published in *Electrochimica Acta* [Stöckl et al. 2016]. Furthermore, the scientific impact was emphasized by the selection as a key scientific article contributing to research excellence in science and engineering by the Journal *Advances in Engineering* [submitted July 2017].

4.2 Materials and Methods

4.2.1 Microorganism

Shewanella oneidensis MR-1 was selected as electroactive model organism for the demonstration of simultaneous EIS and CLSM measurements in the MFC mode in our flow cell. In order to obtain images via CLSM, an engineered *S. oneidensis* MR-1 (ATCC700550) producing the enhanced Green Fluorescent Protein (eGFP) was used.

4.2.1.1 Growth media

Cultivation of *S. oneidensis* included the following two growth media:

Luria broth (LB): 5 g L^{-1} yeast extract, 10 g L^{-1} tryptone, 10 g L^{-1} NaCl and 50 mg L^{-1} kanamycin in deionized water.

Lactate Medium (LM), adapted from Thormann [Thormann et al. 2006]: 19.62 g L^{-1} 50 % sodium lactate solution; 23.83 g L^{-1} HEPES buffer; 0.225 g L^{-1} KH_2PO_4; 0.225 g L^{-1} K_2HPO_4; 0.46 g L^{-1} NaCl; 0.225 g L^{-1} $(NH_4)_2SO_4$; 5 mL L^{-1} trace element solution (23.4 g L^{-1} $MgSO_4 \cdot 7 H_2O$; 26 g L^{-1} $ZnCl_2$; 5 g L^{-1} $Na_2MoO_4 \cdot 2 H_2O$; 4.8 g L^{-1} $NiCl_2$, 5 g L^{-1} $Na_2WO_4 \cdot 2 H_2O$; 1.5 g L^{-1} $C_6H_9NO_6$; 0.452 g L^{-1} $MnSO_4 \cdot H_2O$; 1 g L^{-1} NaCl; 0.1 g L^{-1} $FeSO_4 \cdot 7 H_2O$; 0.1 g L^{-1} $CoCl_2$; 0.1 g L^{-1} $CaCl_2 \cdot 2 H_2O$; 0.01 g L^{-1} $CuSO_4 \cdot 5 H_2O$; 0.01 g L^{-1} $AlK(SO_4)_2 \cdot 12 H_2O$; 0.018 g L^{-1} H_3BO_3 in deionized water); 5 mL L^{-1} vitamin solution (0.002 g L^{-1} biotin; 0.002 g L^{-1} folic acid; 0.01 g L^{-1} pyridoxine hydrochloride; 0.005 g L^{-1} thiamine hydrochloride; 0.005 g L^{-1} riboflavin; 0.005 g L^{-1} nicotinic acid; 0.005 g L^{-1} DL-calcium pentothenate; 0.0001 g L^{-1} cyanocobalamin, 0.005 g L^{-1} 4-aminobenzoic acid; 0.005 g L^{-1} liponic acid in deionized water) set to a pH value of 7.2 with KOH in deionized water. Kanamycin (50 mg L^{-1}) and L-rhamnose (2.2 g L^{-1}) were added for plasmid maintenance and continuous eGFP expression, respectively. For anaerobic cultivation of *S. oneidensis* 49 mL LM with the addition of disodium fumarate (160 g L^{-1}) as electron acceptor were filled in 250 mL septum flasks degassed with N_2 and pressurized to 1 bar with N_2.

4.2.1.2 Heterotrophic cultivation of *S. oneidensis*

All cultivations were carried out at 30 °C and a shaking frequency of 180 rpm (shaking diameter 25 mm). Initially, an aerobic *S. oneidensis* pre-culture was raised from a cryo stock in LB. A small amount of frozen *S. oneidensis* cells were scratched off with a sterile pipette, suspended in 5 mL LB and incubated for 8 h. Experiments were either produced with an aerobic or an anaerobic pre culture. For the anaerobic pre-cultures 50 µL of the LB grown cells were added to 5 mL aerobic LM and incubated for another 16 h. Finally, 1 mL of the aerobic LM culture was added to 49 mL anaerobic LM in a septum flask and incubated for 24 h. *S. oneidensis* cells were harvested by centrifugation (4000 rpm, 24 °C, 12 min) from the anaerobic LM pre-culture, when an OD_{600} of 0.3 was reached ($2 \cdot 10^8$ cells mL^{-1}). For the production of growth curves and aerobic pre-cultures, 50 µL of the LB grown cells were added to 100 mL LM in 300 mL Erlenmeyer flasks. Cells were harvested at an OD_{600} around 0.65 ($4 \cdot 10^8$ cells mL^{-1}). Subsequently, harvested cells were directly used for electrochemical experiments. Development of substrate and metabolite concentrations during growth were monitored by HPLC as mentioned before (section 3.2.1.2).

4.2.1.3 *Shewanella oneidensis* MR-1: eGFP gene introduction

To examine the cells with a CLSM, a plasmid containing a gene promoting the production of the enhanced green fluorescent protein (eGFP) was transformed into *S. oneidensis*. The plasmid pJeM1 Jeske encoding the eGFP gene under the rhamnose inducable promotor rhaPBAD was transformed into *S. oneidensis* by electroporation with modified regeneration at 30 °C for 2 h under constant shaking (800 rpm) [Choi et al. 2006; Jeske and Altenbuchner 2010]. Recombinant cells were selected on LB agar containing 50 mg L^{-1} kanamycin. The resulting strain was stored at –80 °C in LB containing 25 % (v/v) glycerol [Stöckl et al. 2016].

4.2.2 Flow cell construction

Based on custom-built flow cells previously constructed and successfully tested for biofilm cultivation and microscopy [Schlegel 2016] a graphical 3D model of a flow cell compiling with the requirements mentioned above (section 4.1.1) was designed and can be seen in Figure

32. With outer dimensions of 30 · 23 · 75 mm (w · h · d), the reactor consisted of two chambers separated by a membrane and mounted with 4 screws. Prior to the final construction of a flow cell, 3D prototypes were printed with a 3D printer (Institute of Bioprocess Engineering, University of Kaiserslautern, Germany) in order to optimize electrode positioning, dimensions and spacing under a CLSM. Furthermore, electrical connections of the electrodes were optimized and influences of the CLSM on EIS measurements were excluded in a preliminary abiotic experiment (Figure 39; data not shown). Briefly, the prototype cell was placed on the CLSM stage under an objective and EIS of the redox probe $Fe(CN)_6^{4-}$ was measured in parallel to imaging and movement of the stage in z-direction, respectively.

4.2.2.1 Final PEEK flow cell

Based on the graphical 3D model (Figure 32) findings of the 3D printed prototypes and preliminary experiments, the final flow cell was constructed by the DECHEMA workshop and is presented in section 4.3.2.2. Both chambers (upper WE and lower CE chamber) were made from polyetheretherketone (PEEK) by milling with a 5-axis mill. PEEK was chosen because it is lightweight and autoclavable (see current material tables) as well as biologically compatible [US Food and Drug Administration 2015]. Nozzles of 1.5 mm in inner diameter provided fluid flow in and out of the flow cell. In- and outlet areas in both chambers were conically designed, minimizing dead zones and turbulences. At the bottom of the low chamber (CE-chamber) an 18 · 20 mm (W · L) large platinum sheet (Goodfellow Cambridge Ltd., Huntingdon, England) was installed as counter electrode (CE). Contact to instrumentation was provided by a platinum wire through a lateral bore hole of

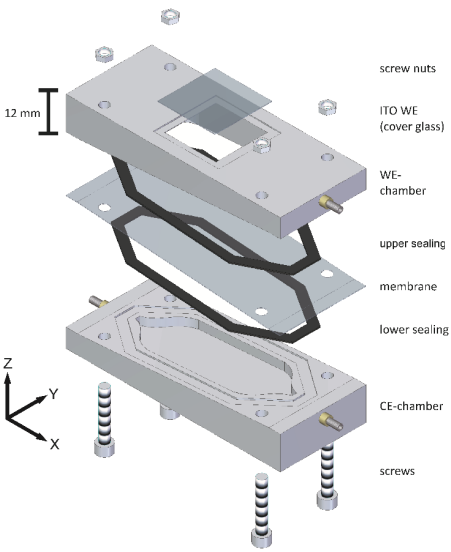

Figure 32: Exploded view of the flow cell in a 3D model [Stöckl et al. 2016].

0.5 mm in inner diameter sealed by silicone (Picodent Twinsil® 22, Picodent® Dental Production & Sales GmbH, Wipperfürth, Germany).

The working electrode (WE) in the WE-chamber consisted of an indium tin oxide (ITO) coated cover glass (20 · 20 · 0.175 mm; 10 Ω cm^{-2}, Precision Glass & Optik GmbH, Iserlohn, Germany), which was glued (Picodent Twinsil® 22) into a rectangular gap on the outer side presenting the conducting side inwards. Resulting surface area of the ITO electrode was 2.89 cm^2. Prior to installation, ITO glasses were rinsed with copious amounts of deionized water and wiped dry with lens tissue. Electrical contact was achieved by a gold foil (Goodfellow Cambridge Ltd., Huntingdon, England) bonded between the chamber housing and the ITO-coated side of the cover glass. Short circuit of the gold foil and electrolyte was avoided by application of silicone.

As reference electrode a platinum wire was positioned as pseudo reference electrode 2 mm below the WE in the WE-chamber through another lateral bore hole with 0.75 mm inner diameter. The platinum wire was inserted and sealed with silicone from the outside of the flow cell.

For sealing of both chambers towards the membrane (Nafion 117, Sigma Aldrich, St. Louis, USA), two gaskets of 0.5 mm thick silicone were embedded between the chamber frame and the membrane. Both chambers were then pressed together by screws. Each chamber (upper WE- and lower CE-chamber) was connected to its own storage vessel by tubing (Norprene® 1.5 mm in inner diameter, Saint-Gobain, Courbevoie, France) and circular fluid transportation was achieved by peristaltic pumping (IPC-N 8 IDEX Health & Science, Lake Forest, USA).

Flow cell conception, printing of 3D prototypes and final construction was conducted in cooperation with Christin Schlegel, Institute of Bioprocess Engineering, University of Kaiserslautern, Germany.

4.2.2.2 Insertion of a Ag/AgCl reference electrode in the flow cell

Based on the evaluation of the experiments the designed flow cell was improved by the introduction of a Ag/AgCl reference electrode [Stöckl et al. 2016]. Therefore, the lateral bore hole and the Pt-wire pseudo reference electrode was replaced by a screw thread and a screw type Ag/AgCl reference electrode (RE-3VT, ALS, Tokyo, Japan).

4.2.3 Electrochemical flow cell characterization

All electrochemical experiments for reactor characterization were performed in an incubation hood (Edmund Bühler GmbH, Tübingen, Germany) at constant temperature of 30 °C. Electrochemical measurements were performed with a Gamry Reference 600 potentiostat (Gamry Instruments, Warminster, USA). The flow cell was equipped with a new ITO WE as working electrode for each experiment. Electrochemical characterization experiments were conducted with the flow cell extended by a screw type Ag/AgCl reference electrode instead of a Pt-pseudo RE.

4.2.3.1 Cyclic Voltammetry with $Fe(CN)_6^{4-}$

Cyclic voltammograms (CV) were performed with 1 mmol L^{-1} potassium hexacyanoferrate in Na_2SO_4 (0.5 mol L^{-1}) in the WE-chamber and Na_2SO_4 (0.5 mol L^{-1}) in the CE-chamber. To avoid chemical oxidation of the dissolved iron (II) anaerobic conditions were ensured in the WE-chamber. Therefore the electrolyte was pumped through at a flow rate of 15 mL min^{-1} and constant N_2 degassing of the WE-chamber storage vessel 30 min before starting the experiment. Subsequently, potassium hexacyanoferrate was added to the WE-chamber. CV measurements were started at open circuit potential (OCP) and first driven to upper vertex potential (E) of +900 mV vs. Ag/AgCl before going to lower vertex potential of –400 mV vs. Ag/AgCl. Scan rate was varied from 1 to 75 mV s^{-1} (step size 1 mV).

4.2.3.2 Electrochemical Impedance Spectroscopy with $Fe(CN)_6^{4-}$

Abiotic EIS measurements for flow cell characterization were performed at the same conditions as described for CV (30 °C, anaerobic, Ag/AgCl RE). As redox probe 10 mM $K_4[Fe(CN)_6]$ in 0.5 M Na_2SO_4 was pumped through the WE-chamber, whereas the CE-chamber was filled with 0.5 M Na_2SO_4 electrolyte. Potentiostatic EIS was performed in a frequency range from 100 kHz to 50 mHz, an amplitude of 10 mV root mean square (rms) and 10 points per decade at an OCP of +125 mV vs. Ag/AgCl. Pumping of

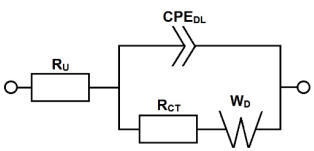

Figure 33: Equivalent electrical circuit for fitting of EIS data obtained from flow cell characterization; R_U: solution resistance; R_{CT}: charge transfer resistance, CPE_{DL}: double layer constant phase element; W_D: Warburg diffusion.

the electrolytes was stopped meanwhile. EIS data were fitted with the equivalent electrical circuit shown in Figure 33, as stated for this reaction before [Ende and Mangold 1993], with: solution resistance (R_U), charge transfer resistance (R_{CT}), double layer constant phase element (CPE_{DL}) and a Warburg diffusion element (W_D).

4.2.4 Simultaneous Electrochemical Impedance Spectroscopy and Confocal Laser Scanning Microscopy

To demonstrate the functionality of the designed flow cell *S. oneidensis* was applied as model organism and the ITO WE was polarized as anode, using the flow cell as MFC.

4.2.4.1 Current and EIS measurements

For the detection of bacterial adhesion on the ITO WE, the flow cell was run in MFC mode. Therefore the whole set up was mounted under sterile conditions. After installation of the ITO WE, (section 4.2.2.1) into the WE-chamber, the two flow cell chambers were heat-sterilized at 80 °C for at least 2 h. The residual parts, namely two storage vessels, tubing, membrane and silicone gaskets were sterilized by autoclaving. Finally, all parts were assembled in a clean bench. 60 mL of 0.5 M Na_2SO_4 or LM (section 4.2.1.1) were filled aseptically into the CE- or WE-chamber, respectively.

Tempered fluids were pumped through the flow cell as bypass of the storage vessels with a peristaltic pump. Flushing of the WE storage vessel with N_2 was started 30 min before the experiment at flow rates of 5 mL min^{-1} to provide anaerobic conditions in the WE-chamber. All electrodes were connected via alligator clips to the potentiostat.

Subsequently, the polarization and EIS measurement routine were started. A potential of +198 mV vs. Pt was applied at the WE, corresponding to a potential of +400 mV vs. a Ag/AgCl reference electrode. The first EIS measurement was performed after 20 min of polarization. EIS was potentiostatically measured at +198 mV vs. Pt. The frequency range varied between 100 kHz and 50 mHz with an amplitude of 10 mV rms and 10 points per decade. With increasing experimental time intervals between the EIS measurements were increased.

Harvested cells of *S. oneidensis* from anaerobic pre-culture (section 4.2.1.2) were added to the WE storage vessel 40 min (arrow in Figure 46 and Figure 47, section4.3.4.1) after starting

the polarization and EIS measurement routine to reach a calculated OD_{600} of 0.1 ($5 \cdot 10^7$ cells mL^{-1}).

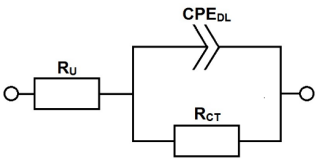

Figure 34: Equivalent electrical circuit for fitting of EIS data obtained from MFC mode operation; R_U: solution resistance; R_{CT}: charge transfer resistance, CPE_{DL}: double layer constant phase element.

EIS measurements performed during MFC operation were fitted with the Randle´s type equivalent circuit, given in Figure 34, that has already been reported before for anodic bacterial adhesion to electrodes; [Srikanth et al. 2008; Ramasamy et al. 2008; Ha et al. 2010]. R_{CT} values for the WE were calculated with Gamry Echem Analyst software (Gamry Instruments, Warminster, USA) in simplex mode.

4.2.4.2 Confocal Laser Scanning Microscopy

During the first hour after inoculation with *S. oneidensis* every 10 min and before and after each EIS measurement confocal microscopic xy-images of adherent cells on a 110 · 110 µm large area of the ITO WE were taken by a Leica TCS SP5 II (Leica Microsystems GmbH, Wetzlar, Germany) with SuperZ galvanometric stage (Märzhäuser Wetzlar GmbH & Co. KG, Wetzlar, Germany) and LAS AF software (Leica Microsystems GmbH, Wetzlar, Germany). Additionally equipped with an incubation hood (THE CUBE 2, Life Imaging Services, Basel, Swiss), the complete cultivation system including the storage vessels and the microscope and the flow cell was tempered at 30 °C. Due to expression of eGFP, no staining of the bacteria was required for detection. Nevertheless, pumping was paused during imaging to avoid movement of the ITO WE in z-direction caused by hydraulic pulsation of the peristaltic pump. Using a HCX PL APO CS water-immersion objective (N.A. 1.2; cover glass 0.14–0.18 mm; free working distance 0.22 mm; LEICA MICROSYSTEMS GMBH, Wetzlar, Germany), laser output power (Argon, visible) was set to 14 %. Power of AOTF for an excitation wavelength of 488 nm was adjusted to 15 % intensity and 1 AU was chosen as pinhole size. Furthermore, a RSP 500 excitation beam splitter was used and PMT detected fluorescence at an emission bandwidth of 500–600 nm as well as a scanning speed of 400 Hz. With increasing experimental time, image stacks in xyz scan mode were taken to make biofilm thickness visible as well. Therefore a step size of 0.13 µm was applied. Cell counting was done manually with a LAS AF draw counter (Leica Microsystems GmbH, Wetzlar, Germany).

4.2.5 Application as MFC with inserted Ag/AgCl reference electrode

As already mentioned in section 4.2.2.2, the Pt-pseudo reference electrode was replaced by a screw type Ag/AgCl reference electrode [Stöckl et al. 2016]. To demonstrate the influence of the improved cell design on current and EIS measurements, the experiments described in section 4.2.4 were repeated, but without the imaging process under the CLSM.
All other experimental conditions remained the same.

4.3 Results

4.3.1 Aerobic heterotrophic growth by *S. oneidensis*

Growth of *S. oneidensis* was observed initially under anaerobic heterotrophic conditions to characterize the organism under standard conditions for the preparation of pre-cultures for the cultivation under electrochemical conditions.

Bacterial cells were cultivated during approximately 70 h until the stationary phase was reached (Figure 35). Optical density (OD_{600}) was used to monitor growth in parallel pH, substrate consumption (Figure 35) and concentration of metabolites excreted during growth (Figure 36). Correlation between cell concentration and total cell count and OD_{600} ($y = 5.485 * 10^8 x$; $R^2 = 0.995$) can be found in Figure 37.

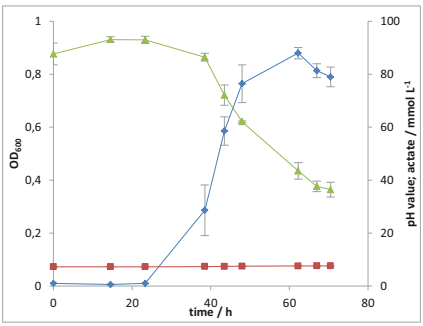

Figure 35: Growth for *S. oneidensis* under standard aerobic heterotrophic cultivation (minimal medium + lactate; aerobic; 30 °C, shaking 180 rpm). Left y-axis: OD_{600} (—◆—); right x-axis: pH (—■—) and lactate (—▲—, in mmol L^{-1}). Mean values of three biologically independent cultures are given with standard deviations presented in grey error bars.

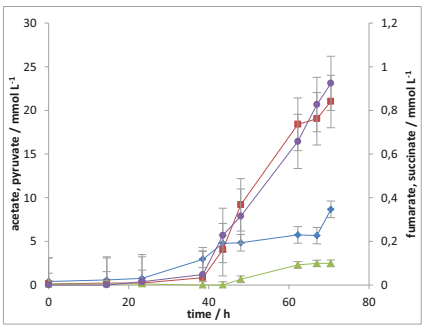

Figure 36: Metabolite concentrations by *S. oneidensis* under standard aerobic heterotrophic cultivation (minimal medium + lactate; aerobic; 30 °C, shaking 180 rpm). Left y-axis: acetate (—◆—) and pyruvate (—■—, in mmol L^{-1}); right y-axis: fumarate (—▲—) and succinate (—●—, in mmol L^{-1}). Mean values of three biologically independent cultures are given with standard deviations presented in grey error bars.

Growth of *S. oneidensis* was characterized initially by a log phase of approximately 24 h, followed by the exponential growth phase. The stationary phase started after 62 h with a maximum OD_{600} of 0.88 ($5 \cdot 10^8$ cells mL^{-1}). At the end of growth monitoring the bacterial cell density was slightly decreased to an OD_{600} of 0.79 ($4 \cdot 10^8$ cells mL^{-1}). The pH increased slightly in the HEPES buffered system from initially 7.3 to 7.6 at the end of the experiment.

Lactate concentration decreased analogous to the increased cell concentration. However, substrate depletion did not occur, since 36.4 mmol L^{-1} lactate were still present at the end of the experiment. All identified metabolites show rising values until the end of the experiment, indicating that cells were still metabolically active. Pyruvate was the main product excreted by *S. oneidensis* with a final concentration of 21.0 mmol L^{-1}, followed by acetate with 8.7 mmol L^{-1}, and succinate and fumarate with minor concentrations of 0.9 mmol L^{-1} and 0.1 mmol L^{-1}, respectively.

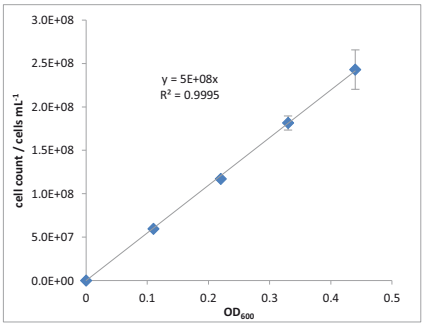

Figure 37: Calibration curve for the correlation between the total cell count with a Neubauer-chamber and the optical density (OD_{600}). Given are mean values of three biologically independent cultivations with standard deviations presented in grey error bars.

4.3.2 Flow cell construction

Towards the production of a flow cell for simultaneously coupled impedance spectroscopy and confocal laser scanning microscopy, a graphical 3D model was designed (section 4.2.2, Figure 32). 3D-printed prototypes were constructed and finally the custom made flow cell was milled from PEEK.

4.3.2.1 Prototypes

Figure 38 illustrates three 3D-printed prototypes leading towards the final PEEK version. Construction was started with a rudimentary prototype (A) matching the outer dimension of the final cell, but with no conical fluid inlet and a deepening in the lower chamber for the CE. The second prototype (B) was already characterized by conical fluid channels and the final prototype (C) was additionally equipped with working and counter electrodes. The deepening in the lower chamber was removed due to the small dimension of the installed Pt-CE.

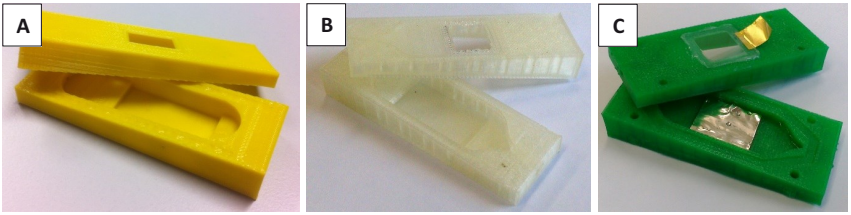

Figure 38: 3 models (images A – C)of 3D-printed prototypes leading to the final flow cell (PEEK version for simultaneous EIS and CLSM).

In Figure 39 the final prototype (Figure 38 C) is presented preliminary abiotic experiments. The flow cell fitted on the microscope stage (Figure 39 A) and the transparent ITO electrode could be accessed with the objective of the microscope without influencing electrical contact of the flow cell with the potentiostat (Figure 39 B). Simultaneously run EIS and CLSM measurements with the redox probe $Fe(CN)_6^{4-}$ did not show any influence on each other (results not shown). However, pumping of the electrolyte was found to interfere with image acquisition due to movement of the ITO WE caused by hydraulic a pulsation of the peristaltic pump.

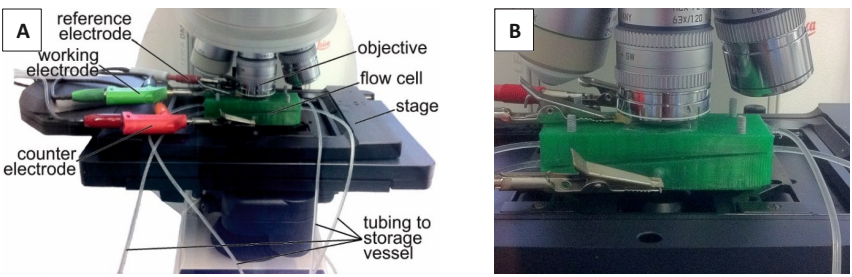

Figure 39: Photographs of the final 3D printed prototype of the flow cell under the CLSM connected to an potentiostat (A) and a more detailed image of the prototype placed under the CLSM objective (B).

4.3.2.2 Flow cell made from PEEK

As mentioned before, the final flow cell was made from PEEK, which is lightweight and autoclavable (see current material tables) as well as biologically compatible [US Food and Drug Administration 2015]. Furthermore, it is advantageous over conventional metallic materials for reactor construction, because of being electrically insulating. Photographs of the respective chambers are presented in Figure 40, as well as the mounted flow cell in Figure 41.

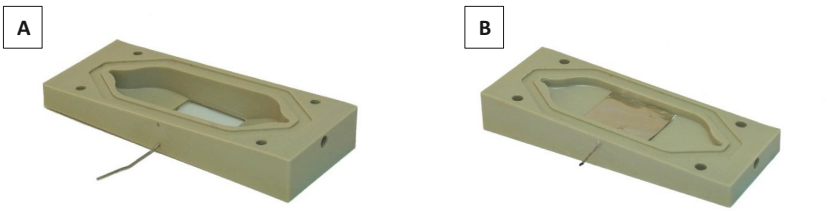

Figure 40: Photographs of the interior of the upper working electrode chamber (A) and the lower counter electrode chamber (B). Pt-pseudo reference electrode wire can be seen in (A) as well as the installed Pt counter electrode (B).

The image of the upper WE chamber shows the installed Pt-pseudo reference electrode wire (Figure 40 A), which was replaced by a screw type Ag/AgCl reference electrode for the final experiments presented in this chapter (section 4.3.5). Milled gaps ensuring the positioning of the silicon gaskets as well as bores for the screws can be seen in images A and B. Furthermore, the gold foil, responsible for the electrical connection of the ITO WE can be found in Figure 41 of the mounted and ready to use flow cell. Finally, the flow cell extended by a Ag/AgCl RE is shown in Figure 41.

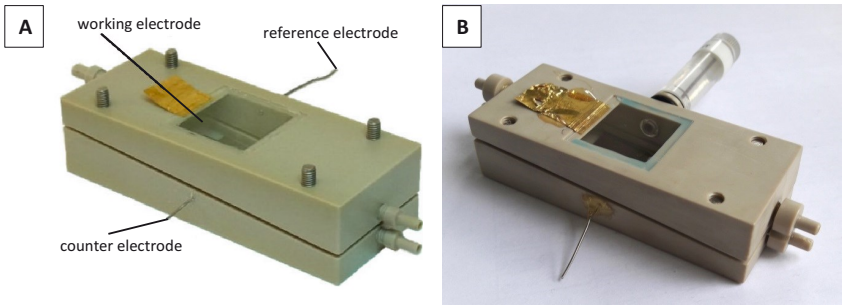

Figure 41: Photographs of the completely mounted flow cell made from PEEK with the installed ITO WE and gold foil for electrical contact, Pt-pseudo RE, CE, and nozzles for tubing connection (A). Image B shows the advanced version of the flow cell upgraded by a Ag/AgCl RE.

4.3.3 Electrochemical flow cell characterization

Cyclic Voltammetry and Electrochemical Impedance Spectroscopy of the model redox couple iron(II)/iron(III) were recorded to demonstrate the applicability and quality of the custom-built flow cell.

4.3.3.1 Cyclic Voltammetry with $Fe(CN)_6^{4-}$

In addition to the EIS measurements (section 4.3.3.2) also CV measurements of the redox probe iron(II) ($Fe(CN)_6^{4-}$) were conducted to demonstrate the applicability of the flow cell for electrochemical measurements. Figure 42 shows the resulting voltammograms obtained with 1 mmol L^{-1} potassium hexacyanoferrate in Na_2SO_4 (0.5 mol L^{-1}) in the flow cell at different scan rates. The shape of the curve is typical for an iron(II) / iron(III) system, with an oxidation peak at a potential around +300 mV vs. Ag/AgCl and the corresponding reduction peak around +100 mV vs. Ag/AgCl. The peak potential difference (ΔE_p) thereby strongly depends on the scan rate and increased with increasing scan rate. At a scan rate of 1 mV s^{-1} ΔE_p was at 98 mV and increased to 158, 200, 243, and 274 mV for scan rates of 10, 25, 50 and 75 mV s^{-1}, respectively. Peak current ratios between the oxidation and reduction peak range around 1.13 and 1.24 for the respective scan rates indicating that the oxidation reaction is slightly favored, eventually resulting from residual oxygen in the system. The

linear regression of the peak currents over the square root of the corresponding scan rate presented in Figure 43 show that the redox reaction at the electrode surface is diffusion limited.

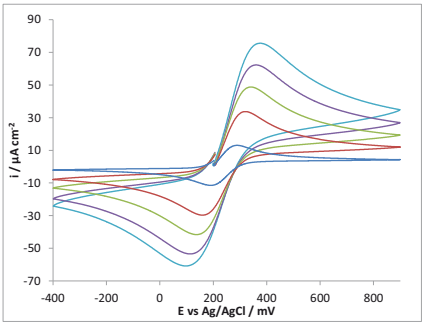

Figure 42: Cyclic voltammograms of $K_4[Fe(CN)_6]$ (1 mmol L^{-1} in 0.5 M Na_2SO_4)at ITO WE installed into the CLSM EIS flow cell; scan rates are 1 (—■—), 10 (—■—), 25 (—■—), 50 (—■—) and 75 mV s^{-1} (—■—); step size: 1 mV.

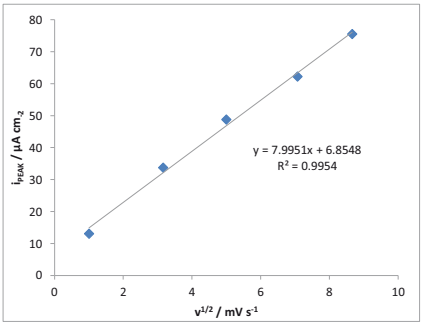

Figure 43: Linear regression of peak currents over square root of scan rate.

4.3.3.2 Electrochemical Impedance Spectroscopy

Results from EIS measurements of 10 mmol L^{-1} potassium hexacyanoferrate in Na_2SO_4 (0.5 mol L^{-1}) are shown in Figure 44 and Figure 45. The Nyquist plot shows the shape of a semicircle in the range of high frequencies to approximately 2 Hz, which is typically indicating kinetically controlled reactions in this frequency range. From 250 to 50 mHz a typical Warburg diffusion line is given for diffusion controlled kinetics in this range [Sundfors et al. 2002]. Furthermore, the angle between total impedance and the y-axis of 45.12 ° is very close to the theoretical value of 45 ° [Ende and Mangold 1993]. Application of the equivalent electrical circuit given in Figure 33 resulted in a reasonable fit with: R_U = 6.50 Ω, R_{CT} = 3.777 kΩ, CPE_{DL} = 10.52 µF s^{α} with an α of 0.918 and a Warburg diffusion (W_D) of 288.7 µS $s^{1/2}$. Furthermore, Bode plot and phase angle of the obtained data given in Figure 45 indicate only one time constant, which is integrated in the applied equivalent circuit (Figure 33).

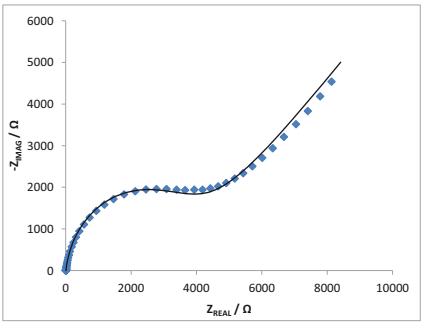

Figure 44: Nyquist plot of EIS measurement of 10 mM $K_4[Fe(CN)_6]$ in 0.5 M Na_2SO_4 with ITO WE installed in the flow cell. Data points (◆) are presented with the corresponding fit (————).

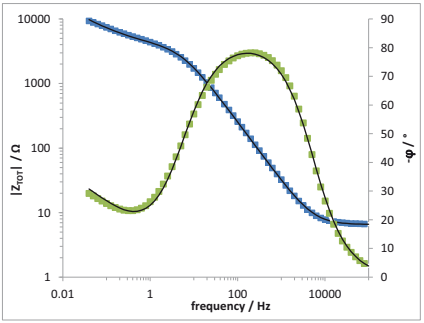

Figure 45: Bode plot of EIS measurement of $K_4[Fe(CN)_6]$ in Na_2SO_4 with ITO WE installed in the flow cell. Data points for total impedance (Z, ■) and phase shift (φ, ■) are presented with the corresponding fits (————).

4.3.4 Simultaneous Electrochemical Impedance Spectroscopy and Confocal Laser Scanning Microscopy in Microbial Fuel Cell Mode

This experiment was performed to demonstrate the applicability of the custom-built flow cell for the electrochemical monitoring of microbial activity and adhesion via chronoamperometry and EIS combined with the simultaneous imaging of adhered biomass on the ITO WE via CLSM.

4.3.4.1 Current and electrochemical impedance spectroscopy measurements

Running the flow cell in MFC mode produced a typical current curve (Figure 46) of a MFC. After addition of *S. oneidensis* to the WE storage vessel (arrows in Figure 46 and Figure 47) a current increase was observed. Within 30 min a current density of 0.35 µA cm^{-2} was reached and after approximately 5 h the current stabilized at around 0.52 µA cm^{-2} for the further time course of the experiment. Current peaks after 12, 14 and 17 h of operation are the result of gas bubbles in the WE-chamber as well as their subsequent removal by slight movement of the flow cell. Missing data points of the current curve result from EIS measurements, where current could not monitored simultaneously.

Calculated charge transfer resistance (R_{CT}) from EIS measurements during MFC mode was plotted together with current density over time in Figure 46.In the beginning of the experiment R_{CT} increased after addition of *S. oneidensis* from 292 kΩ in the abiotic system to a maximum of 390 kΩ 59 min later. This had been observed also in prior experiments without the use of the CLSM (data not shown). Subsequently, the R_{CT} decreased constantly to a value of 120 kΩ after 17 h of operation.

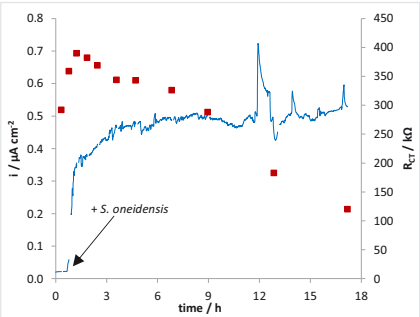

Figure 46: Current density (i, ——) and charge transfer resistance (R_{CT}, ■) obtained from EIS measurements (Figure 48 and Figure 49) of the flow cell polarized (+198 mV vs. Pt) as MFC (substrate: lactate; 30 °C). Black arrow indicates the inoculation with *S. oneidensis* into the WE storage vessel of the polarized ITO WE.

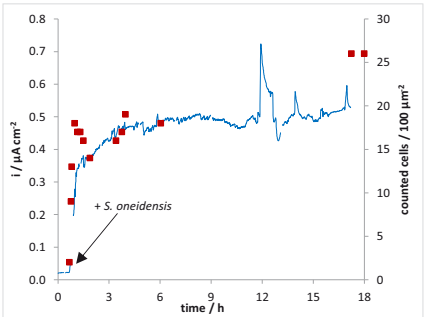

Figure 47: Current density (i, ——) and cell count (■ obtained from CSLM images in Figure 50) of the flow cell polarized (+198 mV vs. Pt) as MFC (substrate: lactate; 30 °C). Black arrow indicates the inoculation with *S. oneidensis* into the WE storage vessel of the polarized ITO WE

Representative EIS measurements before (18 min) and after (59 min and 17h) the addition of *S. oneidensis* cells to the WE chamber are given in Figure 48 and Figure 49.

The Nyquist diagram (Figure 48) displays a semicircle pattern for all curves with different sizes of the circle for the respective points of time. The widest semicircle was measured 59 minutes after inoculation, followed by the measurement of the abiotic system (18 min before inoculation) and the smallest pattern after 17 h of operation. These findings match with the R_{CT} values obtained from the fitting procedure with the equivalent circuit (Figure 34), illustrating an initial increase after addition followed by a subsequent decrease.

The frequency dependent phase angle (φ), shown in Figure 49, confirms the employed electrical equivalent circle (Figure 34) with only one time constant (CPE_{DL}). Differences in the

curves are not as remarkable as in the Nyquist diagram. However, the phase angle of the final EIS measurement shows a clear decrease at reduced frequencies.

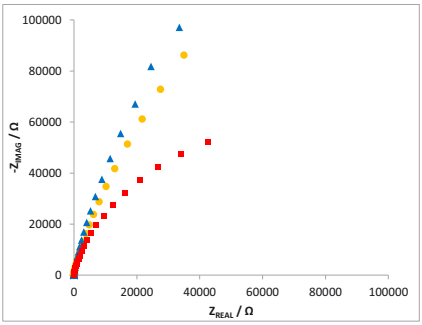

Figure 48: Nyquist presentation of representative EIS measurements during MFC operation (substrate: lactate; 30 °C). Given are measurements before (18 min ●) and after (59 min ▲ and 17 h ■) addition of *S. oneidensis* to the WE chamber system.

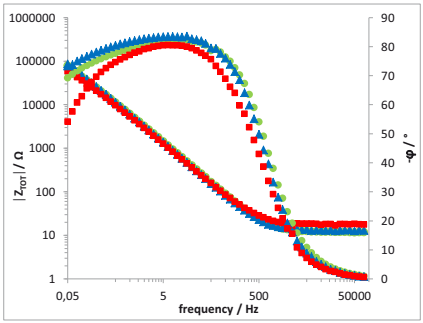

Figure 49: Bode presentation of representative EIS measurements during MFC operation (substrate: lactate; 30 °C). Given are measurements before (18 min ●) and after (59 min ▲ and 17 h ■) addition of *S. oneidensis* to the WE chamber system.

4.3.4.2 Confocal laser scanning microscopy images

CLSM images taken directly after inoculation of the cells to the WE storage vessel parallel to the EIS measurements are shown in Figure 50.At 0 h the addition of *S. oneidensis* to the WE storage vessel took place. The images display that already 5 min after inoculation bacteria adhered to the ITO WE. Though, no ordered spatial orientation of the cells was detected. 5 min later, the number of adherent cells had more than quadrupled. In many positions, a parallel alignment of up to 4 cells can be seen (see circular indication in Figure 50). With increasing experimental time the number of cells on the electrode surface increased, resulting in a dense layer of cells. However, the electrode did not become covered completely. Furthermore, a multilayer arrangement of the biofilm was also not visible at the end of the experiment. The arrangement can rather be described as a monolayer. Darker regions in the upper right of the images indicate a small slope of the ITO WE during the imaging process originating from the gold foil installed between the ITO WE and the WE chamber made from PEEK.

Changes of cell numbers quantified by counting are summarized graphically in combination with the current density in Figure 47. From inoculation up to 23 min the cell number was

increasing to 18 cells per 100 µm². Thereafter, a decrease to 14 cells per 100 µm² in cell count is observable until 77 min. Obviously, many cells detached from the WE again. This was accompanied with a less steep increase in current production. However, the majority of the cells attached irreversibly and started to form an electroactive layer. In the following, the cell count increased up to 26 cells per 100 µm² at 17 h showing a consolidation of the culture with experimental duration. This matched the pattern of the increasing current density curve (Figure 47).

To summarize, EIS and current measurements as well as CLSM imaging were successfully applied to show that the custom-built flow cell allows online biofilm monitoring of electroactive microorganisms.

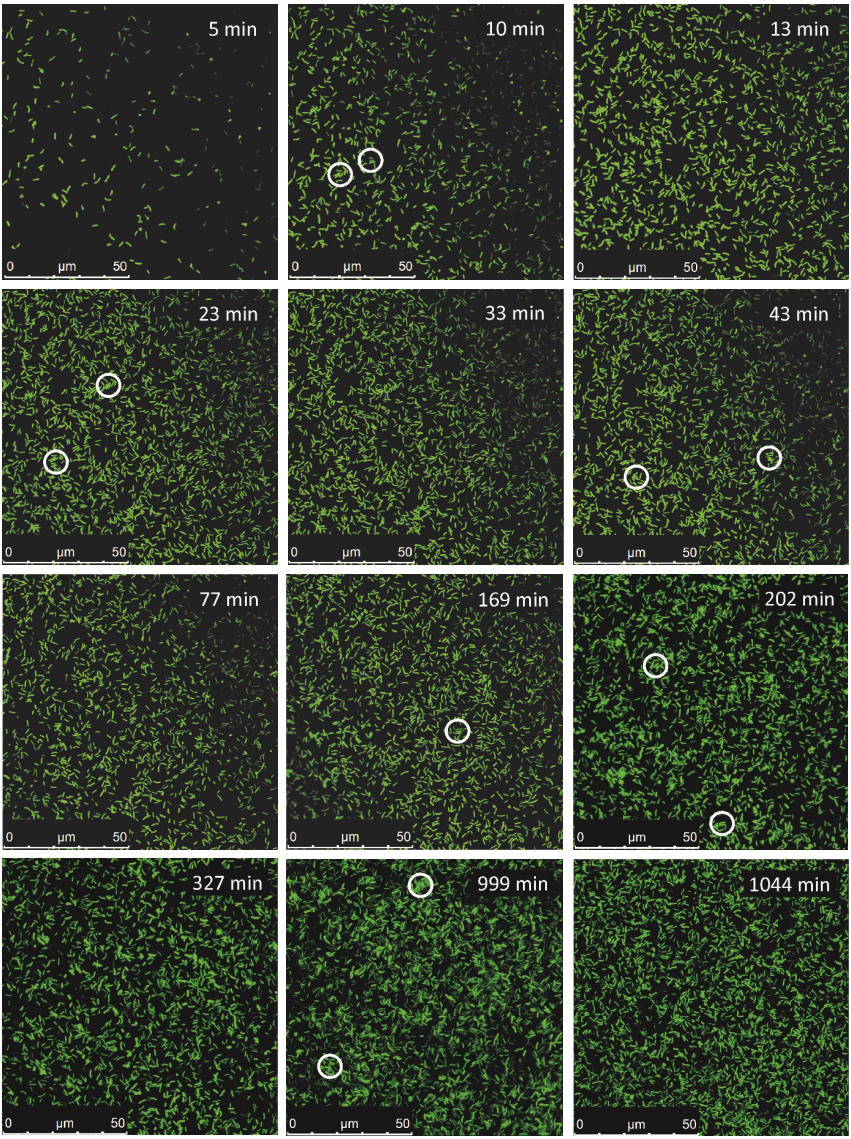

Figure 50: CLSM images of adherent *S. oneidensis* cells after inoculation and in parallel to EIS measurements (flow cell; MFC mode; WE polarized to +198 mV vs. Ag/AgCl; substrate: lactate; 30 °C,). Circles mark parallel alignment of cells on the surface of ITO WE [Stöckl et al. 2016].

4.3.5 Application of flow cell as MFC with inserted Ag/AgCl reference electrode

An extension of the flow cell by a screw type Ag/AgCl reference electrode and the subsequent application as MFC with *S. oneidensis* produced results comparable to those presented before with a Pt-pseudo reference electrode. However, the pattern of the current density curve as well as impedance data appear with significantly better signal to noise ratio compared to the current density curve with a Pt-pseudo RE (section 4.3.4). Data are displayed in Figure 51 to Figure 54. Similar to the system with a Pt-pseudo reference, directly after inoculation of cells to an OD_{600} of 0.1 ($5 \cdot 10^7$ cells mL^{-1}), a current production was observed as shown in Figure 51. Current density increased rapidly, but less rapid than in the experiments using a flow cell with a Pt-pseudo RE.

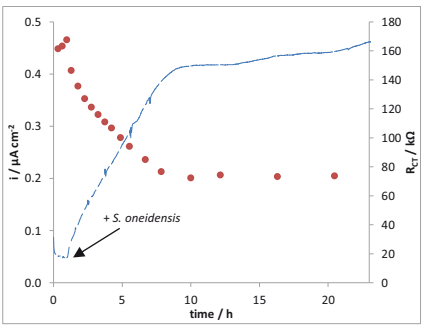

Figure 51: Current density (i ——) and charge transfer resistance (R_{CT} ●) from measurements in Figure 53 and Figure 54 with *S. oneidensis* in a flow cell improved with a Ag/AgCl reference electrode. Black arrow marks inoculation of cells into WE chamber system of the MFC (substrate: lactate; 30 °C).

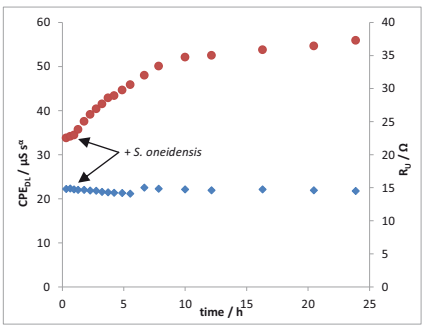

Figure 52: Double layer constant phase element capacity (CPE_{DL} ●) and solution resistance (R_U ◆) from measurements in Figure 53 and Figure 54 with *S. oneidensis* in a flow cell with a Ag/AgCl reference electrode. Black arrow marks inoculation of cells into WE chamber system of the MFC (substrate: lactate; 30 °C).

Current density reached a plateau of 0.42 µA cm^{-2} after approximately 9 h, whereas in the previous experiment with a Pt-pseudo RE it needed 5 h. Subsequently, the current density increased only slightly to a final value of 0.48 µA cm^{-2},similar to the previous experiment with the Pt-pseudo RE (0.52 µA cm^{-2}, section 4.3.4).

The course of the charge transfer resistance displayed exactly an opposite pattern to the one of the current density (Figure 51). Again, an initial increase in R_{CT} from 161.4 to 167.6 kΩ was

observed after the addition of the cells, followed by a rapid decrease to a plateau around 72 kΩ after 10 h. In contrast to the current density, R_{CT} was not lowered further during the following time course. Additionally to the calculated R_{CT} values, values for double layer capacitance from constant phase element (CPE_{DL}) and solution resistance (R_U) are presented in Figure 52. R_U remained constant between 14.09 and 15.01 Ω throughout the whole experiment, whereas the CPE_{DL} increased with a similar pattern as observed for the current density from 33.80 to 52.11 µS s^{α} after 9 h and further to 55.91 until the end of the experiment. The α-value for the CPE_{DL} remained constant between 0.891 and 0.898 throughout the whole experiment.

A selection of the corresponding single EIS measurements can be found in Figure 53 and Figure 54. Nyquist presentation is given in Figure 53, whereas Figure 54 shows Bode presentation of the respective measurements. The pattern of the curves were similar to those described before and confirm the application of the equivalent circuit described in Figure 34 [Stöckl et al. 2016].

In the Nyquist diagram a minor extension of the semicircle was observed after cell addition (10 min), before smaller semicircles were obtained with increasing experimental time indicating the R_{CT} decrease. In the Bode diagram, the decrease of the total impedance can be seen over time as well as a small decrease in phase shift at low frequency.

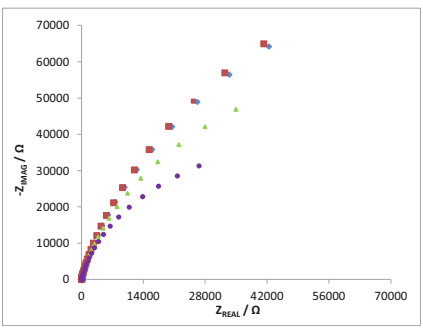

Figure 53: Nyquist presentation of representative EIS measurements during MFC operation of a flow cell (substrate: lactate; 30 °C) with *S. oneidensis* and implemented Ag/AgCl reference electrode. Given are measurements before (50 min ◆) and after (10 min ■, 3 ▲ and 23 h●) inoculation with *S. oneidensis* to the WE chamber system.

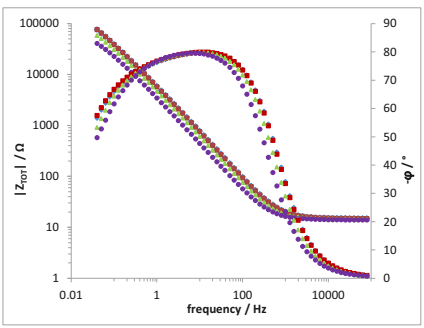

Figure 54: Bode presentation of representative EIS measurements during MFC operation of a flow cell (substrate: lactate; 30 °C) with *S. oneidensis* and implemented Ag/AgCl reference electrode. Given are measurements before (50 min ◆) and after (10 min ■, 3 ▲ and 23 h●) inoculation with *S. oneidensis* into the WE chamber system of the MFC

4.4 Discussion and Conclusions

The development of a membrane separated flow cell, which enables simultaneous EIS and CLSM measurements for the detection of electro-active bacteria and their surface attachment, was demonstrated successfully in this study.

4.4.1 Flow cell construction

The requirements for the construction of a flow cell to simultaneously apply EIS and CLSM for biofilm monitoring were:

I. Applicability as a bioelectrochemical system (e.g. microbial fuel cell)
II. Enabling continuous and non-destructive in-situ microscopy for the characterization of cell attachment or biofilm growth on the electrode surface
III. Suitable design for EIS measurements and further electrochemical measurements such as cyclic voltammetry
IV. Separated working and counter electrode (two chamber system in order to separate the electrodes, electrochemically formed products and corresponding electrolytes)

The applicability of the flow cell as bioelectrochemical system **(I)** has been shown in sections 4.3.4 and 4.3.5. The flow cell was polarized as microbial fuel cell and *S. oneidensis* was cultivated electrochemically with electrode respiration and consequent current generation. The flow cell was made from polyetheretherketone (PEEK), which is lightweight and autoclavable as well as biologically compatible and electrically insulating. However, the design is not optimal for a MFC demonstrated by the relatively low current densities, resulting mainly from the 2D morphology of the indium tin oxide working electrode.
Continuous and non-destructive in-situ microscopy to monitor cell attachment to the electrode surface **(II)** was successfully demonstrated by the performed CLSM imaging presented in Figure 50. Employing a transparent WE allowed the formation of an electroactive biofilm on the inwards facing side of the conducting cover glass, which could be examined by CLSM at any time without influencing microbial activity.

CV and EIS measurements with the ferrocyanide redox probe in the custom-built flow cell proved that this construction is suitable for electrochemical experiments, as it was stated in requirement (**III**). Peak potential differences ranged at 158 and 200 mV for scan rates of 10 and 25 mV s^{-1}, indicating less optimal electron transfer kinetics at the electrode material, an increased IR drop or non-ideal flow cell geometry , than reported by Zudans for the same redox reaction at an ITO WE (ΔE_{PEAK} = 160 mV, scan rate = 20 mV s^{-1}) [Zudans et al. 2004].

Separation of the working and the counter electrode by a membrane as final requirement (**IV**) was successfully proven, since both CV and EIS measurements with iron(II) showed reasonable results. Furthermore, the CE chamber system in MFC-mode remained sterile in all experiments with *S. oneidensis*. This indicates that changes in current, EIS or cell count on the electrode exclusively result from the WE and are not influenced by the CE.

Finally, the implementation of a screw type reference electrode instead of the Pt-pseudo reference electrode wire further improved the flow cell design. Both current density and charge transfer resistance curves produced with *S. oneidensis* in MFC mode showed a more constant and less error-prone pattern. General trends remain equal to the data obtained with the pseudo RE, but precision and reliability were improved significantly with the Ag/AgCl reference electrode.

4.4.2 Simultaneous Electrochemical Impedance Spectroscopy and Confocal Laser Scanning Microscopy in the Microbial Fuel Cell Mode

Running the flow cell in MFC mode produced a typical MFC current curve (Figure 46) as reported [Cho and Ellington 2007; Roy et al. 2014]. Directly after inoculation the current increased and reached a plateau after 5 h. The fast current stabilization, compared to the H-cell systems employing *G. sulfurreducens* for example (section 3.3.2), can be explained by the planar and small WE surface and high cell concentration of the inoculum. On one hand the current increase is assumed to originate from cell attachment and on the other hand from mediator excretion by *S. oneidensis* [Marsili et al. 2008; Brutinel and Gralnick 2012]. A precise differentiation between bacterial cells that contribute to current production via DET from cells using a mediator for electron shuttling might be possible with our flow cell in future studies. The amount of cells respiring by DET can be determined by microscopy,

whereas mediator concentration and planktonic cells may be quantified from the aqueous phase.

The observed general decrease of R_{CT} with the maturation of an electroactive culture on the electrode surface has been measured before and was explained as activation loss due to increased biocatalyst density [Ramasamy et al. 2008]. However, to the best of the authors knowledge, the initial increase of R_{CT} after inoculation with *S. oneidensis* in an MFC has not been described in literature so far. One possible explanation may be that even with an electron transfer of *S. oneidensis* to the electrode the initial attachment could lead to a short term blocking of the electrode surface [Stöckl et al. 2016]. Initial electron transfer from the bacteria to the electrode might be of mediated nature, such as it has been reported for *S. oneidensis* [Marsili et al. 2008]. Cells on the electrode surface might then rather block electrode kinetics, leading to a short increase of R_{CT}. With increasing time, the direct electron transfer mechanism of *S. oneidensis* is supposed to become involved increasingly [Xiong et al. 2006]. Hence, electrode kinetics are elevated, which might lead to a decrease of R_{CT}. Especially for the understanding of initial attachment of *S. oneidensis* and the initially increasing R_{CT} values further studies with the flow cell may give more information and a deepened understanding.

CLSM images taken in parallel to the above mentioned EIS measurements and chronoamperometry showed a fast cell attachment to the electrode and constant coverage of the WE surface after 17 h of operation. However, morphology and thickness of the biofilm still have to be described as a monolayer. Since *S. oneidensis* is known for the formation of monolayers/thin biofilms under anaerobic conditions, no thick and multilayered biofilm was expected [Rosenbaum et al. 2010]. Furthermore, a parallel alignment of up to 4 cells was detected. Synergistic effects may be one possible reason for that, since if two cells are not only attached to the WE but also to each other this may cause an overall increased binding strength at this certain attachment point resulting in decreased shear stress for a single cell. Cell division of adherent cells was not observed, but will occur also. However, it is assumed that the majority of the sessile cells attached from the planktonic phase, since the starting cell number was relatively high ($5 \cdot 10^7$ cells mL^{-1}) and that these cells were in the lag-phase.

Summarizing, a flow cell for simultaneous electrochemical impedance spectroscopy and confocal laser scanning microscopy was designed and employed successfully with the

electroactive model organism *S. oneidensis* as a microbial fuel cell. Abiotic EIS and CV measurements with the model molecule iron(II) demonstrate that reliable electrochemical measurements can be performed. A general decrease of the R_{CT} was observed with an increased current production and an increasing cell number on the WE electrode surface under MFC conditions.

Biofilm formation of *S. oneidensis* has been observed in numerous studies, also with EIS or CLSM. However, to the best of the author's knowledge no simultaneous application of these two methods has been reported so far. The development of the custom-built flow cell will allow the investigation of less studied and established electro-active bacteria or mixed species biofilms. With this powerful combination of two noninvasive methods, a monitoring tool is presented, which will give interesting insights in the biofilm formation process of mixed and cocultures, e.g. by different staining procedures. Furthermore, an interpretation of EIS measurements is significantly improved by the simultaneous imaging with CLSM. This allows a deepened insight into mechanisms of bacterial adhesion to electrodes and extracellular electron transfer.

5 Development of magnetic electrode particles

5.1 Introduction

In 1983 Stirling already pointed out five key challenges that have to be overcome to obtain optimum yields of power output from a MFC [Stirling et al. 1983]. Besides the selection of fuel and organism (1), the development of a high performance cathode (2), the identification of redox mediators (3) and the rapid reversible mediator oxidation (4), the improvement of the cell design (5) was identified as a crucial factor for the establishment of BES. Even though these limiting factors were pointed out more than 30 years ago, most of them are still valid. When focusing on the industrial application of BES, scaling-up and the selection of a reactor system are essential. Thereby, an adequate electrode surface-to-volume ratio was identified as one limiting factor, since the productivity directly depends on the electrode surface [Krieg et al. 2014]. Different reactor designs have been already reviewed [Krieg et al. 2014] and problems of scale-up were discussed [Janicek et al. 2014].

5.1.1 Electrochemical fluidized bed reactor

Concerning a high electrode surface-to-volume ratio (specific electrode surface area), electrochemical fluidized bed reactors represent a promising approach. In general, fluidized bed reactors are comprised of a particulate material, which is kept in suspension in the reactor by an inflowing gas or a liquid stream with high velocity. Biological or chemical reactions are catalyzed on the surface of the suspended material. The catalyst density in this type of reactor is smaller compared to packed bed reactors, but characterized by an increased homogeneity due to uniform particle mixing, reduced temperature gradients and decreased formation of dead zones.

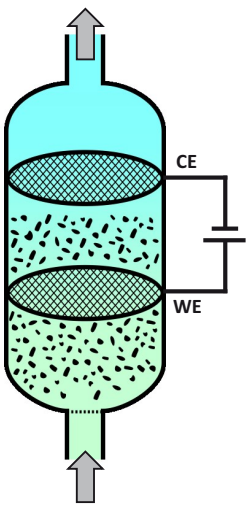

Figure 55: Schematic illustration of an electrochemical fluidized bed reactor. Current collectors of the working (WE) and counter electrode (CE) are grid structured. Fluidized electrode particles are presented in black and grey arrows indicate direction of flow.

A scheme of an electrochemical fluidized bed reactor is presented in Figure 55. The fluidized bed particles represent the enlarged working electrode. Electrical contact between the current collector/distributor and the electrode particles is realized by randomized collision. Furthermore, electrons might also shuttle between the particles themselves by physical contact.

Since BES are characterized by slow substrate degradation kinetics compared to chemical systems, fluidized bed reactors have been successfully applied as MFC. Liu presented a MFC with fluidized anode particles [Liu et al. 2014]. They showed a biocapacitor-like behavior of the employed activated carbon particles. The electroactive bacteria could release/store electrons to the activated carbon particles, which were subsequently released to the current collector during intermittent physical contact. Rabaey published a tubular MFC with a granular graphite matrix fed with wastewater for the production of current [Rabaey et al. 2005].

Furthermore, Deeke presented a MFC with granular carbon based electrode material. Electroactive bacteria located on a fluidized capacitive bioanode were fed with acetate and the system was employed over 220 d with increasing current. However, they also reported a rather long start-up period of 100 d [Deeke et al. 2015].

5.1.2 Magnetic particles in fluidized bed reactors

Besides the application as MFC, fluidized bed reactors have been used also by stabilization with an external magnetic field [Özkara et al. 2004; Liu et al. 2009; Ursu et al. 2010]. Converting the approach of magnetic stabilization of a fluidized bed reactor to a BES might lead to two improvements during operation. Physical contact between the current collector/distributor is no longer of randomized nature but might be controlled by the external magnetic field. Moreover, particles size can be decreased without lowering the fluid velocity, leading to an increased electrode surface.

However, the possibility to stabilize an electrochemically fluidized bed reactor magnetically requires magnetic electrode particles. Several approaches towards the synthesis of magnetic particles have been reported so far. The generation of polypyrrol hollow sphere particles including the synthesis of magnetite particles from iron (0) has been reported [Mangold et al. 2011]. Moreover, the microwave assisted synthesis of magnetite was found to be an appropriate route to produce electric particles. Zheng presented a fast microwave synthesis

of magnetite using iron(II) as precursor [Zheng et al. 2010]. Based on these results, a method to magnetize different organic compounds such as spent grain or yeast cells was developed [Pospiskova and Safarik 2013; Pospiskova et al. 2013]. Briefly, magnetite was initially synthesized with a microwave and subsequently combined with the respective organic compounds.

Based on these findings, the aim of the research presented in this chapter was the synthesis of magnetic electrode particles and the subsequent immobilization of electroactive bacteria.

5.1.3 Artificial immobilization of electroactive bacteria

The artificial immobilization of electroactive bacteria on electrode materials for the application as MFC or in MES is an interesting way to design a ready-for-use electrodes for BES. Different approaches range from the incorporation into polymers [Yu et al. 2011; Le et al. 2015; Estévez-Canales et al. 2017] to the layer-by-layer approach based on different surface polarities [Xia et al. 2015].
Claimed advantages of the artificial biofilms are:

- direct application in BES without initial biofilm formation, leading to a significant decrease of the start-up time of BES (bioelectrical sensors).
- pre-selection of the bacterial consortium.
- higher current densities due to the artificial incorporation of conductive materials such as activated carbon or carbon nanotubes.

As mentioned before, prominent examples for the formation of artificial biofilms or the durable fixation of single cells on electrodes employ (electrochemical) polymerization techniques. Thereby, bacterial cells are suspended in buffered monomer solutions. Subsequently, electrodes are placed in the monomer-bacteria-suspension and polymerization is conducted either by the application of a certain potential to the electrode or induced chemically. Consequently, the bacterial cells are incorporated in the polymer layer formed on the electrode surface.

In 2015, Le presented the capturing of *P. aeruginosa, E. coli* and *S. oneidensis* cells on an ITO electrode with EDOT (3,4-ethylenedioxythiophene) [Le et al. 2015]. When applying a potential between 1.0 and 1.2 V vs. Ag/AgCl, the bacterial cells were immobilized during the electrochemical polymerization of PEDOT (poly-3,4-ethylenedioxythiophene). Artificial biofilms were characterized by a thickness of 0.3 to 1.5 µm.

Yu published the fabrication of a conductive artificial biofilm with *S. oneidensis* by the electrochemical polymerization of pyrrole on a carbon cloth electrode [Yu et al. 2011]. Cells were immobilized in the combination with graphite particles on the electrode by layer-by-layer fabrication. Polymerization was repeated several times, leading to several layers of electroactive cells and an eleven-fold increased current output in a MFC. However, the increased electrode surface by the incorporation of particulate graphite was taken into consideration.

Xia also described the application of the layer-by-layer technique for the production of a hierarchical artificial biofilm based anode [Xia et al. 2015]. Based on different zeta-potentials, several layers of positively and negatively charged components attached to an electrode surface. This step-by-step electrode modification produced a biofilm based bioanode, characterized by a hierarchical assembly of bacteria, mediators, multiwall carbon nanotubes and carbon paper.

Finally, Estévez-Canales published the fixation of *G. sulfurreduces* on a carbon felt fibre electrode by an encapsulation into silica gel [Estévez-Canales et al. 2017]. Bacterial cells were incorporated during the polymerization process with a reported viability of around 70 %. Due to limited space in the silica layer cells were not able to grow and cell density was rather low as visible in EFM images.

A variety of scientific approaches concerning artificial cell fixation has been published. These findings indicate that the artificial fixation of electroactive bacteria on electrode materials is an appropriate way to decrease startup time of a BES. However, all presented immobilization techniques were quite complex methods and used agents (such as polymers) or cross-linker (layer-by-layer) to bind cells on the electrode surface. Long term performance of these systems has not been proven yet and might be questionable due to inhibited self-reproduction of the bacterial catalysts.

The aim of the research presented in this chapter was the synthesis of magnetic electrode particles and the subsequent immobilization of electroactive bacteria on these particles without the application of a fixation agent.

The findings presented in this chapter have been patented [Stöckl, et al. 2016, DE102014112685A, Frankfurt, Germany].

5.2 Materials and Methods

5.2.1 Production of magnetic electrode particles

Based on the production described by Zheng and Pospiskova, two different types of magnetic electrode particles were developed [Zheng et al. 2010; Pospiskova et al. 2013]. Briefly, the two approaches differed in the incorporation of particulate activated carbon in the particles: the first approach did not employ activated carbon, whereas in the second approach activated carbon was used as backbone of the particle structure.

5.2.1.1 Electrode particles without activated carbon P_{MAG}

As mentioned before, one production route for magnetic particles (P_{MAG}) was based on the technique described by Pospiskova [Pospiskova et al. 2013]. A schematic of the preparation can be found in Figure 56. Iron (II) sulfate-heptahydrate (1 g) was dissolved in distilled water (200 mL) in an 800 mL glass beaker (Figure 56 / **1**). Sodium hydroxide pellets were added (**2**)

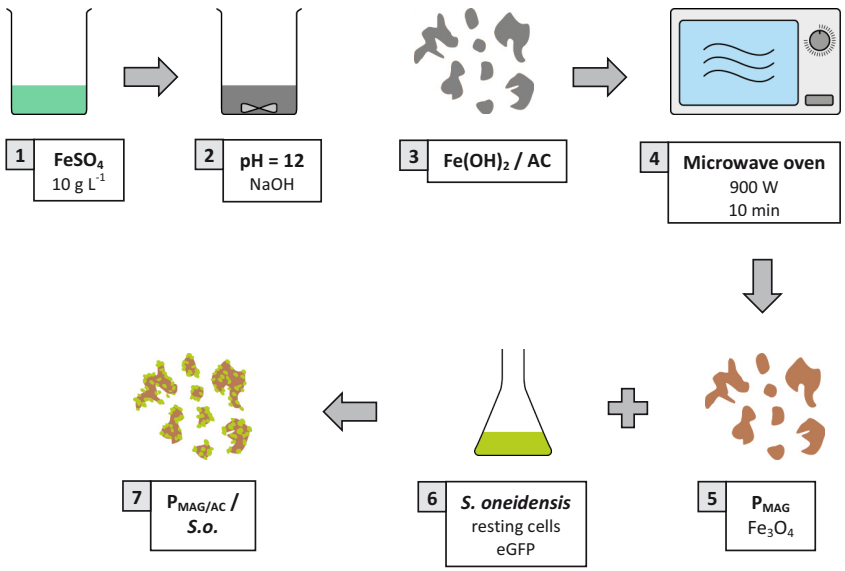

Figure 56: Scheme of the production route for the preparation of magnetic particles without activated carbon (P_{MAG}). Production steps include the alkaline precipitation by iron(II) hydroxide (1–3), microwave assisted conversion of iron(II) hydroxide to magnetite (4–5) and the combination of synthezised particles with *Shewanella oneidensis* resting cells (6–7). Abbreviations: P_{MAG}: magnetic electrode particles; *S.o.: Shewanella oneidensis* resting cells.

under constant stirring with a magnetic stirring bar, until the pH was around 12 and dark greyish iron hydroxide precipitates were observed (**3**). Consequently, the stirring bar was removed, the beaker was placed into a microwave oven (Siemens, München, Germany) and covered with a watch glass. The microwave assisted magnetite synthesis was carried out with the microwave oven set to 900 W for 10 min (**4**). Followed by a cooling phase to room temperature, the magnetic particles were neutralized by washing steps with distilled water in a Falcon tube or a snap cap vial made from glass. Therefore, particles were suspended in water, attracted to the inner wall of the Falcon tube with an external neodymium disc magnet (15 · 10 mm; Webcraft GmbH, Gottmadingen, Germany) and the supernatant was discarded (Figure 57). This process was repeated 12 to 15 times until the pH remained neutral. Two subsequent washing steps with ethanol (70 % v/v) were made to remove excess organic impurities. Ethanol was removed by another cascade of 10–15 washing steps with water. Particles were always freshly prepared in aliquots (1 g of iron(II) sulfate), before starting an experiment. Steps **6** and **7** presented in Figure 56 are described in section 5.2.3.

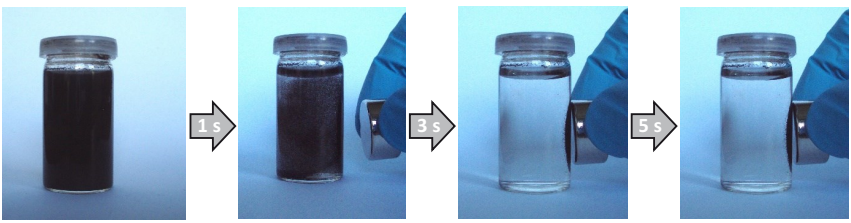

Figure 57: Series of images illustrating the separation of magnetic particles from the supernatant with a magnet. Time interval between the images is given in seconds written in the grey arrows.

5.2.1.2 Electrode particles with activated carbon $P_{MAG/AC}$

The preparation of magnetic particles with activated carbon ($P_{MAG/AC}$) is schematically displayed in Figure 58. For the production of $P_{MAG/AC}$ 0.1 g of activated carbon with a size distribution of 45 to 180 µm (Alcarbon DC, Donau Carbon, DE) was added to distilled water (200 mL) containing 1 g of dissolved iron(II) sulfate heptahydrate (Figure 58 / **1+2**). Particulate activated carbon was produced from coconut shells and activated with steam by

the manufacturer. Precipitation of iron hydroxide (**3+4**), the subsequent microwave assisted magnetite synthesis (**5+6**) and washing steps were conducted as described before for the production P_{MAG}. Again, particles were always freshly prepared prior to the experiments. Steps **7** and **8** presented in Figure 58 are described in section 5.2.3.

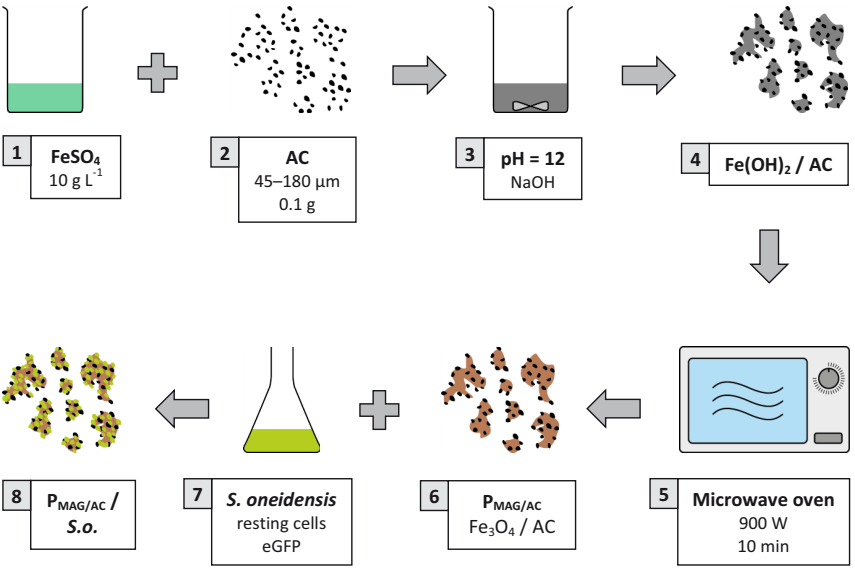

Figure 58: Scheme of the production route for the preparation of magnetic particles with activated carbon ($P_{MAG/AC}$). Production steps include the alkaline precipitation by iron(II) hydroxide in the presence of activated carbon (1–4), microwave assisted conversion of iron(II) hydroxide to magnetite (5–6) and the combination of synthesized particles with *Shewanella oneidensis* resting cells (7–8). Abbreviations: AC: activated carbon; $P_{MAG/AC}$: magnetic electrode particles with acticated carbon; *S.o.: Shewanella oneidensis* resting cells.

5.2.2 SEM imaging of prepared electrode particles

In order to visualize surface morphology and composition of the particles, SEM images were made. Freshly prepared particles with and without activated carbon were dried for 3 h at 50 °C in an oven and fixed on SEM sample holders. For fixation and electrical contact, samples were immobilized via conducting carbon tape (Leit-Tabs 9 mm, Plano GmbH, Wetzlar, Germany). Particles were manually scattered on the conducting tape and surplus or

unbound particles were subsequently discarded with compressed air. Imaging conditions were the same as already mentioned in section 3.2.7.2.

5.2.3 Combination of *S. oneidensis* and magnetic electrode particles

To characterize the binding capacity and attachment of an electroactive bacterium to the particles, *S. oneidensis* was used as model organism. The latter was chosen due to its tolerance towards oxygen, the well-studied EET and the possibility to monitor bacterial attachment via epifluoresece microscopy due to the use of an eGFP producing strain (section 4.2.1.3). Combination of *S. oneidensis* cells and magnetic electrode particles always followed the same experimental pattern. The attachment was evaluated by the application of resting cells of *S. oneidensis*. Resting cells are metabolically active but do not divide, mainly due to nitrogen limitation. This type of cells was selected because attachment studies could be evaluated without considering possible growth during attachment experiments.

GFP synthesizing resting cells of *S. oneidensis* were produced in the following way: *S. oneidensis* was grown aerobically to stationary phase as described before (section 4.2.1.3), harvested by centrifugation (Sigma 3K30) and washed twice with sterile 154 mM sodium chloride buffer (SCB). Subsequently, the freshly prepared particles, also suspended in sodium chloride buffer, were added to the resting cells in a snap-cap glass vail. Resting cells and particles were incubated for 30 min by shaking (400 rpm; IKA KS 130) under aerobic conditions and room temperature (Figure 58/**7+8**). Particles were then attracted to the glass wall of the vial by a magnet as is shown in Figure 57. The supernatant, containing resting cells, not bound to particles, was discarded and particle cell agglomerates were resuspended in sodium chloride buffer. This process was repeated until OD_{600} of the supernatant was zero, indicating the presence of immobilized cells only. Depending on the experiment, cell density, particle concentration and incubation time varied in the following experiments.

5.2.3.1 Qualitative evaluation of surface attachment

Initially, the attachment of resting cells of *S. oneidensis* to the electrode particles was evaluated qualitatively via microscopy. Bacterial cells were combined with the particles as

mentioned before, followed by a series of washing steps involving magnetic attraction and resuspension. Experiments were performed in 5 mL snap-cap glass vials. Resting cells (100 µL) with an OD_{600} of 22 were combined with 1 mL SCB containing either 0.051 g P_{MAG} or 0.061 g $P_{MAG/AC}$, respectively (resulting OD_{600} = 2; $1 \cdot 10^9$ cells mL^{-1}). After 15 min of incubation 10 washing steps were performed. For microscopy 25 µL samples were taken prior and after the washing steps. Samples were transferred to glass slides, covered with a glass and imaged directly with an upright epifluorescence microscope (section 3.2.7.1). Initially, particles were visualized in transmission mode. Subsequently, eGFP producing cells were imaged at the same spot in fluorescence mode, detecting emitted light at a wavelength of 509 nm.

5.2.3.2 Time dependent attachment of *S. oneidensis* to $P_{MAG/AC}$ particles

The time dependent attachment behavior of resting cells of *S. oneidensis* to $P_{MAG/AC}$ was characterized by the detection of the OD_{600} decrease during the incubation time of resting cells and particles. Resting cells were produced as mentioned before in section 5.2.3.

Resting cells (0.5 mL, OD_{600} = 6) were combined with 3 mL sterile SCB in a snap-cap vial (5 mL). Vials were placed on a rotating shaker and mixed at 400 rpm. Subsequently, 0.5 mL SCB containing 0.0152 g particles were added under constant agitation to a total volume of 4 mL. For sampling, vials were taken from the shaker and the particles were separated from the solution by attraction to the glass wall with an external magnet (Figure 57). Unbound cells in the supernatant were quantified by OD_{600} measurement. Samples were taken after 5 s, 90 s, 3, 9, 18, 36, 72, 120 and 240 min and each experiment was done in duplicate. Particles were not resuspended for further incubation. Each two snap-cap vials with resting cells and $P_{MAG/AC}$ have been used for the respective sampling times.

Based on the findings of the time dependent attachment of resting cells of *S. oneidensis* to $P_{MAG/AC}$ particles, the concentration of cells related to the particle mass was calculated. The amount of cells in the supernatant after 240 min of incubation with $P_{MAG/AC}$ was subtracted from the amount of cells without the addition of particles. This value was then related to the mass of $P_{MAG/AC}$ and the respective surface area.

5.2.4 Surface area determination with BET

The mass-related specific surface was determined based on the Brunauer-Emmett-Teller (BET) theory on gas ad- and desorption onto solid surfaces with an Autosorb iQ (Quantachrome GmbH & Co. KG, Odelzhausen, Germany) [Brunauer et al. 1938]. BET measurements were conducted to determine the specific surface of $P_{MAG/AC}$ particles as well as the specific surfaces of the single substituents AC and P_{MAG} particles. On one hand, the amount of attached cells was related to the mass specific surface of $P_{MAG/AC}$. On the other hand, specific surfaces of AC and P_{MAG} lead to information concerning the in-situ magnetite synthesis in the presence of AC leading to $P_{MAG/AC}$ particles.

The samples were activated at 250°C under vacuum for 3 h. The measurements were performed at –196°C by taking measuring points between 0.02 and 1. The specific surface area was calculated by the Brunauer-Emmett-Teller equation from a linearized isotherm equation between 0.03 and 0.25.

5.2.5 Electrochemical characterization

The magnetic electrode particles were electrochemically characterized to determine electrochemical behavior and potential dependent stability against oxidation or reduction. Cyclic voltammetry (CV) and linear sweep voltammetry (LSV) were performed in order to fulfill this aim. Both experiments were conducted under anaerobic conditions in the WE chamber (degassing with nitrogen; 20 mL min^{-1}) and at room temperature.

5.2.5.1 Cyclic voltammetry of magnetically immobilized $P_{MAG/AC}$ particles

Cyclic voltammograms were conducted in order to indicate anodic or cathodic potential borders for the application of $P_{MAG/AC}$ in a magnetically stabilized fluidized bed reactor. Experiments were performed in a modified H-cell, as it has been described already in section 3.2.2. Briefly, the glass reactor consisted of two chambers (V_{WE} = 120 mL; V_{CE} = 110 mL) separated by a membrane. As WE a glassy carbon (GC) plate (HTW Hochtemperatur-Werkstoffe GmbH, Thierhaupten, Germany) was installed at the outer flange. A platinum

mesh (30 · 30 mm) served as CE and the Ag/AgCl RE was inserted via a Luggin capillary. Sodium sulfate (0.5 mol L^{-1}) was applied as electrolyte in both chambers. The scan rate was 50 mV s^{-1} and data points were recorded with a step size of 2.5 mV. CV was started at the OCP, driven to an upper vertex potential of +1000 mV vs. Ag/AgCl before the potential scan was inverted to a lower vertex potential of –1000 mV vs. Ag/AgCl.

An external neodymium disc magnet (20 · 8 mm; Webcraft GmbH, Gottmadingen, Germany) was located at the outer side of the WE. Dispersed particles were attracted consequently from the solution directly onto the GC-WE, establishing electrical contact between the particles and the GC. Physical contact of the magnet with both the WE and the connecting spring wire was avoided via insulation with PTFE-tape (VWR chemicals, Radnor, Pennsylvania, USA).

Initially, no $P_{MAG/AC}$ was added for the control measurement. Subsequently, $P_{MAG/AC}$ was added in 5 steps of 0.12 g increments each (in sodium sulfate, 0.5 mol L^{-1}), until a final mass of 0.61 g $P_{MAG/AC}$ was achieved. This was magnetically immobilized on the GC-WE (geometrical surface = 4.91 cm^2). The system was degassed for 2 h prior to the start of the experiments and for 15 min after the respective addition of dispersed particles. During CV measurement the nitrogen inlet was set above the electrolyte level to avoid fluid convection.

5.2.5.2 Cathodic linear sweep voltammetry of $P_{MAG/AC}$ in a stirred fluidized bed reactor

Linear sweep voltammetry (LSV) of $P_{MAG/AC}$ was the final experiment to electrochemically characterize the particles under application oriented conditions in a stirred fluidized bed reactor. Based on the findings of CV measurements, LSV measurements were run exclusively with a cathodic particle polarization. The electrochemical reactor was again a glass H-cell comprising of two chambers divided by a membrane (Figure 59). In contrast to previous experiments, the WE was not a carbon based plate electrode installed from the outside of the reactor, but a platinum plated titanium expanded metal (Metakem GmbH, Usingen, Germany). The expanded metal structure was selected in order to allow perfusion of the $P_{MAG/AC}$ containing electrolyte and thereby realizing electrical contact by randomized collision. Electrical contact towards the expanded metal WE was maintained via a platinum

wire. As CE a carbon based fleece was connected also with a platinum wire. As can be seen in Figure 59, a magnetic stirrer was placed under the CE chamber. The RE was again a Ag/AgCl electrode inserted via a Luggin capillary and sodium sulfate (0.5 mol L^{-1}) served as electrolyte. Anaerobic conditions were achieved by degassing with nitrogen (20 mL min^{-1}). Fluid convection was realized with an agitator from above (Lab-egg, IKA), since a magnetic stirrer would interfered with the magnetic properties of $P_{MAG/AC}$.

The WE chamber was degassed for 2 h, before the experiments were started. Initially, LSV without $P_{MAG/AC}$ was tested as a control. Subsequently, 0.608 g $P_{MAG/AC}$ were added and the system was degassed for additional 15 min. LSV started at OCP with a scan rate of 50 mV s^{-1} and a step size of 5 mV. Both experiments, control measurements and polarization of $P_{MAG/AC}$, were run in triplicates and the whole set-up was placed in a Faradaic cage.

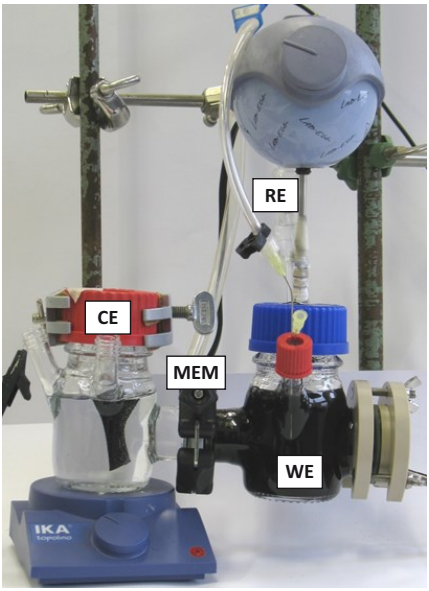

Figure 59: Fluidized bed reactor for the electrochemical characterization of $P_{MAG/AC}$ with LSV. The black colored chamber is filled with fluidized $P_{MAG/AC}$. Abbreviations: CE: counter electrode (carbon based fleece); MEM: membrane; WE: working electrode ($P_{MAG/AC}$ and current collector); RE: reference electrode.

5.3 Results

5.3.1 Particle preparation

Preparation of magnetic electrode particles was based on the production described by Zheng and Pospiskova [Zheng et al. 2010; Pospiskova et al. 2013]. In general, the preparation contained two subsequent steps, namely the precipitation of iron(II) hydroxide from iron(II) sulfate and the subsequent microwave assisted oxidation of iron(II) hydroxide. As it was postulated by Zheng and Pospiskova, iron(II) hydroxide is oxidized to magnetite (Fe_3O_4) during the microwave assisted conversion, leading to 0.508 g magnetite per gram iron hydroxide (the postulated reaction mechanism can be found in section 5.4.1).

Based on the findings presented in section 5.3.2.1, the production according to Zheng and Pospiskova was modified further. Additional to pure magnetite, activated carbon was included in the synthesis. This resulted in two different approaches for magnetic electrode particles: the first approach employed only iron(II) sulfate as precursor (P_{MAG}), whereas in the second approach particulate activated carbon was added prior to the precipitation of iron(II) hydroxide ($P_{MAG/AC}$).

The magnetic properties of the particles (P_{MAG}) are illustrated in Figure 60. P_{MAG}–particles were placed on a watch glass located above a magnet. As can be seen, particles aligned accurately with the magnetic field and formed elongated agglomerates.

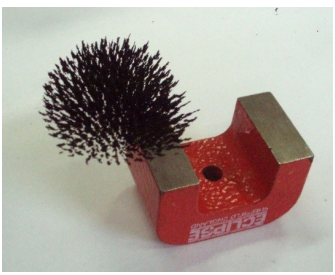

Figure 60: Dried magnetic electrode particles made from iron(II) hydroxide (P_{MAG}). A magnet was placed under a watch glass with the particles demonstrates the magnetic properties.

5.3.1.1 SEM imaging of P_{MAG} and $P_{MAG/AC}$ particles

SEM images of the magnetic particles without activated carbon (P_{MAG}) are given in Figure 61. The 5000-fold magnification (Figure 61 A) indicates that the particles are characterized by a rough and amorphous surface. P_{MAG} appears as loosely attached agglomerates of small particles in the nanometer scale. This is indicated by the particulate structure and small fragments forming the surface of P_{MAG}. The size of P_{MAG} given in the 1000-fold magnification

SEM image (Figure 61 B) ranges from 20 µm to the sub-micrometer range. Average particle size is around 10 to 15 µm.

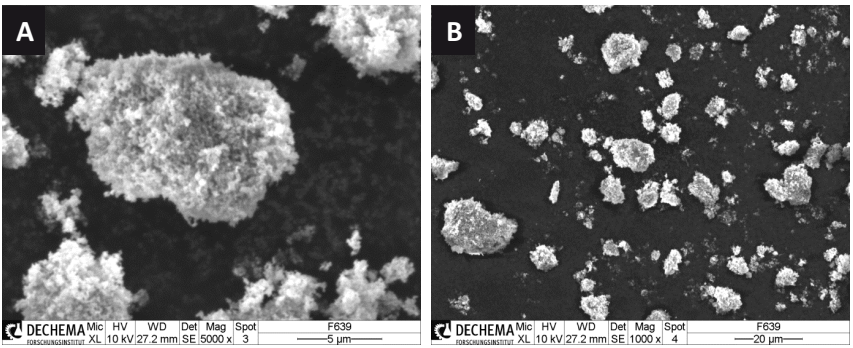

Figure 61: Images of SEM with SE-detector of magnetic particles (P_{MAG}). Image A shows P_{MAG} with 5000-fold magnification and 1000-fold magnification is used in image B. For sample preparation particles were dried (3 h, 50 °C) and immobilized on SEM sample holders with conducting carbon tape. Unbound particles were discarded with compressed air.

Since for the second type of particles ($P_{MAG/AC}$) activated carbon (AC) was used as precursor additionally to iron(II) sulfate, the AC was imaged initially by SEM. Again, images of 5000-fold and 1000-fold magnification are presented in Figure 62. Compared to P_{MAG}, the surface of the AC was rather smooth and unstructured, if seen at the nanometer scale. Small pores are visible on the surface as well as larger cavities reaching inside the particulate AC (Figure 62 A). A few small particles in the sub-micrometer range were located on the AC surface. The 1000-fold magnification indicates that cavities were distributed over the AC particle surface. Furthermore, the AC appeared as fragments of big particles, since straight edges indicating mechanical breaking down can be observed (Figure 62 B). Size of the AC particles was significantly higher compared to P_{MAG} and ranged between 20 and 200 µm.

Finally, $P_{MAG/AC}$ was visualized with SEM, which is shown in Figure 63. The surface morphology, as visible in the image with 5000-fold magnification (Figure 63 A), can be compared to the observations described for P_{MAG}. The surface pattern is dominated by an amorphous structure of particles in the nanometer scale. However, big particles between 1 and 2 µm were also located on the surface.

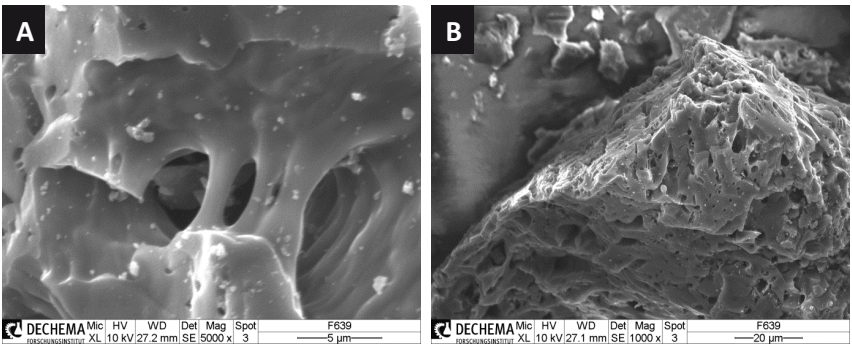

Figure 62: Images of SEM with SE-detector of particulate activated carbon. Image A shows AC with 5000-fold magnification and 1000-fold magnification is displayed in image B. For sample preparation activated carbon was immobilized on SEM sample holders with conducting carbon tape. Unbound particles were discarded with compressed air.

The surface is more structured compared to P_{MAG}, but pores and cavities, as they were observed for activated carbon, are less detectable and are assumed to be filled with P_{MAG}. The bigger scale visualization presented by the 1000-fold SEM image (Figure 63 B) emphasizes $P_{MAG/AC}$ shape and surface homogeneity. It can be seen clearly that the macroscopic appearance of $P_{MAG/AC}$ mainly resulted from the AC. Both shape and rough edges of $P_{MAG/AC}$ were identical to observations of AC. The homogenous distribution of cavities of AC was not observed for $P_{MAG/AC}$, since the majority of the particle surface was covered with the amorphous pattern described for P_{MAG}. The size of $P_{MAG/AC}$ was between 20 and 200 µm.

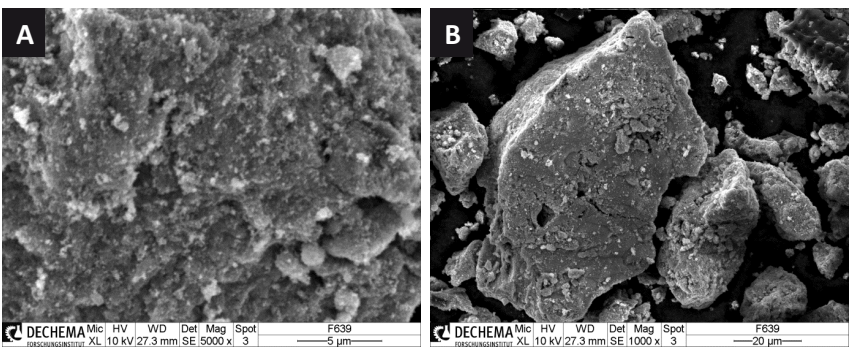

Figure 63: Images of SEM with SE-detector of $P_{MAG/AC}$. Image A shows $P_{MAG/AC}$ with 5000-fold magnification and 1000-fold magnification is displayed in image B. For sample preparation particles were dried (3 h, 50 °C) and immobilized on SEM sample holders with conducting carbon tape. Unbound particles were discarded with compressed air.

In conclusion $P_{MAG/AC}$ can be described as hybrid particles from P_{MAG} and AC. Shape and size distribution of the particles were mainly dominated by the applied AC, whereas the surface pattern indicated coverage with magnetite.

5.3.2 Fixation of resting cells of *S. oneidensis* on magnetic electrode particles

The aim in this section was to characterize the attachment of resting cells of *S. oneidensis* to P_{MAG} and $P_{MAG/AC}$. The attachment was monitored qualitatively by microscopy. A quantitative evaluation was performed subsequently by the determination of the time dependent attachment behavior and the surface loading with bacterial cells.

5.3.2.1 Qualitative evaluation of the attachment by microscopy

For the qualitative evaluation of the attachment of bacterial cells to P_{MAG} and $P_{MAG/AC}$ eGFP producing resting cells of *S. oneidensis* were combined with such particles and after a series of washing steps imaged by EFM. Particles were visualized in transmission mode, whereas *S. oneidensis* cells were detected by fluorescence. Resting cells were selected, because cell division was negligible and attachment studies could be evaluated without considering possible growth during attachment experiments.

Figure 64 shows the initial combination of P_{MAG} with eGFP producing resting cells. As can be seen in the transmission image in Figure 64 A size distribution of P_{MAG} was between 20 and 100 µm. The particles were characterized by an elongated shape. The fluorescence image taken at the same position (Figure 64 B) shows clearly that green fluorescent cells accumulated at the same position, where the particles have been imaged before. Thus, intensity of fluorescence or amount of cells was not equal for all particles. Besides, a high concentration of planktonic cells was visible, indicating that many cells did not attach to P_{MAG}.

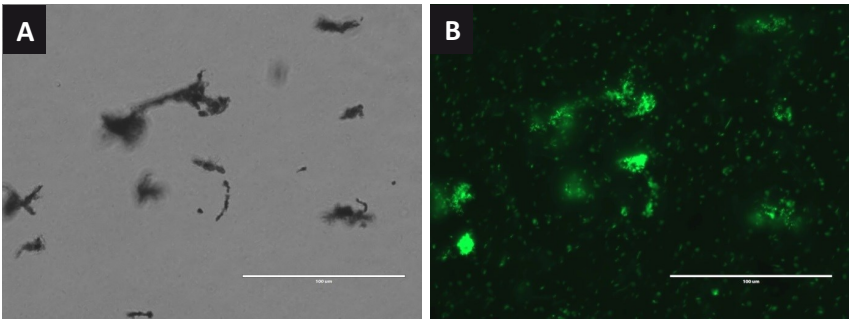

Figure 64: Microscopic images of the initial combination of resting cells of *S. oneidensis* (aerobic, heterotrophic cultivation: minimal medium + lactate; 30 °C, shaking 180 rpm) and P_{MAG}. Bacterial cells were washed twice with SCB (154 mM) to obtain resting cells. Image A: 400-fold, transmission mode. Image B: 400-fold, fluorescence mode with GFP filter. Scale bars indicate 100 µm.

Images from P_{MAG} with attached cells of *S. oneidensis* after several washing steps are presented in Figure 65. Again, the initial transmission image (Figure 65 A) shows the size and shape of the particles. The shape is also elongated and the presented P_{MAG} has a length of approximately 85 µm. In contrast to the previous image showing fluorescent cells attached to the particles, almost no attached cells were detectable on the particle. Planktonic cells have been removed by the washing steps as well as the majority of cells that have been immobilized on the P_{MAG} surface.

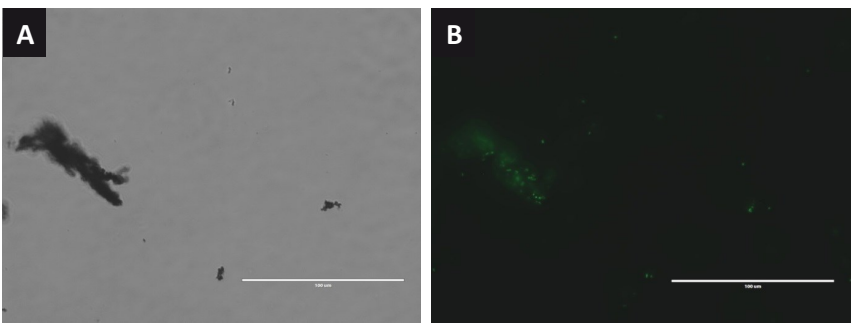

Figure 65: Microscopic images of P_{MAG} combined with resting cells of *S. oneidensis* (aerobic, heterotrophic cultivation: minimal medium + lactate; 30 °C, shaking 180 rpm; cells washed twice with SCB (154 mM)) after several washing steps. Image A: 400-fold, transmission mode. Image B: 400-fold, fluorescence mode with GFP filter. Scale bars indicate 100 µm.

As second type of the synthesized particles $P_{MAG/AC}$ was tested for qualitative attachment. Transmission and fluorescence images after planktonic cell elimination by washing steps with SCB are presented in Figure 66. The size of the particles ranged between 10 and 120 µm and particles were less elongated than P_{MAG} particles (Figure 66 A). Resting cells of *S. oneidensis* were still attached on $P_{MAG/AC}$ particles after a series of washing steps (Figure 66 B). Planktonic cells had been removed, but agglomerates of eGFP producing bacterial cells occurred at the same location as observed for $P_{MAG/AC}$ (Figure 66 A). Furthermore, the distribution of resting cells on the particles was more homogenous compared to the pattern observed for P_{MAG}.

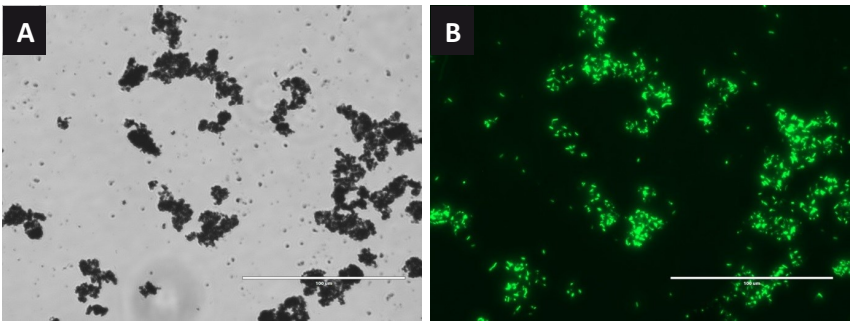

Figure 66: Microscopic images of $P_{MAG/AC}$ combined with resting cells of *S. oneidensis* (aerobic, heterotrophic cultivation: minimal medium + lactate; 30 °C, shaking 180 rpm; cells washed twice with SCB (154 mM)) after several washing steps. Image A: 400-fold, transmission mode. Image B: 400-fold, fluorescence mode with GFP filter. Scale bars indicate 100 µm.

In conclusion eGFP producing resting cells of *S. oneidensis* were immobilized on $P_{MAG/AC}$ without the addition of fixation agents. Bacterial cells remained on $P_{MAG/AC}$ even after a series of 10 washing steps and were more homogenously distributed on the particle surface than on P_{MAG} particles. Consequently, $P_{MAG/AC}$ particles were chosen as preferable particle type for further experiments.

To illustrate the distribution of resting cells of *S. oneidensis* on the $P_{MAG/AC}$ surface, a series of Z-sectional images taken from a $P_{MAG/AC}$ particle combined with resting cells is presented in Figure 67. The size of the particle was approximately $75 \cdot 110$ µm and Z-sectional images were made to a depth of 23 µm.

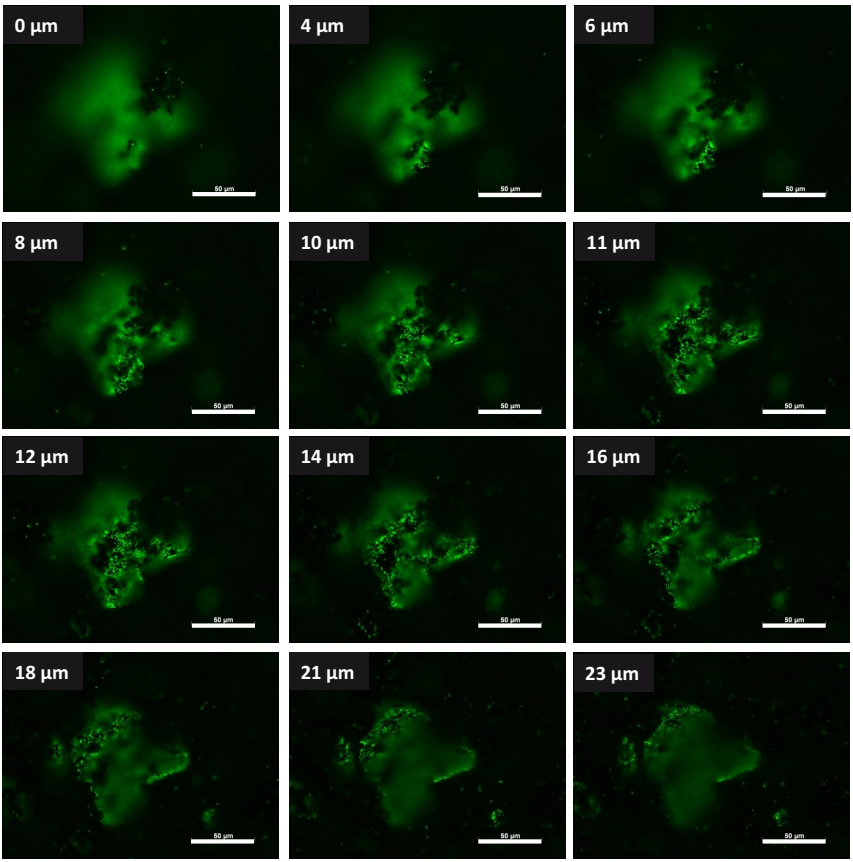

Figure 67: Series of Z-sectional EFM images taken from a $P_{MAG/AC}$ particle combined with fluorescent resting cells of *S. oneidensis* (aerobic, heterotrophic cultivation: minimal medium + lactate; 30 °C; shaking 180 rpm; cells washed twice with SCB (154 mM)). White numbers given on the upper left corner of each image illustrate the distance in Z-direction correlated to the initial (0 µm) image. Scale bars represent 50 µm.

The $P_{MAG/AC}$ particle was almost homogenously covered with a monolayer of fluorescent bacterial cells. However, a few regions of the particle remained uncovered. Fluorescence of the initial images (starting at 0 µm in Z-direction) was higher compared to the final images of the cross sectional imaging process (23 µm in Z-direction). Since no anti-fading agent was used in this experiments, photo-bleaching was observed while stack imaging. Consequently, the intensity of the fluorescence was decreased from the initial (0 µm) to the final (23 µm) image.

5.3.2.2 Time dependent attachment of *S. oneidensis* to $P_{MAG/AC}$ particles

In addition to the qualitative attachment of resting cells to P_{MAG} and $P_{MAG/AC}$ particles, the time dependent attachment behavior of *S. oneidensis* cells to $P_{MAG/AC}$ particles was measured. Additionally, the particle loading with resting cells was calculated and also graphically displayed over time.

Time dependent attachment of resting cells of *S. oneidensis* to $P_{MAG/AC}$ particles is presented in Figure 68. Before $P_{MAG/AC}$ particles were added, the initial OD_{600} was around 0.75 ($4 \cdot 10^8$ cells mL^{-1}). 90 s after addition of $P_{MAG/AC}$ particles to the resting cells and the subsequent separation of $P_{MAG/AC}$ by an external magnet the OD_{600} was already lowered to 0.61 ($3 \cdot 10^8$ cells mL^{-1}). After 36 min of incubation the OD_{600} decreased further to 0.28 ($2 \cdot 10^8$ cells mL^{-1}). A constant OD_{600} indicating either an equilibrium of attaching and detaching cells or completely loaded $P_{MAG/AC}$ particles was observed after 240 min at an OD_{600} of 0.21 ($1 \cdot 10^8 \pm 3 \cdot 10^6$cells mL^{-1}). In generate the decrease of resting cells in the solution followed a typical isothermal adsorptive behavior. It was characterized initially by a fast decrease of the cell concentration followed by a steady state phase at the end of the experiment.

Based on these findings as shown in Figure 68, the calculated amount of resting cells referred to the particle mass is displayed in Figure 69. Starting with no cells on $P_{MAG/AC}$, the particle loading was increased to $2 \cdot 10^{10}$ cells per g $P_{MAG/AC}$ particles. Analogue to the decrease of planktonic cells presented in Figure 68, the amount of cells on $P_{MAG/AC}$ reached a plateau at the end of the incubation time. The final calculated particle loading with resting cells of *S. oneidensis* was around $8 \cdot 10^{10} \pm 3 \cdot 10^9$ g^{-1}. The pattern of the curve also indicates an isothermal adsorptive behavior, precisely described by a Langmuir isotherm [Hameed et

al. 2007]. According to the adsorption model by Langmuir, these results indicate the formation of a monolayer of the sorbate (resting cells) on the sorbent ($P_{MAG/AC}$ particles) [Langmuir 1932].

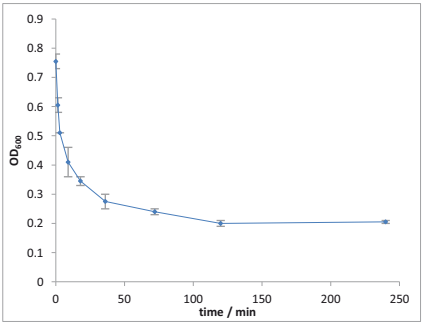

Figure 68: Attachmet of resting cells of *S. oneidensis* (aerobic, heterotrophic cultivation: minimal medium; + lactate; 30 °C, shaking 180 rpm; cells washed twice with SCB (154 mM)) to $P_{MAG/AC}$ particles. Decrease of bacterial cell concentration in the liquid phase was monitored by OD_{600}. Mean values of three biologically independent cultures are given with standard deviations in grey error bars.

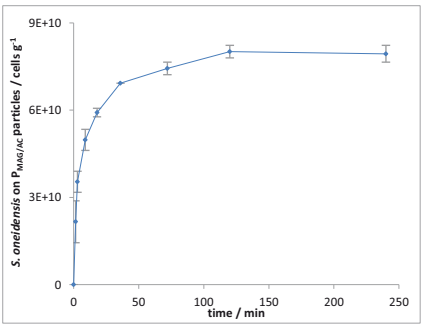

Figure 69: Loading of $P_{MAG/AC}$ particles with resting cells of *S. oneidensis* (aerobic, heterotrophic cultivation: minimal medium; + lactate; 30 °C, shaking 180 rpm; cells washed twice with SCB (154 mM)) calculated from OD_{600} decrease. Mean values of three biologically independent cultures are given with standard deviations in grey error bars.

5.3.3 Surface determination via BET measurement

The surface area of P_{MAG}, AC and $P_{MAG/AC}$ particles were measured via BET analysis in order to correlate with the mechanisms during particle formation and for final characterization of $P_{MAG/AC}$ particles. Mass specific surface areas of the three samples are displayed in Table 1. P_{MAG} was found to have the smallest surface area with 41 $m^2 g^{-1}$, followed by $P_{MAG/AC}$ with 300 $m^2 g^{-1}$ and AC with 1020 $m^2 g^{-1}$, respectively.

Table 1: Surface areas of P_{MAG}, AC and $P_{MAG/AC}$ determined with BET (activation at 250 °C in vacuum for 3 h, measurement at –196 °C).

Sample	Specific surface [$m^2 g^{-1}$]
P_{MAG}	41
AC	1020
$P_{MAG/AC}$	300

The mass specific surface area was mainly determined by the added AC, since 0.1 g AC were used to produce $P_{MAG/AC}$ particles with 1 g iron hydroxide. Based on the calculated particle loading presented in Figure 69, a density of $3 \cdot 10^8 \pm 9.621 \cdot 10^6$ resting cells m^{-2} was calculated.

5.3.4 Electrochemical characterization

The final experimental part of this chapter was the electrochemical characterization of the synthesized $P_{MAG/AC}$ particles. Cyclic voltammetry of magnetically immobilized particles was performed as well as linear sweep voltammetry in a fluidized bed reactor.

5.3.4.1 CV with particles magnetically attracted to an electrode

Cyclic voltammograms obtained from different amounts of $P_{MAG/AC}$ particles can be seen in Figure 70. CV´s were conducted with $P_{MAG/AC}$ particles magnetically immobilized on the WE with an external magnet. Current densities were referred to the geometrical surface area of the current collector WE.

CV measurements were started at the OCP. For the control without $P_{MAG/AC}$ an OCP of +130 mV vs. Ag/Ag/Cl was measured, which was lowered continuously to –201 mV vs. Ag/Ag/Cl at the highest particle load (124 mg cm^{-2}) on the WE. The decrease of the OCP with particle addition is related to the reductive properties of $P_{MAG/AC}$ particles and a contamination with iron(II) due to the particle synthesis.

The initial voltammogram without the addition of $P_{MAG/AC}$ particles (0 mg cm^{-2}) produced a maximum current density under 100 µA cm^{-2}, hence, anodic (water electrolysis, oxygen reduction) and cathodic (water electrolysis, proton reduction) peak currents appear around 0 mA cm^{-2}. The addition of 25 mg cm^{-2} particles to the current collector WE led to a significant increase in anodic and cathodic current density. The highest anodic current density was observed at +1000 mV vs. Ag/AgCl (+0.49 mA cm^{-2}) and the highest cathodic current was observed at –1000 mV vs. Ag/AgCl (0.58 mA cm^{-2}), presumably indicating water electrolysis. However, a formation of gas was not observed. With increasing mass of immobilized $P_{MAG/AC}$ particles on the WE, maximum current densities increased to final values of +1.31 and –1.47 mA cm^{-2} (124 mg $P_{MAG/AC}$ cm^{-2}). The pattern of the anodic current

densities show a minor peak or a shoulder at a potential around +300 mV vs. Ag/AgCl, eventually indicating the oxidation of iron(II) to iron(III). At the cathodic part of the curves no peaks or shoulders are visible.

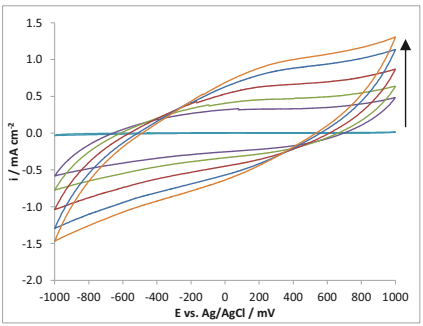

Figure 70: Cyclic voltammograms of increasing masses of $P_{MAG/AC}$ particles magnetically immobilized on the WE. Black arrow indicates the increase of mass. $P_{MAG/AC}$ masses on the WE surface: 0 (—■—), 25 (—■—), 49 (—■—),74 (—■—), 99 (—■—) and 124 (—■—) mg cm^{-2}. Electrolyte: sodium sulfate (0.5 mol L^{-1}); scan rate: 50 mv s^{-1}; step size: 2.5 mV.

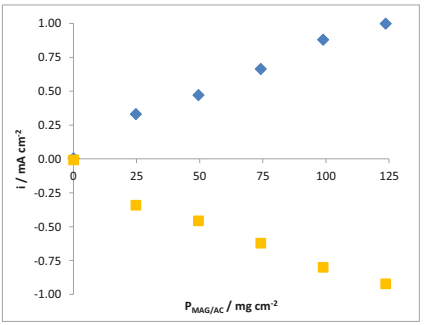

Figure 71: Current densities (i) at potentials of +400 (◆) and –400 mV (■) vs. Ag/AgCl over the mass of immobilized $P_{MAG/AC}$ obtained from CV´s presented in Figure 70. Linear regression curves gave the following correlations between immobilized mass of $P_{MAG/AC}$ and current density (i): anodic (◆): $y = 0.0079x + 0.07$; $R^2 = 0.9825$; cathodic (■): $y = -0.0071x - 0.09$; $R^2 = 0.9726$.

In general, anodic and cathodic current densities obtained at the OCP are characterized by a high difference from 0.58 up to 1.27 mA cm^{-2} for 25 up to 124 mg cm^{-2} $P_{MAG/AC}$ particles, respectively. The shape of the CV curves indicates capacitive-like currents resulting from a rough electrode surface. This points out that the electrode surface significantly increased by the addition and immobilization of $P_{MAG/AC}$, and that $P_{MAG/AC}$ are characterized by a capacitor-like behavior. Secondly, an increasing tilt of the curves can be observed with increasing mass of immobilized $P_{MAG/AC}$, indicating an increasing resistance within the layer of $P_{MAG/AC}$ on the current collector WE.

Current densities at an anodic potential of +400 mV and a cathodic potential of –400 mV vs. Ag/AgCl are additionally plotted in dependence of the immobilized particle mass (Figure 71). Both, anodic and cathodic current densities, show a linear correlation to the immobilized particle mass. On one hand this indicates that electrical contract of $P_{MAG/AC}$ was achieved by the attraction with an external magnet. On the other hand the current per g of $P_{MAG/AC}$ was calculated on the basis of these correlations. At a potential of +400 mV vs. Ag/AgCl 1.67 mA g^{-1} were measured and 1.55 mA g^{-1} at–400 mV vs. Ag/AgCl.

In conclusion, $P_{MAG/AC}$ was found to be electrochemically stable with cathodic polarization under these conditions.

Additionally, electrochemical impedance measurements have been performed. However, due to the external magnet an interference-free signal recording from EIS measurements was not possible.

5.3.4.2 Cathodic LSV of $P_{MAG/AC}$ particles

The electrochemical characterization of the particles was completed by linear sweep voltammetry. Presented CV measurement (Figure 70) showed a small anodic peak at a potential around +300 mV vs. Ag/AgCl. As mentioned before, this observation might indicate an oxidation of the iron(II) present in the magnetite fraction of $P_{MAG/AC}$ particles leading to non-magnetic iron(III) oxide (hematite). Due to these findings, LSV was driven to the cathodic direction exclusively. Furthermore, the use for reductive synthesis processes (cathodic polarization) was the aimed application for $P_{MAG/AC}$. The aim of this experiment was to test the electrochemical stability of $P_{MAG/AC}$ particles in view of a technical application. This included on one hand the application in a fluidized bed reactor. On the other hand, the development of the magnetic electrode particles points to an application in the field of MES (reductive electrode conditions).

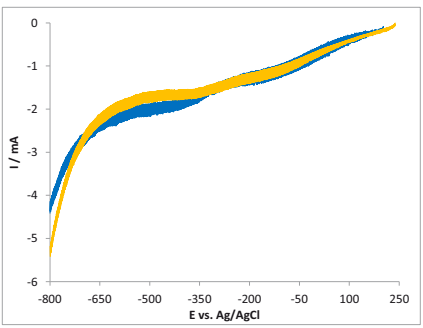

Figure 72: Linear sweep voltammograms in fluidized bed reactor with the addition of $P_{MAG/AC}$ particles (5.1 g L^{-1}) and without (control). Curves represent mean values of triplicate measurements. Electrolyte: sodium sulfate (0.5 mol L^{-1}); scan rate: 50 mv s^{-1}; step size: 5 mV.

The results of the LSV can be found in Figure 72. OCP of the current collector electrode without and with the addition of $P_{MAG/AC}$ particles was around +200 mV vs. Ag/AgCl. Down to a potential of –350 mV vs. Ag/AgCl the controls and the system with $P_{MAG/AC}$ showed the same current response (–1.9 mA). Going to lower potentials, a small plateau around –1.9 mA to a potential of –550 mV vs. Ag/AgCl was observed for $P_{MAG/AC}$ particles while the current of the control without particles was further

increased to negative values. At potentials lower than –680 mV vs. Ag/AgCl both samples showed an increasing current response, most probably due to hydrogen development. However, $P_{MAG/AC}$ particles showed a higher current at a potential negative to –700 mV vs. Ag/AgCl compared the control (no $P_{MAG/AC}$). This finding might suggest a reduction of $P_{MAG/AC}$ particles namely the iron(III) present in the magnetite. A second option might be accelerated hydrogen production due to a catalytic activity of $P_{MAG/AC}$ or an increased electrode surface area by the fluidized particles.

The electrochemical characterization of the magnetic electrode particles revealed that $P_{MAG/AC}$ are electrochemically stable to a potential of –680 mV vs. Ag/AgCl. Furthermore, when magnetically immobilized on a current collector WE, $P_{MAG/AC}$ particles were shown to significantly increase the active surface.

5.4 Discussion and Conclusions

The aim of the research presented in this chapter was the development of magnetic electrode particles for a magnetically stabilized fluidized BES. In order to achieve this aim, the experimental approach was structured in the following three sub-points:

- Establishment of production for magnetic particles
- Fixation of electroactive resting cells on particles
- Electrochemical characterization of particles

5.4.1 Production of magnetic electrode particles

As mentioned before, the production route of magnetic particles was based on the findings presented by Zheng [Zheng et al. 2010]. They established a fast microwave assisted synthesis with iron(II) as precursor. Based on the mechanisms described by Briehl and Zhang, the microwave assisted magnetite synthesis was assumed to follow these reaction mechanisms [Briehl 2008; Zheng et al. 2010]:
Initially, iron(II) hydroxide precipitates by the addition of sodium hydroxide to iron(II) sulfate.

$$Fe^{2+} + SO_4^{2-} + 2Na^+ + 2\,OH^- \rightarrow Fe(OH)_2 + 2Na^+ + SO_4^{2-}$$

During the microwave assisted magnetization, iron(II) hydroxide oxidized incompletely to magnetite hydrate under oxygen limitation.

$$6\,Fe(OH)_2 + {}^1/_2\,O_2 \rightarrow 2\,(Fe_2O_3 \cdot FeO) \cdot H_2O + 4\,H_2O$$

Subsequently, magnetite (*sum formula: Fe_3O_4*) is formed from magnetite hydrate under the separation of a water molecule.

$$Fe_3O_4 \cdot H_2O \rightarrow Fe_3O_4 + H_2O$$

This magnetite was reported to be initially present as spherical nanoparticles with an average round size of 80 ± 5 nm [Zheng et al. 2010]. SEM and light microscopy images produced in this study show that the magnetite particles (P_{MAG}) mainly present as agglomerates ranging around 10 to 15 µm. In contrast to the findings presented by Pospiskova with yeast cells, the agglomerates of *S. oneidensis* resting cells and P_{MAG} particles were not stable [Pospiskova et al. 2013]. The resting cells detached from the P_{MAG} agglomerates during several washing steps. Consequently, particulate activated carbon (AC) was involved in the production pathway of the magnetic particles. AC has been applied before as electrode particles and showed a biocapacitor-like behavior in a fluidized bed MFC [Liu et al. 2014; Deeke et al. 2015].

In the developed production route particulate AC was combined with iron(II) prior to the precipitation of iron(II) hydroxide. It is assumed that during alkalization with sodium hydroxide precipitation of iron(II) hydroxide appeared on the AC surface as well as partly inside the porous structure of the AC. Consequently, magnetite was formed on the AC particles and in the porous system in the subsequent microwave assisted magnetization step. SEM images of the $P_{MAG/AC}$ particles revealed that the surface is dominated by structures previously observed for magnetite. Moreover, the initially porous structure of the AC is almost not visible in SEM images any more for $P_{MAG/AC}$ particles. However, BET analysis of $P_{MAG/AC}$ particles pointed out that the surface area of $P_{MAG/AC}$ (300 $m^2 g^{-1}$) still is significantly higher compared to pure magnetite (41 $m^2 g^{-1}$). This might indicate that the porous structure of the AC was partially maintained.

In conclusion this procedure presents a fast and effective approach for the synthesis of magnetite in the presence of activated carbon leading to a formation of magnetite–activated carbon agglomerates. The size of the particles can be adjusted by the size of the particulate AC, whereby AC serves as structural backbone for the production of $P_{MAG/AC}$ particles. Customization in terms of size adaptation to the requirements of electrochemical fluidized bed reactors might be one of the subsequent steps towards their practical application in BES.

Since the resting cells combined with P_{MAG} particles were only weakly bound to P_{MAG} and detached, $P_{MAG/AC}$ particles were used for further experiments.

5.4.2 Fixation of electroactive resting cells on particles

The evaluation of the immobilization of resting cells of *S. oneidensis* on P_{MAG} and $P_{MAG/AC}$ particles revealed that agglomerates of P_{MAG} and resting cells were not stable. In contrast, resting cells remained sessile on $P_{MAG/AC}$ even after the conduction of washing steps and showed a homogenous coverage of the $P_{MAG/AC}$ surface. It was assumed that P_{MAG} – resting cell agglomerates were instable due to the dis- and re-agglomeration of particles. Breaking down the particle structure and their rearrangement might lead to instable particle cell agglomerates and a consequent detachment of the cells. Contrarily, $P_{MAG/AC}$ comprised AC as structural backbone, avoiding a breaking down of the loosely agglomerated structure by P_{MAG} and thereby conserving stable attachment conditions for the bacteria.

The time dependent experiments on the attachment of *S. oneidensis* were characterized by an isothermal adsorption profile. According to the adsorption model by Langmuir, this profile indicates the formation of a monolayer on the sorbent ($P_{MAG/AC}$), which was confirmed by EFM imaging of sessile cells of *S. oneidensis* on $P_{MAG/AC}$ particles [Langmuir 1932]. Moreover, attachment was very fast, since the maximum particle loading was observed after 120 min. Similar observations have been made for the attachment of *S. oneidensis* to a polarized ITO electrode. Even though that system was completely different from the $P_{MAG/AC}$ particle system, the majority of cells became immobilized initially within the first 120–180 min [Stöckl, et al. 2016].

Due to the combination of Langmuir adsorptive behavior and the fast attachment of *S. oneidensis* to an electrode, a differentiation between active attachment and passive adsorption was not possible. However, electroactive bacterial cells have been immobilized successfully on $P_{MAG/AC}$ particles surface without the addition of a (chemical) cross linker. Long term experiments and EPS analysis focusing on the surface attachment on $P_{MAG/AC}$ might give further information on the attachment behavior and the stability of the agglomerates under application oriented conditions.

5.4.3 Electrochemical characterization of particles

The electrochemical characterization of $P_{MAG/AC}$ was the last experimental part to characterize the particles with the focus on the possible application in a fluidized bed BES.

Linear sweep voltammetry measurements revealed that the synthesized $P_{MAG/AC}$ particles were stable under cathodic polarization conditions up to –680 mV vs. Ag/AgCl. Furthermore, CV measurements indicated that mainly capacitive-like currents were measured. Faradaic currents originating from the reduction of the iron(II) in the magnetite were not monitored. These findings are in contrast to previous electrochemical studies on magnetite. The following mechanism was postulated for the electrochemical reduction of magnetite [White et al. 1994]:

$$Fe_3O_4 + 8\,H^+ + 2\,e^- \rightarrow 3\,Fe^{2+} + 4\,H_2O$$

Studies on Fe_3O_4 – poly porrole core shell particles showed a reduction peak around +180 mV vs. Ag/AgCl, which was related to the equation mentioned above [Mangold et al. 2011]. However, reduction peaks originated from the latter were not observed, leading to the assumption that $P_{MAG/AC}$ particles were chemically inert under the tested conditions.
Furthermore, CV measurements showed a significant increase of the electrode surface when $P_{MAG/AC}$ particles were magnetically immobilized

Based on these results $P_{MAG/AC}$ particles might be suitable for the application in MES systems for methane production for example. A potential around –160 mV vs. SHE (–360 mV vs. Ag/AgCl) is required to biologically catalyze methane production in a MES [Beese-Vasbender et al. 2015]. Furthermore, the methanogens have been found to poorly form biofilms on the cathode. Consequently, the immobilization on $P_{MAG/AC}$ particles might present a promising approach to enhance direct electron transfer for non-biofilm forming synthesis organisms. Besides the application in MES conducting methane production, approaches for acetate generation with MES have been reported to use potentials in the possible range found for $P_{MAG/AC}$. A system for the bioelectrochemical acetate production at –600 mV vs. Ag/AgCl in a MES was reported [Soussan et al. 2013].

In conclusion, the synthesized $P_{MAG/AC}$ particles represent a straight forward approach to in-situ produce magnetite – activated carbon agglomerates for the artificial immobilization of electroactive bacteria.

In systems with controlled sterile conditions, artificial biofilms/immobilized cells might play a role in future applications. Reactor systems designed for MES production of valuable chemicals might present a possible field of industrial operation. Controlling the inflow of the systems is thereby essential, since the introduction of bacteria other than those immobilized on the electrode include the risk that the bacterial consortium might change.

Our $P_{MAG/AC}$ particles aim to optimize the utilization in MES for the reductive production of valuable substances.

6 Summary and Outlook

The combination of electroactive bacteria and electrochemical techniques offers a wide range of application opportunities. Bioelectrochemical systems merge the advantages of microorganisms and electrochemical systems. The systems are characterized by high reaction specificity, self-replication of the biocatalyst, high reaction control and high coulombic efficiencies [Krieg et al. 2014].
The two most prominent examples are the sustainable generation of electricity from (organic) waste (MFC) and the consumption of current to produce valuable substances such as biofuels or process chemicals (MES). Thereby, research in the field of BES is focused on a plethora of single aspects of BES. The main addressed aspects towards an implementation into industrial processes are the interactions of electrodes with electroactive bacteria, expanding the product spectrum or optimization of reactor designs.

In this thesis, several aspects of microbial electrochemistry were addressed. Research ranged from fundamentals of microbial attachment to electrodes to the development of electrode material for advanced reactor concepts.
The aims of this thesis were:

- The analysis of the EPS excreted by an electroactive organism under electroactive conditions (chapter 3).

- The development of a platform for the simultaneous electrochemical and optical monitoring of electroactive microbial attachment to electrodes (chapter 4).

- The development of a three-dimensional electrode material providing the artificial fixation of electroactive bacteria for an advanced reactor system (chapter 5).

Fulfilling these aims was supposed to contribute to the progress of BES leading towards their application and establishment for future energy management.

The first aim was the biochemical analysis of the EPS secreted by an electroactive bacterium under electroactive conditions. In order to fulfill this aim *G. sulfurreducens* was cultivated on

graphite based electrodes in MFC mode (WE polarized to +400 mV vs. Ag/AgCl) for 8 d reaching a current density of 172 ± 29 µA cm^{-2}. Routines for both, the biofilm harvest and the EPS processing (biofilm harvest, EPS extraction and fractionation) were established for *G. sulfurreducens* biofilms. Additionally, DOWEX was evaluated as TB EPS extraction reagent. Finally, EPS fractions were analyzed for their main components proteins, carbohydrates, lipids, uronic acids and eDNA.

The electrochemical cultivation of *G. sulfurreducens* was found to strongly promote the production of EPS. Electroactive cultures secreted significantly more EPS compared to cells grown under standard heterotrophic conditions using fumarate respiration. With 116 pg $cell^{-1}$, the highest amount of EPS was measured for the soluble fraction of the EPS of *G. sulfurreducens* using anode respiration. Proteins were found to dominate all EPS fractions (TB, LB and SOL EPS) of the biofilms grown under electrochemical conditions, followed by carbohydrates. Under electrochemical conditions the protein concentration in the SOL EPS (97 ± 18 pg $cell^{-1}$) was tenfold higher as compared to the controls harvested in EXP phase (12 ± 1 pg $cell^{-1}$) and more than 30 times higher as compared to the cells harvested in STAT phase (3 ± 0.2 pg $cell^{-1}$). These findings underline the importance of proteins for the EET of *G. sulfurreducens* and indicate a strong promoting effect of an anodically polarized electrode on EPS production.

To the best of the author's knowledge, these experiments are the first approach towards a complete analysis of the main EPS components of *G. sulfurreducens* under electroactive conditions. Since microbial EPS are very complex and the results strongly depend on the type of analysis, further studies are needed. A more detailed analysis of the major EPS compounds such as preparative proteins or carbohydrate analysis should be performed. This will lead to a deepened understanding of electroactive biofilm formation and function. Furthermore, varying electrochemical parameters such as the applied anode potential might also influence the EPS composition and should therefore be tested in future studies

To accomplish the second aim, a membrane separated flow cell for the parallelized EIS and CLSM measurement was developed. Based on a variety of 3D-printed prototypes a flow cell made from PEEK was constructed using a transparent ITO electrode as working electrode allowing parallel EIS and CLSM measurements. The flow cell was electrochemically

characterized using iron(II) with CV and EIS. Subsequently, surface attachment, current production and development of the charge transfer resistance were monitored for *S. oneidensis* under MFC conditions. Finally, the quality of the electrochemical signal monitoring was improved by the implementation of a screw type Ag/AgCl electrode into the flow cell.

The results show that a flow cell for simultaneous EIS and CLSM was successfully designed and employed with the model organism *S. oneidensis* as microbial fuel cell. A general decrease of the R_{CT} from 292 kΩ to 120 kΩ was observed with an increased current to 0.52 µA cm^{-2} after 17 h of operation. The parallel CLSM images revealed an increasing cell number of *S. oneidensis* on the WE electrode to a monolayer with a 26 cells μm^{-2} after 17 h under MFC conditions.

To the best of the author's knowledge no simultaneous application of these two methods has been reported so far. With this powerful combination of two noninvasive methods, a monitoring tool is presented, which might give interesting insights into the biofilm formation process of mixed and cocultures. Future studies should focus on different types of cultures as well as on the influence of different electrode potential or the direction of electron flow (MFC vs. MES) on the biofilm formation.

Finally, magnetic electrode particles were developed to fulfill the aim of a three-dimensional electrode material providing the artificial fixation of electroactive bacteria. Initially, a production routine for the magnetic electrode particles was developed, including the microwave assisted magnetization of activated carbon. The attachment of *S. oneidensis* resting cells was evaluated and the synthesized particles ($P_{MAG/AC}$) were examined electrochemically.

Developed particles provide a high surface area around 300 $m^2 g^{-1}$ and the size ranges between 20 and 200 µm. Both size and morphology of the particles is determined mainly by the AC, which served as structural backbone. The attachment of *S. oneidensis* resting cells to the particles was characterized by a Langmuir profile, forming a monolayer on the surface with a maximum concentration of $8 \cdot 10^{10} \pm 3 \cdot 10^9$ resting cells g^{-1} $P_{MAG/AC}$ particles. CV experiments with magnetically immobilized $P_{MAG/AC}$ particles showed that particles are

characterized by a capacitive current response. LSV revealed that particles were stable down to a potential of –680 mV vs. Ag/AgCl.

A straight forward approach to in-situ produce magnetite – activated carbon agglomerates for the artificial immobilization of electroactive bacteria was presented by this series of experiments. The magnetic electrode particles are suitable for the application in a magnetically stabilized fluidized bed reactor. However, further experiments focusing on the long-time stability of $P_{MAG/AC}$ particles are needed. These should also include the application in a MES system and the observation of biofilm formation on the particles surface.

In conclusion three approaches focusing on different aspects of bioelectrochemical systems have been presented in this thesis. The EPS of *G. sulfurreducens* has been analyzed for 5 main components, a flow cell for simultaneous EIS and CLSM has been developed and magnetic electrode particles have been synthesized. This multidisciplinary research approach provided detailed information about different aspects of BES. Fundamentals like the electrode attachment and electron transfer were addressed as well as an application oriented reactor system for the electrochemical cultivation of bacteria. New methods to analyze electroactive bacteria are presented as two powerful approaches to investigate the bacteria-electrode-interaction. The methods and results presented in this thesis might promote the application and establishment of BES for future energy management, and thereby may contribute to the minimization of global warming.

7 References

Alhede, M.; Qvortrup, K.; Liebrechts, R.; Høiby, N.; Givskov, M.; Bjarnsholt, T., **2012**. *Combination of microscopic techniques reveals a comprehensive visual impression of biofilm structure and composition*. FEMS Immunology and Medical Microbiology, Vol. 65, Issue 2, pp. 335–342. doi:10.1111/j.1574-695X.2012.00956.x.

Allen, M.J., **1966**. *The Electrochemical Aspects of some Biochemical Systems - IX. The Anomalous Behaviour of E. Coli with Mixed Substrates*. Electrochimica Acta, Vol. 11, , pp. 1503–1508.

Ausfelder, F.; Beilmann, C.; Bertau, M.; Bräuninger, S.; Heinzel, A.; Hoer, R.; Koch, W.; Mahlendorf, F.; Metzelthin, A.; Peuckert, M.; Plass, L.; Räuchle, K.; Reuter, M.; Schaub, G.; Schiebahn, S.; Schwab, E.; Schüth, F.; Stolten, D.; Teßmer, G.; Wagemann, K.; Ziegahn, K.F., **2015**. *Energiespeicherung als Element einer sicheren Energieversorgung*. Chemie-Ingenieur-Technik, Vol. 87, Issue 1–2, pp. 17–89. doi:10.1002/cite.201400183.

Barnett, C., **1931**. *The Bacterial Culture as an Electrical Half-Cell*. Journal of Bacteriology, Vol. 21, , pp. 18–19.

Beese-Vasbender, P.F.; Grote, J.P.; Garrelfs, J.; Stratmann, M.; Mayrhofer, K.J.J., **2015**. *Selective microbial electrosynthesis of methane by a pure culture of a marine lithoautotrophic archaeon*. Bioelectrochemistry, Vol. 102, , pp. 50–55. doi:10.1016/j.bioelechem.2014.11.004.

Ben-Yoav, H.; Freeman, A.; Sternheim, M.; Shacham-Diamand, Y., **2011**. *An electrochemical impedance model for integrated bacterial biofilms*. Electrochimica Acta, Vol. 56, Issue 23, pp. 7780–7786. doi:10.1016/j.electacta.2010.12.025.

Blanchet, E.; Duquenne, F.; Rafrafi, Y.; Etcheverry, L.; Erable, B.; Bergel, A., **2015**. *Importance of the hydrogen route in up-scaling electrosynthesis for microbial CO_2 reduction*. Energy Environ. Sci., Vol. 8, Issue 12, pp. 3731–3744. doi:10.1039/C5EE03088A.

Blumenkrantz, N.; Asboe-Hansen, G., **1973**. *New method for quantitative determination of uronic acids*. Analytical Biochemistry, Vol. 54, Issue 2, pp. 484–489. doi:10.1016/0003-2697(73)90377-1.

Boles, B.R.; Thoendel, M.; Singh, P.K., **2004**. *Self-generated diversity produces "insurance effects" in biofilm communities*. Proceedings of the National Academy of Sciences, Vol. 101, Issue 47, pp. 16630–16635. doi:10.1073/pnas.0407460101.

Bond, D.R.; Holmes, D.E.; Tender, L.M.; Lovley, D.R., **2002**. *Electrode-Reducing*

Microorganisms That Harvest Energy from Marine Sediments. Science, Vol. 295, Issue 5554, pp. 483–485. doi:10.1126/science.1066771.

Bond, D.R.; Lovley, D.R., **2003**. *Electricity Production by Geobacter sulfurreducens Attached to Electrodes*. Applied and Environmental Microbiology, Vol. 69, Issue 3, pp. 1548–1555. doi:10.1128/AEM.69.3.1548.

Borole, A.P.; Aaron, D.; Hamilton, C.Y.; Tsouris, C., **2010**. *Understanding long-term changes in microbial fuel cell performance using electrochemical impedance spectroscopy.* Environmental science & technology, Vol. 44, Issue 7, pp. 2740–2745. doi:10.1021/es9032937.

Borole, A.P.; Reguera, G.; Ringeisen, B.; Wang, Z.-W.; Feng, Y.; Kim, B.H., **2011**. *Electroactive biofilms: Current status and future research needs*. Energy & Environmental Science, Vol. 4, Issue 12, p. 4813. doi:10.1039/c1ee02511b.

Bressel, A.; Schultze, J.W.; Khan, W.; Wolfaardt, G.M.; Rohns, H.P.; Irmscher, R.; Schöning, M.J., **2003**. *High resolution gravimetric, optical and electrochemical investigations of microbial biofilm formation in aqueous systems*. Electrochimica Acta, Vol. 48, Issue 20–22, pp. 3363–3372. doi:10.1016/S0013-4686(03)00406-7.

Briehl, H., **2008**. *Chemie der Werkstoffe – Werkstoffspezifische Chemie und Anwendungen einiger nichtmetallischer Elemente*. B.G. Teubner Verlag, Wiesbaden. doi:10.1007/978-3-658-06225-5.

Brunauer, S.; Emmett, P.H.; Teller, E., **1938**. *Adsorption of Gases in Multimolecular Layers*. Journal of the American Chemical Society, Vol. 60, Issue 2, pp. 309–319. doi:10.1021/ja01269a023.

Brutinel, E.D.; Gralnick, J.A., **2012**. *Shuttling happens: Soluble flavin mediators of extracellular electron transfer in Shewanella*. Applied Microbiology and Biotechnology, Vol. 93, Issue 1, pp. 41–48. doi:10.1007/s00253-011-3653-0.

Bundesministerium für Wirtschaft und Energie, **2017**. *Bundesbericht Energieforschung 2017*. Federal Ministry for Economic Affairs and Energy, Berlin, Germany.

Bundesumweltamt, **2016a**. *Klimaschutzplan 2050 der Bundesregierung, Diskussionsbeitrag des Umweltbundesamtes*. Federal Environment Agency, Vol. Position A, , p. 65. doi:ISSN 1862-4359 Dessau-Roßlau.

Bundesumweltamt, **2016b**. *Submission under the United Nations Framework Convention on Climate Change and the Kyoto Protocol 2016 - National Inventory Report for the*

German Greenhouse Gas Inventory 1990 to 2014. Federal Environment Agency. doi:ISSN 1862-4359 Dessau-Roßlau.

Caccavo, F.; Lonergan, D.J.; Lovley, D.R.; Davis, M., **1994**. *Acetate- Oxidizing Dissimilatory Metal-Reducing Microorganism*. Microbiology, Vol. 60, Issue 10, pp. 3752–3759. http://aem.asm.org/content/60/10/3752.full.pdf

Call, D.; Logan, B.E., **2008**. *Hydrogen production in a single chamber microbial electrolysis cell lacking a membrane*. Environmental Science and Technology, Vol. 42, Issue 9, pp. 3401–3406. doi:10.1021/es8001822.

Carbajosa, S.; Malki, M.; Caillard, R.; Lopez, M.F.; Palomares, F.J.; Martín-Gago, J.A.; Rodríguez, N.; Amils, R.; Fernández, V.M.; De Lacey, A.L., **2010**. *Electrochemical growth of Acidithiobacillus ferrooxidans on a graphite electrode for obtaining a biocathode for direct electrocatalytic reduction of oxygen*. Biosensors and Bioelectronics, Vol. 26, Issue 2, pp. 877–880. doi:10.1016/j.bios.2010.07.037.

Castro, L.; Zhang, R.; Muñoz, J. a; González, F.; Blázquez, M.L.; Sand, W.; Ballester, A., **2014**. *Characterization of exopolymeric substances (EPS) produced by Aeromonas hydrophila under reducing conditions.* Biofouling, Vol. 30, Issue 4, pp. 501–511. doi:10.1080/08927014.2014.892586.

Catal, T.; Li, K.; Bermek, H.; Liu, H., **2008**. *Electricity production from twelve monosaccharides using microbial fuel cells*. Journal of Power Sources, Vol. 175, Issue 1, pp. 196–200. doi:10.1016/j.jpowsour.2007.09.083.

Cheng, S.; Xing, D.; Call, D.F.; Logan, B.E., **2009**. *Direct biological conversion of electrical current into methane by electromethanogenesis.* Environmental science & technology, Vol. 43, Issue 10, pp. 3953–3958. http://www.ncbi.nlm.nih.gov/pubmed/19544913

Cho, E.J.; Ellington, A.D., **2007**. *Optimization of the biological component of a bioelectrochemical cell*. Bioelectrochemistry, Vol. 70, , pp. 165–172. doi:10.1016/j.bioelechem.2006.03.031.

Choi, K.H.; Kumar, A.; Schweizer, H.P., **2006**. *A 10-min method for preparation of highly electrocompetent Pseudomonas aeruginosa cells: Application for DNA fragment transfer between chromosomes and plasmid transformation*. Journal of Microbiological Methods, Vol. 64, Issue 3, pp. 391–397. doi:10.1016/j.mimet.2005.06.001.

Clauwaert, P.; Desloover, J.; Shea, C.; Nerenberg, R.; Boon, N.; Verstraete, W., **2009**. *Enhanced nitrogen removal in bio-electrochemical systems by pH control.* Biotechnology

letters, Vol. 31, Issue 10, pp. 1537–43. doi:10.1007/s10529-009-0048-8.

Coppi, M. V.; Leang, C.; Sandler, S.J.; Lovley, D., **2001**. *Development of a genetic system for Geobacter sulfurreducens*. Applied and Environmental Microbiology, Vol. 67, Issue 7, pp. 3180–3187. doi:10.1128/AEM.67.7.3180-3187.2001.

Daniel, D.K.; Das Mankidy, B.; Ambarish, K.; Manogari, R., **2009**. *Construction and operation of a microbial fuel cell for electricity generation from wastewater*. International Journal of Hydrogen Energy, Vol. 34, Issue 17, pp. 7555–7560. doi:10.1016/j.ijhydene.2009.06.012.

Davey, M.E.; Caiazza, N.C.; Toole, G. a O., **2003**. *Rhamnolipid Surfactant Production Affects Bio lm Architecture in*. Microbiology, Vol. 185, Issue 3, pp. 1027–1036. doi:10.1128/JB.185.3.1027.

Deeke, A.; Sleutels, T.H.J. a.; Donkers, T.F.W.; Hamelers, H.V.M.; Buisman, C.J.N.; Ter Heijne, A., **2015**. *Fluidized Capacitive Bioanode As a Novel Reactor Concept for the Microbial Fuel Cell*. Environmental Science & Technology, Vol. 49, Issue 3, pp. 1929–1935. doi:10.1021/es503063n.

Deng, L.; Zhou, M.; Liu, C.; Liu, L.; Liu, C.; Dong, S., **2010**. *Development of high performance of Co/Fe/N/CNT nanocatalyst for oxygen reduction in microbial fuel cells*. Talanta, Vol. 81, Issue 1–2, pp. 444–448. doi:10.1016/j.talanta.2009.12.022.

Deng, Q.; Li, X.; Zuo, J.; Ling, A.; Logan, B.E., **2010**. *Power generation using an activated carbon fiber felt cathode in an upflow microbial fuel cell*. Journal of Power Sources, Vol. 195, Issue 4, pp. 1130–1135. doi:10.1016/j.jpowsour.2009.08.092.

Deutzmann, J.; Sahin, M.; Spormann, A., **2015**. *Extracellular Enzymes Facilitate Electron Uptake in Biocorrosion and*. mBio, Vol. 6, Issue 2, pp. 1–8. doi:10.1128/mBio.00496-15.Editor.

Dietrich, L.E.P.; Price-Whelan, A.; Petersen, A.; Whiteley, M.; Newman, D.K., **2006**. *The phenazine pyocyanin is a terminal signalling factor in the quorum sensing network of Pseudomonas aeruginosa*. Molecular Microbiology, Vol. 61, Issue 5, pp. 1308–1321. doi:10.1111/j.1365-2958.2006.05306.x.

Dominguez-Benetton, X.; Sevda, S.; Vanbroekhoven, K.; Pant, D., **2012**. *The accurate use of impedance analysis for the study of microbial electrochemical systems*. Chemical Society Reviews, Vol. 41, Issue 21, p. 7228. doi:10.1039/c2cs35026b.

Du, Z.; Li, H.; Gu, T., **2007**. *A state of the art review on microbial fuel cells: A promising*

technology for wastewater treatment and bioenergy. Biotechnology Advances, Vol. 25, Issue 5, pp. 464–482. doi:10.1016/j.biotechadv.2007.05.004.

Dubois, M.; Gilles, K. a.; Hamilton, J.K.; Rebers, P. a.; Smith, F., **1956**. *Colorimetric method for determination of sugars and related substances*. Analytical Chemistry, Vol. 28, Issue 3, pp. 350–356. doi:10.1021/ac60111a017.

Ende, D.; Mangold, K., **1993**. *Impedanzspektroskopie*. Chemie in unserer Zeit, Vol. 27, Issue 3, pp. 134–140. doi:0009-281s1/93/0306-0134.

Estévez-Canales, M.; Pinto, D.; Coradin, T.; Laberty-Rober, C.; Esteve-Núñez, A., **2017**. *Silica-immobilization of Geobacter sulfurreducens for constructing ready-to-use artificial bioelectrodes. Microbial Biotechnology*. Microbial Biotechnology., Vol. In press, . doi:ISSN 17517915.

Fang, H.H.; Chan, K.Y.; Xu, L.C., **2000**. *Quantification of bacterial adhesion forces using atomic force microscopy (AFM).* Journal of microbiological methods, Vol. 40, Issue 1, pp. 89–97. doi:10.1016/S0167-7012(99)00137-2.

Flemming, H.-C.; Wingender, J., **2010**. *The biofilm matrix.* Nature reviews. Microbiology, Vol. 8, Issue 9, pp. 623–33. doi:10.1038/nrmicro2415.

Franks, A.E.; Nevin, K.P.; Jia, H.; Izallalen, M.; Woodard, T.L.; Lovley, D.R., **2009**. *Novel strategy for three-dimensional real-time imaging of microbial fuel cell communities: monitoring the inhibitory effects of proton accumulation within the anode biofilm*. Energy Environ. Sci., Vol. 2, Issue 1, pp. 113–119. doi:10.1039/B816445B.

Fricke, K.; Harnisch, F.; Schröder, U., **2008**. *On the use of cyclic voltammetry for the study of anodic electron transfer in microbial fuel cells*. Energy & Environmental Science, Vol. 1, Issue 1, p. 144. doi:10.1039/b802363h.

Fultz, M. Lou; Durst, R.A., **1982**. *Mediator compounds for the electrochemical study of biological redox systems: a compilation*. Analytica Chimica Acta, Vol. 140, Issue 1, pp. 1–18. doi:10.1016/S0003-2670(01)95447-9.

Galushko, A.S.; Schink, B., **2000**. *Oxidation of acetate through reactions of the citric acid cycle by Geobacter sulfurreducens in pure culture and in syntrophic coculture*. Archives of Microbiology, Vol. 174, Issue 5, pp. 314–321. doi:10.1007/s002030000208.

Ganigué, R.; Puig, S.; Batlle-Vilanova, P.; Balaguer, M.D.; Colprim, J., **2015**. *Microbial electrosynthesis of butyrate from carbon dioxide*. Chem. Commun., Vol. 51, Issue 15, pp. 3235–3238. doi:10.1039/C4CC10121A.

Ha, P.T.; Moon, H.; Kim, B.H.; Ng, H.Y.; Chang, I.S., **2010**. *Determination of charge transfer resistance and capacitance of microbial fuel cell through a transient response analysis of cell voltage*. Biosensors and Bioelectronics, Vol. 25, Issue 7, pp. 1629–1634. doi:10.1016/j.bios.2009.11.023.

Hameed, B.H.; Din, A.T.M.; Ahmad, A.L., **2007**. *Adsorption of methylene blue onto bamboo-based activated carbon: Kinetics and equilibrium studies*. Journal of Hazardous Materials, Vol. 141, Issue 3, pp. 819–825. doi:10.1016/j.jhazmat.2006.07.049.

Van Handel, E., **1985**. *Rapid determination of total lipids in mosquitoes*. Journal of the American Mosquito Control Association, Vol. 1, Issue 3, pp. 302–304.

Hau, H.H.; Gilbert, A.; Coursolle, D.; Gralnick, J.A., **2008**. *Mechanism and consequences of anaerobic respiration of cobalt by Shewanella oneidensis strain MR-1*. Applied and Environmental Microbiology, Vol. 74, Issue 22, pp. 6880–6886. doi:10.1128/AEM.00840-08.

He, Z.; Mansfeld, F., **2009**. *Exploring the use of electrochemical impedance spectroscopy (EIS) in microbial fuel cell studies*. Energy & Environmental Science, Vol. 2, Issue 2, pp. 215–219. doi:10.1039/b814914c.

He, Z.; Wagner, N.; Minteer, S.D.; Angenent, L.T., **2006**. *An upflow microbial fuel cell with an interior cathode: assessment of the internalresistance by impedance spectroscopy*. Environ Sci Technol, Vol. 40, Issue 17, p. 5212–5217. doi:10.1021/es060394f.

Heijne, A. Ter; Liu, F.; Weijden, R. van der; Weijma, J.; Buisman, C.J.N.; Hamelers, H.V.M., **2010**. *Copper Recovery Combined with Electricity Production in a Microbial Fuel Cell*. Environmental Science & Technology, Vol. 44, Issue 11, pp. 4376–4381. doi:10.1021/es100526g.

Hiegemann, H.; Herzer, D.; Nettmann, E.; Lübken, M.; Schulte, P.; Schmelz, K.G.; Gredigk-Hoffmann, S.; Wichern, M., **2016**. *An integrated 45 L pilot microbial fuel cell system at a full-scale wastewater treatment plant*. Bioresource Technology, Vol. 218, Issue June, pp. 115–122. doi:10.1016/j.biortech.2016.06.052.

Huang, L.; Logan, B.E., **2008**. *Electricity generation and treatment of paper recycling wastewater using a microbial fuel cell*. Applied Microbiology and Biotechnology, Vol. 80, Issue 2, pp. 349–355. doi:10.1007/s00253-008-1546-7.

Ieropoulos, I.; Melhuish, C.; Greenman, J.; Horsfield, I., **2005**. *EcoBot-II: An artificial agent with a natural metabolism*. International Journal of Advanced Robotic Systems, Vol. 2,

Issue 4, pp. 295–300. doi:10.5772/5777.

Jain, A.; Gazzola, G.; Panzera, A.; Zanoni, M.; Marsili, E., **2011**. *Visible spectroelectrochemical characterization of Geobacter sulfurreducens biofilms on optically transparent indium tin oxide electrode*. Electrochimica Acta, Vol. 56, Issue 28, pp. 10776–10785. doi:10.1016/j.electacta.2011.02.073.

Janicek, A.; Fan, Y.; Liu, H., **2014**. *Design of microbial fuel cells for practical application: a review and analysis of scale-up studies*. Biofuels, Vol. 5, Issue 1, pp. 79–92. doi:10.4155/bfs.13.69.

Janknecht, P.; Melo, L., **2003**. *Online biofilm monitoring*. Reviews in Environmental Science and Biotechnology, Issue 2002, pp. 269–283. doi:10.1023/B:RESB.0000040461.69339.04.

Jeske, M.; Altenbuchner, J., **2010**. *The Escherichia coli rhamnose promoter rhaPBAD is in Pseudomonas putida KT2440 independent of Crp-cAMP activation*. Applied Microbiology and Biotechnology, Vol. 85, Issue 6, pp. 1923–1933. doi:10.1007/s00253-009-2245-8.

Kim, J.R.; Jung, S.H.; Regan, J.M.; Logan, B.E., **2007**. *Electricity generation and microbial community analysis of alcohol powered microbial fuel cells*. Bioresource Technology, Vol. 98, Issue 13, pp. 2568–2577. doi:10.1016/j.biortech.2006.09.036.

Kim, T.S.; Kim, B.H., **1988**. *Electron flow shift in Clostridiumacetobutylicum fermentation by electrochemically introduced reducing equivalent*. Biotechnology Letters, Vol. 10, Issue 2, pp. 123–128. doi:10.1007/BF01024638.

Kipf, E.; Koch, J.; Geiger, B.; Erben, J.; Richter, K.; Gescher, J.; Zengerle, R.; Kerzenmacher, S., **2013**. *Systematic screening of carbon-based anode materials for microbial fuel cells with Shewanella oneidensis MR-1*. Bioresource Technology, Vol. 146, , pp. 386–392. doi:10.1016/j.biortech.2013.07.076.

Kouzuma, A.; Meng, X.Y.; Kimura, N.; Hashimoto, K.; Watanabe, K., **2010**. *Disruption of the putative cell surface polysaccharide biosynthesis Gene SO3177 in Shewanella oneidensis MR-1 enhances adhesion to electrodes and current generation in microbial fuel cells*. Applied and Environmental Microbiology, Vol. 76, Issue 13, pp. 4151–4157. doi:10.1128/AEM.00117-10.

Krieg, T.; Sydow, A.; Schröder, U.; Schrader, J.; Holtmann, D., **2014**. *Reactor concepts for bioelectrochemical syntheses and energy conversion*. Trends in Biotechnology, Vol. 32,

Issue 12, pp. 645–655. doi:10.1016/j.tibtech.2014.10.004.

Kuntke, P.; Sleutels, T.H.J.A.; Saakes, M.; Buisman, C.J.N., **2014**. *Hydrogen production and ammonium recovery from urine by a Microbial Electrolysis Cell*. International Journal of Hydrogen Energy, Vol. 39, Issue 10, pp. 4771–4778. doi:10.1016/j.ijhydene.2013.10.089.

Langmuir, I., **1932**. *Surface chemistry**. Noble Lecture.

Le, D.Q.; Tokonami, S.; Nishino, T.; Shiigi, H.; Nagaoka, T., **2015**. *Electrochemical evaluation of poly(3,4-ethylenedioxythiophene) films doped with bacteria based on viability analysis*. Bioelectrochemistry, Vol. 105, , pp. 50–55. doi:10.1016/j.bioelechem.2015.05.003.

Lebedev, N.; Strycharz-Glaven, S.M.; Tender, L.M., **2014**. *Spatially resolved confocal resonant Raman microscopic analysis of anode-grown Geobacter sulfurreducens biofilms*. ChemPhysChem, Vol. 15, Issue 2, pp. 320–327. doi:10.1002/cphc.201300984.

Li, S.-W.; Sheng, G.-P.; Cheng, Y.-Y.; Yu, H.-Q.; Zhang, P.; Gonzalez-Gil, G.; Thomas, L.; Emwas, A.H.; Lens, P.N.; Saikaly, P.E.; Zeng, J.; Cao, B.; Yu, G.H.; Tang, Z.; Xu, Y.C.; Shen, Q.R.; Tourney, J.; Ngwenya, B.T.; Flemming, H.-C.; Neu, T.R.; Payne, S.M.; et al., **2016**. *Redox properties of extracellular polymeric substances (EPS) from electroactive bacteria*. Scientific Reports, Vol. 6, Issue Table 1, p. 39098. doi:10.1038/srep39098.

Liu, C.Z.; Wang, F.; Ou-Yang, F., **2009**. *Ethanol fermentation in a magnetically fluidized bed reactor with immobilized Saccharomyces cerevisiae in magnetic particles*. Bioresource Technology, Vol. 100, Issue 2, pp. 878–882. doi:10.1016/j.biortech.2008.07.016.

Liu, H.; Fang, H.H.P., **2002**. *Extraction of extracellular polymeric substances (EPS) of sludges*. Journal of Biotechnology, Vol. 95, Issue 3, pp. 249–256. doi:10.1016/S0168-1656(02)00025-1.

Liu, J.; Zhang, F.; He, W.; Zhang, X.; Feng, Y.; Logan, B.E., **2014**. *Intermittent contact of fluidized anode particles containing exoelectrogenic biofilms for continuous power generation in microbial fuel cells*. Journal of Power Sources, Vol. 261, , pp. 278–284. doi:10.1016/j.jpowsour.2014.03.071.

Logan, B.E.; Murano, C.; Scott, K.; Gray, N.D.; Head, I.M., **2005**. *Electricity generation from cysteine in a microbial fuel cell*. Water Research, Vol. 39, Issue 5, pp. 942–952. doi:10.1016/j.watres.2004.11.019.

Logan, B.E.; Regan, J.M., **2006**. *Microbial fuel cells-challenges and applications.*

Environmental science & technology, Vol. 40, Issue 17, pp. 5172–5180. doi:10.1021/es0627592.

Lovley, D.R., **2011**. *Live wires: direct extracellular electron exchange for bioenergy and the bioremediation of energy-related contamination*. Energy & Environmental Science, Vol. 4, Issue 12, p. 4896. doi:10.1039/c1ee02229f.

Lovley, D.R.; Giovannoni, S.J.; White, D.C.; Champine, J.E.; Phillips, E.J.P.; Gorby, Y.A.; Goodwin, S., **1993**. *Geobacter metallireducens gen. nov. sp. nov., a microorganism capable of coupling the complete oxidation of organic compounds to the reduction of iron and other metals*. Archives of Microbiology, Vol. 159, Issue 4, pp. 336–344. doi:10.1007/BF00290916.

Lovley, D.R.; Phillips, E.J.P., **1988**. *Novel Mode of Microbial Energy Metabolism: Organic Carbon Oxidation Coupled to Dissimilatory Reduction of Iron or Manganese*. Appl. Envir. Microbiol., Vol. 54, Issue 6, pp. 1472–1480. doi:10.1103/PhysRevLett.50.1998.

Lovley, D.R.; Ueki, T.; Zhang, T.; Malvankar, N.S.; Shrestha, P.M.; Flanagan, K.A.; Aklujkar, M.; Butler, J.E.; Giloteaux, L.; Rotaru, A.E.; Holmes, D.E.; Franks, A.E.; Orellana, R.; Risso, C.; Nevin, K.P., **2011**. *Geobacter. The Microbe Electric's Physiology, Ecology, and Practical Applications*,. doi:10.1016/B978-0-12-387661-4.00004-5.

Luo, H.; Liu, G.; Zhang, R.; Jin, S., **2009**. *Phenol degradation in microbial fuel cells*. Chemical Engineering Journal, Vol. 147, Issue 2–3, pp. 259–264. doi:10.1016/j.cej.2008.07.011.

Madigan, M.T.; Martinko, J.M., **2006**. *Brock - Biology of Microorganisms*. Pearson Education Inc.

Malvankar, N.S.; Tuominen, M.T.; Lovley, D.R., **2012**. *Biofilm conductivity is a decisive variable for high-current-density Geobacter sulfurreducens microbial fuel cells*. Energy & Environmental Science, Vol. 5, Issue 2, p. 5790. doi:10.1039/c2ee03388g.

Malvankar, N.S.; Vargas, M.; Nevin, K.P.; Franks, A.E.; Leang, C.; Kim, B.-C.; Inoue, K.; Mester, T.; Covalla, S.F.; Johnson, J.P.; Rotello, V.M.; Tuominen, M.T.; Lovley, D.R., **2011**. *Tunable metallic-like conductivity in microbial nanowire networks.* Nature nanotechnology, Vol. 6, Issue 9, pp. 573–9. doi:10.1038/nnano.2011.119.

Mangold, K.-M.; Schuster, J.; Weidlich, C., **2011**. *Synthesis and properties of magnetite/polypyrrole core–shell nanocomposites and polypyrrole hollow spheres*. Electrochimica Acta, Vol. 56, Issue 10, pp. 3616–3619. doi:10.1016/j.electacta.2010.11.044.

Mangold, S.; Harneit, K.; Rohwerder, T.; Claus, G.; Sand, W., **2008**. *Novel combination of atomic force microscopy and epifluorescence microscopy for visualization of leaching bacteria on pyrite*. Applied and Environmental Microbiology, Vol. 74, Issue 2, pp. 410–415. doi:10.1128/AEM.01812-07.

Manohar, A.K.; Bretschger, O.; Nealson, K.H.; Mansfeld, F., **2008**. *The use of electrochemical impedance spectroscopy (EIS) in the evaluation of the electrochemical properties of a microbial fuel cell*. Bioelectrochemistry, Vol. 72, Issue 2, pp. 149–154. doi:10.1016/j.bioelechem.2008.01.004.

Manohar, A.K.; Mansfeld, F., **2009**. *The internal resistance of a microbial fuel cell and its dependence on cell design and operating conditions*. Electrochimica Acta, Vol. 54, Issue 6, pp. 1664–1670. doi:10.1016/j.electacta.2008.06.047.

Marcus, P.; Mansfeld, F., **2005**. *Analytical Methods In Corrosion Science and Engineering*. Taylor & Francis, p. 776. doi:10.1201/9781420028331.

Marshall, C.W.; Ross, D.E.; Fichot, E.B.; Norman, R.S.; May, H.D., **2013**. *Long-term operation of microbial electrosynthesis systems improves acetate production by autotrophic microbiomes*. Environmental Science and Technology, Vol. 47, Issue 11, pp. 6023–6029. doi:10.1021/es400341b.

Marsili, E.; Baron, D.B.; Shikhare, I.D.; Coursolle, D.; Gralnick, J. a; Bond, D.R., **2008**. *Shewanella secretes flavins that mediate extracellular electron transfer*. Proceedings of the National Academy of Sciences of the United States of America, Vol. 105, Issue 10, pp. 3968–3973. doi:10.1073/pnas.0710525105.

Mohan, S.V.; Srikanth, S.; Sarma, P.N., **2009**. *Non-catalyzed microbial fuel cell (MFC) with open air cathode for bioelectricity generation during acidogenic wastewater treatment*. Bioelectrochemistry, Vol. 75, Issue 2, pp. 130–135. doi:10.1016/j.bioelechem.2009.03.002.

Mohan, V.S.; Saravanan, R.; Raghavulu, S.V.; Mohanakrishna, G.; Sarma, P.N., **2008**. *Bioelectricity production from wastewater treatment in dual chambered microbial fuel cell (MFC) using selectively enriched mixed microflora: Effect of catholyte*. Bioresource Technology, Vol. 99, Issue 3, pp. 596–603. doi:10.1016/j.biortech.2006.12.026.

Mohanakrishna, G.; Seelam, J.S.; Vanbroekhoven, K.; Pant, D., **2015**. *An enriched electroactive homoacetogenic biocathode for the microbial electrosynthesis of acetate through carbon dioxide reduction*. Faraday Discuss., Vol. 183, , pp. 445–462.

doi:10.1039/C5FD00041F.

Möhle, R.B.; Langemann, T.; Haesner, M.; Augustin, W.; Scholl, S.; Neu, T.R.; Hempel, D.C.; Horn, H., **2007**. *Structure and shear strength of microbial biofilms as determined with confocal laser scanning microscopy and fluid dynamic gauging using a novel rotating disc biofilm reactor*. Biotechnology and Bioengineering, Vol. 98, Issue 4, pp. 747–755. doi:10.1002/bit.21448.

Monroe, D., **2007**. *Looking for Chinks in the Armor of Bacterial Biofilms*. PLoS Biology, Vol. 5, Issue 11, p. e307. doi:10.1371/journal.pbio.0050307.

Müller, H.; Bosch, J.; Griebler, C.; Damgaard, L.R.; Nielsen, L.P.; Lueders, T.; Meckenstock, R.U., **2016**. *Long-distance electron transfer by cable bacteria in aquifer sediments*. The ISME Journal, Vol. 10, Issue 8, pp. 2010–2019. doi:10.1038/ismej.2015.250.

Nancharaiah, Y.; Mohan, S.; Lens, P., **2015**. *Metals removal and recovery in bioelectrochemical systems: a review*. Bioresource technology, Vol. 195, , pp. 102–114. doi:org/10.1016/j.biortech.2015.06.058.

Neu, T.R.; Lawrence, J.R., **2014**. *Investigation of Microbial Biofilm Structure by Laser Scanning Microscopy*. Advances in Biochemical Engineering/Biotechnology, Vol. 146, , pp. 1–51. doi:10.1007/10_2014_272.

Nevin, K.P.; Hensley, S. a.; Franks, A.E.; Summers, Z.M.; Ou, J.; Woodard, T.L.; Snoeyenbos-West, O.L.; Lovley, D.R., **2011**. *Electrosynthesis of organic compounds from carbon dioxide is catalyzed by a diversity of acetogenic microorganisms*. Applied and Environmental Microbiology, Vol. 77, Issue 9, pp. 2882–2886. doi:10.1128/AEM.02642-10.

Nevin, K.P.; Kim, B.-C.; Glaven, R.H.; Johnson, J.P.; Woodard, T.L.; Methé, B. a; Didonato, R.J.; Covalla, S.F.; Franks, A.E.; Liu, A.; Lovley, D.R., **2009**. *Anode biofilm transcriptomics reveals outer surface components essential for high density current production in Geobacter sulfurreducens fuel cells.* PloS one, Vol. 4, Issue 5, p. e5628. doi:10.1371/journal.pone.0005628.

Nevin, K.P.; Richter, H.; Covalla, S.F.; Johnson, J.P.; Woodard, T.L.; Orloff, A.L.; Jia, H.; Zhang, M.; Lovley, D.R., **2008**. *Power output and columbic efficiencies from biofilms of Geobacter sulfurreducens comparable to mixed community microbial fuel cells*. Environmental Microbiology, Vol. 10, Issue 10, pp. 2505–2514. doi:10.1111/j.1462-2920.2008.01675.x.

Nevin, K.P.; Woodard, T.L.; Franks, A.E.; Summers, Z.M.; Lovley, D.R., **2010**. *Microbial Electrosynthesis : Feeding Microbial Electrosynthesis : Feeding Microbes Electricity To Convert Carbon Dioxide and Water to Multicarbon Extracellular Organic Compounds*. mbio, Vol. 1, , p. 4. doi:10.1128/mBio.00103-10.Editor.

Oh, S.; Logan, B.E., **2005**. *Hydrogen and electricity production from a food processing wastewater using fermentation and microbial fuel cell technologies*. Water Research, Vol. 39, Issue 19, pp. 4673–4682. doi:10.1016/j.watres.2005.09.019.

Özkara, S.; Akgöl, S.; Çanak, Y.; Denizli, A., **2004**. *A novel magnetic adsorbent for immunoglobulin-G purification in a magnetically stabilized fluidized bed*. Biotechnology Progress, Vol. 20, Issue 4, pp. 1169–1175. doi:10.1021/bp049896s.

Pant, D.; Van Bogaert, G.; Diels, L.; Vanbroekhoven, K., **2010**. *A review of the substrates used in microbial fuel cells (MFCs) for sustainable energy production*. Bioresource Technology, Vol. 101, Issue 6, pp. 1533–1543. doi:10.1016/j.biortech.2009.10.017.

Pasupuleti, S.B.; Srikanth, S.; Venkata Mohan, S.; Pant, D., **2015**. *Continuous mode operation of microbial fuel cell (MFC) stack with dual gas diffusion cathode design for the treatment of dark fermentation effluent*. International Journal of Hydrogen Energy, Vol. 40, Issue 36, pp. 12424–12435. doi:10.1016/j.ijhydene.2015.07.049.

Patil, S.A.; Arends, J.B.A.; Vanwonterghem, I.; Van Meerbergen, J.; Guo, K.; Tyson, G.W.; Rabaey, K., **2015**. *Selective Enrichment Establishes a Stable Performing Community for Microbial Electrosynthesis of Acetate from CO2*. Environmental Science and Technology, Vol. 49, Issue 14, pp. 8833–8843. doi:10.1021/es506149d.

Pirbadian, S.; Barchinger, S.E.; Leung, K.M.; Byun, H.S.; Jangir, Y.; Bouhenni, R.A.; Reed, S.B.; Romine, M.F.; Saffarini, D.A.; Shi, L.; Gorby, Y.A.; Golbeck, J.H.; El-Naggar, M.Y., **2014**. *Shewanella oneidensis MR-1 nanowires are outer membrane and periplasmic extensions of the extracellular electron transport components.* Proceedings of the National Academy of Sciences of the United States of America, Vol. 111, Issue 35, pp. 12883–8. doi:10.1073/pnas.1410551111.

Pospiskova, K.; Prochazkova, G.; Safarik, I., **2013**. *One-step magnetic modification of yeast cells by microwave-synthesized iron oxide microparticles.* Letters in applied microbiology, Vol. 56, Issue 6, pp. 456–461. doi:10.1111/lam.12069.

Pospiskova, K.; Safarik, I., **2013**. *Magnetically modified spent grain as a low-cost, biocompatible and smart carrier for enzyme immobilisation*. Journal of the Science of

Food and Agriculture, Vol. 93, Issue 7, pp. 1598–1602. doi:10.1002/jsfa.5930.

Potter, M.C., **1912**. *Electrical Effects accompanying the Decomposition of Organis Compounds*. Proceedings of the Royal Society (London), Vol. 84, Issue Part B, pp. 260–276.

Priester, J.H.; Horst, A.M.; Van De Werfhorst, L.C.; Saleta, J.L.; Mertes, L.A.K.; Holden, P.A., **2007**. *Enhanced visualization of microbial biofilms by staining and environmental scanning electron microscopy*. Journal of Microbiological Methods, Vol. 68, Issue 3, pp. 577–587. doi:10.1016/j.mimet.2006.10.018.

Rabaey, K.; Angenent, L.; Schröder, U.; Keller, J., **2008**. *Bioelectrochemical systems*. IWA Publishing Alliance House, Issue May.

Rabaey, K.; Clauwaert, P.; Aelterman, P.; Verstraete, W., **2005**. *Tubular microbial fuel cell for efficient electricity generation*. Environmental Science and Technology, Vol. 39, Issue 20, pp. 8077–8082. doi:10.1021/es050986i.

Rabaey, K.; Girguis, P.; Nielsen, L.K., **2011**. *Metabolic and practical considerations on microbial electrosynthesis*. Current Opinion in Biotechnology, Vol. 22, Issue 3, pp. 371–377. doi:10.1016/j.copbio.2011.01.010.

Rabaey, K.; Rozendal, R. a, **2010**. *Microbial electrosynthesis - revisiting the electrical route for microbial production.* Nature reviews. Microbiology, Vol. 8, Issue 10, pp. 706–716. doi:10.1038/nrmicro2422.

Ramasamy, R.P.; Ren, Z.; Mench, M.M.; Regan, J.M., **2008**. *Impact of initial biofilm growth on the anode impedance of microbial fuel cells*. Biotechnology and Bioengineering, Vol. 101, Issue 1, pp. 101–108. doi:10.1002/bit.21878.

Reguera, G.; Nevin, K.P.; Nicoll, J.S.; Covalla, S.F.; Woodard, T.L.; Lovley, D.R., **2006**. *Biofilm and nanowire production leads to increased current in Geobacter sulfurreducens fuel cells*. Applied and Environmental Microbiology, Vol. 72, Issue 11, pp. 7345–7348. doi:10.1128/AEM.01444-06.

Richter, H.; Nevin, K.P.; Jia, H.; Lowy, D. a.; Lovley, D.R.; Tender, L.M., **2009**. *Cyclic voltammetry of biofilms of wild type and mutant Geobacter sulfurreducens on fuel cell anodes indicates possible roles of OmcB, OmcZ, type IV pili, and protons in extracellular electron transfer*. Energy Environ. Sci., Vol. 2, Issue 5, p. 506. doi:10.1039/b816647a.

Rodrigo, M.A.; Cañizares, P.; Lobato, J.; Paz, R.; Sáez, C.; Linares, J.J., **2007**. *Production of electricity from the treatment of urban waste water using a microbial fuel cell*. Journal

of Power Sources, Vol. 169, Issue 1, pp. 198–204. doi:10.1016/j.jpowsour.2007.01.054.

Rohwerder, T.; Gehrke, T.; Kinzler, K.; Sand, W., **2003**. *Bioleaching review part A: progress in bioleaching: fundamentals and echanisms of bacterial metal sulfide oxidation*. Research Journal of Biotechnology, Vol. 63, , pp. 239–248. doi:10.1007/s00253-003-1448-7.

Rollefson, J.B.; Stephen, C.S.; Tien, M.; Bond, D.R., **2011**. *Identification of an extracellular polysaccharide network essential for cytochrome anchoring and biofilm formation in Geobacter sulfurreducens*. Journal of Bacteriology, Vol. 193, Issue 5, pp. 1023–1033. doi:10.1128/JB.01092-10.

Rosenbaum, M.; Cotta, M. a.; Angenent, L.T., **2010**. *Aerated Shewanella oneidensis in continuously fed bioelectrochemical systems for power and hydrogen production*. Biotechnology and Bioengineering, Vol. 105, Issue 5, pp. 880–888. doi:10.1002/bit.22621.

Rosenbaum, M.; Schröder, U.; Scholz, F., **2005**. *Utilizing the green alga Chlamydomonas reinhardtii for microbial electricity generation: A living solar cell*. Applied Microbiology and Biotechnology, Vol. 68, Issue 6, pp. 753–756. doi:10.1007/s00253-005-1915-4.

Ross, D.E.; Flynn, J.M.; Baron, D.B.; Gralnick, J. a; Bond, D.R., **2011**. *Towards electrosynthesis in shewanella: energetics of reversing the Mtr pathway for reductive metabolism.* PloS one, Vol. 6, Issue 2, p. e16649. doi:10.1371/journal.pone.0016649.

Roy, J.N.; Babanova, S.; Garcia, K.E.; Cornejo, J.; Ista, L.K.; Atanassov, P., **2014**. *Catalytic biofilm formation by Shewanella oneidensis MR-1 and anode characterization by expanded uncertainty*. Electrochimica Acta, Vol. 126, , pp. 3–10. doi:10.1016/j.electacta.2013.07.075.

Sand, W.; Gehrke, T., **2006**. *Extracellular polymeric substances mediate bioleaching/biocorrosion via interfacial processes involving iron(III) ions and acidophilic bacteria*. Research in Microbiology, Vol. 157, Issue 1, pp. 49–56. doi:10.1016/j.resmic.2005.07.012.

Sand, W.; Rohde, K.; Sobotke, B.; Zenneck, C., **1992**. *Evaluation of Leptospirillum ferrooxidans for leaching*. Applied and Environmental Microbiology, Vol. 58, Issue 1, pp. 85–92. doi:0099-2240/92/010085-08$02.00/0.

Schippers, A.; Jozsa, P.G.; Sand, W., **1996**. *Sulfur chemistry in bacterial leaching of pyrite*. Applied and Environmental Microbiology, Vol. 62, Issue 9, pp. 3424–3431. doi:0099-2240/96/$04.00+0.

Schlegel, C., **2016**. *Produktive Biofilme auf mikrostrukturierten Metalloberflächen*. Göttingen. doi:ISBN: 9783736992092.

Soussan, L.; Riess, J.; Erable, B.; Delia, M.L.; Bergel, A., **2013**. *Electrochemical reduction of CO2 catalysed by Geobacter sulfurreducens grown on polarized stainless steel cathodes*. Electrochemistry Communications, Vol. 28, , pp. 27–30. doi:10.1016/j.elecom.2012.11.033.

Srikanth, S.; Marsili, E.; Flickinger, M.C.; Bond, D.R., **2008**. *Electrochemical characterization of Geobacter sulfurreducens cells immobilized on graphite paper electrodes*. Biotechnology and Bioengineering, Vol. 99, Issue 5, pp. 1065–1073. doi:10.1002/bit.21671.

Staudt, C.; Horn, H.; Hempel, D.C.; Neu, T.R., **2004**. *Volumetric measurements of bacterial cells and extracellular polymeric substance glycoconjugates in biofilms.* Biotechnology and bioengineering, Vol. 88, Issue 5, pp. 585–592. doi:10.1002/bit.20241.

Stirling, J.L.; Bennetto, P.H.; Delaney, G.M.; Mason, J.R.; Roller, S.D.; Tanaka, K.; Thurston, C., **1983**. *Microbial fuel cells*. Biochemical Society Transactions, Vol. 11, Issue 1969, pp. 451–453. doi:10.1042/bst0110451.

Stöckl, M.; Schlegel, C.; Sydow, A.; Holtmann, D.; Ulber, R.; Mangold, K.-M., **2016**. *Membrane Separated Flow Cell for Parallelized Electrochemical Impedance Spectroscopy and Confocal Laser Scanning Microscopy to Characterize Electro-Active Microorganisms*. Electrochimica Acta, Vol. 220, , pp. 444–452. doi:10.1016/j.electacta.2016.10.057.

Stöckl, M.; Schrader, J.; Mangold, K.-M., **2016**. *Verfahren zur mikrobiologisch-elektrochemischen Synthese von chemischen Stoffen durch elektroaktive Mikroorganismen*. doi:DE102014112685A.

Sun, D.; Chen, J.; Huang, H.; Liu, W.; Ye, Y.; Cheng, S., **2016**. *The effect of biofilm thickness on electrochemical activity of Geobacter sulfurreducens*. International Journal of Hydrogen Energy, Vol. 41, Issue 37, pp. 16523–16528. doi:10.1016/j.ijhydene.2016.04.163.

Sundfors, F.; Bobacka, J.; Ivaska, A.; Lewenstam, A., **2002**. *Kinetics of electron transfer between Fe(CN)63−/4− and poly(3,4-ethylenedioxythiophene) studied by electrochemical impedance spectroscopy*. Electrochimica Acta, Vol. 47, , pp. 2245–2251. doi:10.1016/S0013-4686(02)00063-4.

Surman, S.B.; Walker, J.T.; Goddard, D.T.; Morton, L.H.G.; Keevil, C.W.; Weaver, W.; Skinner, A.; Hanson, K.; Caldwell, D.; Kurtz, J., **1996**. *Comparison of microscope techniques for the examination of biofilms*. Journal of Microbiological Methods, Vol. 25, Issue 1, pp.

57–70. doi:10.1016/0167-7012(95)00085-2.

Sydow, A.; Krieg, T.; Mayer, F.; Schrader, J.; Holtmann, D., **2014**. *Electroactive bacteria - molecular mechanisms and genetic tools*. Applied Microbiology and Biotechnology, Vol. 98, Issue 20, pp. 8481–8495. doi:10.1007/s00253-014-6005-z.

Takahashi, E.; Ledauphin, J.; Goux, D.; Orvain, F., **2009**. *Optimising extraction of extracellular polymeric substances (EPS) from benthic diatoms: Comparison of the efficiency of six EPS extraction methods*. Marine and Freshwater Research, Vol. 60, Issue 12, pp. 1201–1210. doi:10.1071/MF08258.

Tang, Y.; Hwang, J.S.; Wemmer, D.E.; Keasling, J.D., **2007**. *Shewanella oneidensis MR-1 fluxome under various oxygen conditions*. Applied and Environmental Microbiology, Vol. 73, Issue 3, pp. 718–729. doi:10.1128/AEM.01532-06.

Tang, Y.; Meadows, A.L.; Keasling, J.D., **2007**. *A kinetic model describing Shewanella oneidensis MR-1 growth, substrate consumption, and product secretion.* Biotechnology and bioengineering, Vol. 96, Issue 1, pp. 125–33. doi:10.1002/bit.21101.

Tang, Y.; Meadows, A.L.; Kirby, J.; Keasling, J.D., **2007**. *Anaerobic central metabolic pathways in Shewanella oneidensis MR-1 reinterpreted in the light of isotopic metabolite labeling*. Journal of Bacteriology, Vol. 189, Issue 3, pp. 894–901. doi:10.1128/JB.00926-06.

Tartakovsky, B.; Manuel, M.F.; Wang, H.; Guiot, S.R., **2009**. *High rate membrane-less microbial electrolysis cell for continuous hydrogen production*. International Journal of Hydrogen Energy, Vol. 34, Issue 2, pp. 672–677. doi:10.1016/j.ijhydene.2008.11.003.

Thormann, K.M.; Duttler, S.; Saville, R.M.; Hyodo, M.; Shukla, S.; Hayakawa, Y.; Spormann, A.M., **2006**. *Control of formation and cellular detachment from Shewanella oneidensis MR-1 biofilms by cyclic di-GMP.* Journal of bacteriology, Vol. 188, Issue 7, pp. 2681–91. doi:10.1128/JB.188.7.2681-2691.2006.

Torres, C.I.; Marcus, A.K.; Lee, H.S.; Parameswaran, P.; Krajmalnik-Brown, R.; Rittmann, B.E., **2010**. *A kinetic perspective on extracellular electron transfer by anode-respiring bacteria*. FEMS Microbiology Reviews, Vol. 34, Issue 1, pp. 3–17. doi:10.1111/j.1574-6976.2009.00191.x.

Tremblay, P.L.; Zhang, T., **2015**. *Electrifying microbes for the production of chemicals*. Frontiers in Microbiology, Vol. 6, Issue MAR, pp. 1–10. doi:10.3389/fmicb.2015.00201.

United Nations, **1998**. *Kyoto Protocol to the United Nations Framework Convention on Climate Change*. , Vol. 2, , p. 21.

United Nations, **2015a**. *Paris Agreement*. Conference of the Parties on its twenty-first session, p. 32. doi:FCCC/CP/2015/L.9/Rev.1.

United Nations, **2015b**. *World Population Prospects: The 2015 Revision, Key Findings and Advance Tables. Working Paper No. ESA/P/WP.241.* United Nations, Department of Economic and Social Affairs, Population Division, pp. 1–59. doi:10.1017/CBO9781107415324.004.

Ursu, A.-V.; Nistor, I.D.; Gros, F.; Arus, A.V.; Isopencu, G.; Mares, A.M., **2010**. *Hydrodynamic aspects of fluidized bed stabilized in magnetic field*. UPB Scientific Bulletin, Series B: Chemistry and Materials Science, Vol. 72, Issue 3, pp. 85–98.

US Food and Drug Administration, **2015**. *§ 177.2415*. Electronic Code of Federal Regulations, Vol. 3, Issue 177.2415. doi:21CFR177.2415.

Vardanyan, A.; Vardanyan, N.; Markosyan, L.; Sand, W.; Vera, M.; Zhang, R.Y., **2015**. *Biofilm Formation and Extracellular Polymeric Substances (EPS) Analysis by New Isolates of* Leptospirillum*,* Acidithiobacillus *and* Sulfobacillus *from Armenia*. Advanced Materials Research, Vol. 1130, , pp. 153–156. doi:10.4028/www.scientific.net/AMR.1130.153.

Venkateswaran, K.; Moser, D.P.; Dollhopf, M.E.; Lies, D.P.; Saffarini, D. a; MacGregor, B.J.; Ringelberg, D.B.; White, D.C.; Nishijima, M.; Sano, H.; Burghardt, J.; Stackebrandt, E.; Nealson, K.H., **1999**. *Polyphasic taxonomy of the genus Shewanella and description of Shewanella oneidensis sp. nov.* International journal of systematic bacteriology, Vol. 49 Pt 2, Issue 1 999, pp. 705–724. doi:10.1099/00207713-49-2-705.

Villano, M.; Aulenta, F.; Ciucci, C.; Ferri, T.; Giuliano, A.; Majone, M., **2010**. *Bioelectrochemical reduction of CO2 to CH4 via direct and indirect extracellular electron transfer by a hydrogenophilic methanogenic culture*. Bioresource Technology, Vol. 101, Issue 9, pp. 3085–3090. doi:10.1016/j.biortech.2009.12.077.

Virdis, B.; Harnisch, F.; Batstone, D.J.; Rabaey, K.; Donose, B.C., **2012**. *Non-invasive characterization of electrochemically active microbial biofilms using confocal Raman microscopy*. Energy & Environmental Science, Vol. 5, Issue 5, p. 7017. doi:10.1039/c2ee03374g.

Wang, X.; Feng, Y.J.; Lee, H., **2008**. *Electricity production from beer brewery wastewater using single chamber microbial fuel cell*. Water Science and Technology, Vol. 57, Issue 7, pp. 1117–1121. doi:10.2166/wst.2008.064.

White, A.F.; Peterson, M.L.; Hochella, M.F., **1994**. *Electrochemistry and dissolution kinetics of*

magnetite and ilmenite. Geochimica et Cosmochimica Acta, Vol. 58, Issue 8, pp. 1859–1875. doi:10.1016/0016-7037(94)90420-0.

Wikiel, A.J., **2013**. *Role of extracellular polymeric substances on biocorrosion initiation or inhibition*. Dissertation, Essen Germany, p. 202.

Wingender, J.; Neu, T.R.; Flemming, H.C., **1999**. *Microbial extracellular polymeric substances: characterization, structure, and function.* In *Springer*. doi:10.1007/BF00582584.

Wloka, M.; Rehage, H.; Flemming, H.-C.; Wingender, J., **2004**. *Rheological properties of viscoelastic biofilm extracellular polymeric substances and comparison to the behavior of calcium alginate gels*. Colloid and Polymer Science, Vol. 282, Issue 10, pp. 1067–1076. doi:10.1007/s00396-003-1033-8.

Wolf, G.; Wolf, G.; Reis, M.A.M.; Reis, M.A.M., **2002**. *Optical and spectroscopic methods for bio lm examination and monitoring*. Reviews in Environmental Science and Biotechnology, Vol. 1, Issue 3, pp. 227–251.

Xia, L.; Ravenna, Y.; Alfonta, L., **2015**. *Layer-by-layer assembly of a redox enzyme displayed on the surface of elongated bacteria into a hierarchical artificial biofilm based anode*. Chem. Commun., Vol. 51, Issue 13, pp. 2633–2636. doi:10.1039/C4CC09781E.

Xiong, Y.; Shi, L.; Chen, B.; Mayer, M.U.; Lower, B.H.; Londer, Y.; Bose, S.; Hochella, M.F.; Fredrickson, J.K.; Squier, T.C., **2006**. *High-Affinity Binding and Direct Electron Transfer to Solid Metals by Purified Metal Reducing Protein OmcA Decaheme Cytochrome .* , pp. 1–9.

Yang, Y.; Wikieł, A.J.; Dall'Agnol, L.T.; Eloy, P.; Genet, M.J.; Moura, J.J.G.; Sand, W.; Dupont-Gillain, C.C.; Rouxhet, P.G., **2016**. *Proteins dominate in the surface layers formed on materials exposed to extracellular polymeric substances from bacterial cultures*. Biofouling, Vol. 32, Issue 1, pp. 95–108. doi:10.1080/08927014.2015.1114609.

Yang, Y.; Xu, M.; Guo, J.; Sun, G., **2012**. *Bacterial extracellular electron transfer in bioelectrochemical systems*. Process Biochemistry, Vol. 47, Issue 12, pp. 1707–1714. doi:10.1016/j.procbio.2012.07.032.

You, S.-J.; Wang, X.-H.; Zhang, J.-N.; Wang, J.-Y.; Ren, N.-Q.; Gong, X.-B., **2011**. *Fabrication of stainless steel mesh gas diffusion electrode for power generation in microbial fuel cell*. Biosensors and Bioelectronics, Vol. 26, Issue 5, pp. 2142–2146. doi:10.1016/j.bios.2010.09.023.

Yu, Y.-Y.; Chen, H.-L.; Yong, Y.-C.; Kim, D.-H.; Song, H., **2011**. *Conductive artificial biofilm*

dramatically enhances bioelectricity production in Shewanella-inoculated microbial fuel cells. Chemical communications, Vol. 47, Issue 48, pp. 12825–12827. doi:10.1039/c1cc15874k.

Yuvraj, C.; Aranganathan, V., **2016**. *Enhancement of Voltage Generation Using Isolated Dissimilatory Iron-Reducing (DIR) Bacteria Klebsiella pneumoniae in Microbial Fuel Cell*. Arabian Journal for Science and Engineering. doi:10.1007/s13369-016-2108-4.

Zhang, R.Y.; Neu, T.R.; Bellenberg, S.; Kuhlicke, U.; Sand, W.; Vera, M., **2015**. *Use of lectins to in situ visualize glycoconjugates of extracellular polymeric substances in acidophilic archaeal biofilms*. Microbial Biotechnology, Vol. 8, Issue 3, pp. 448–461. doi:10.1111/1751-7915.12188.

Zheng, B.; Zhang, M.; Xiao, D.; Jin, Y.; Choi, M.M.F., **2010**. *Fast microwave synthesis of Fe3O4 and Fe3O4/Ag magnetic nanoparticles using Fe2+ as precursor*. Inorganic Materials, Vol. 46, Issue 10, pp. 1106–1111. doi:10.1134/S0020168510100146.

Zudans, I.; Paddock, J.R.; Kuramitz, H.; Maghasi, A.T.; Wansapura, C.M.; Conklin, S.D.; Kaval, N.; Shtoyko, T.; Monk, D.J.; Bryan, S.A.; Hubler, T.L.; Richardson, J.N.; Seliskar, C.J.; Heineman, W.R., **2004**. *Electrochemical and optical evaluation of noble metal– and carbon–ITO hybrid optically transparent electrodes*. Journal of Electroanalytical Chemistry, Vol. 565, Issue 2, pp. 311–320. doi:10.1016/j.jelechem.2003.10.025.

8 Declaration

Herewith I declare that the presented thesis with the title

“Attachment under current – biofilm formation by electroactive bacteria”

is the result of my independent work. All sources and auxiliary materials used by me in this thesis are cited completely.

Frankfurt am Main, 25th of August 2017